DETECTION AND CHARACTERIZATION OF GENE-FUSIONS IN BREAST AND OVARIAN CANCER USING HIGH-THROUGHPUT SEQUENCING

A Dissertation
Presented to
The Academic Faculty

By

Vinay K. Mittal

In Partial Fulfillment
of the Requirements for the Degree
Doctor of Philosophy in Bioinformatics in the
School of Biology

Georgia Institute of Technology
August 2014

Copyright © 2014 by Vinay K. Mittal

DETECTION AND CHARACTERIZATION OF GENE-FUSIONS IN BREAST AND OVARIAN CANCER USING HIGH-THROUGHPUT SEQUENCING

Approved by:

Dr. John F. McDonald, Advisor
School of Biology
Georgia Institute of Technology

Dr. Gregory Gibson
School of Biology
Georgia Institute of Technology

Dr. I. King Jordan
School of Biology
Georgia Institute of Technology

Dr. Nathan J. Bowen
Department of Biological Sciences
Clark Atlanta University

Dr. Jung Choi
School of Biology
Georgia Institute of Technology

Date Approved: June 16, 2014

To my parents…

ACKNOWLEDGEMENTS

Firstly, I would like to thank my advisor, Dr. McDonald, who has supported and supervised my research throughout my Masters and PhD. I wouldn't have been able to accomplish my research goals without his advice. I can't thank him enough for being my 'guru' for which I will forever be grateful. I thank my committee members, Drs. Nathan Bowen, King Jordan, Jung Choi and Greg Gibson who have taken time out of their busy schedules for committee meetings, to conduct written exams, read and critique my proposal and guide me throughout this endeavor. I would like to especially thank Nathan Bowen for being one of my best mentors in the early days in the lab and for teaching me all the basics of cancer biology and computational genomics; and for his thoughtful suggestions during my research.

I am also thankful to the members of McDonald lab who have shared with me and supported me during my time spent at Georgia Tech. I would specifically like to express my sincere gratitude to Dr. DeEtte Walker and Dr. Lilya Matyunina for their moral support, kindness and motherly affection. My special thanks to my seniors and fellow students in the lab without whom everyday work wouldn't be as much fun and a learning experience.

On a personal note, I would like to thank my mother for her affection and confidence in me; my father for his unconditional support, advice and the best guidance throughout my life. I want to thank my brother, Rahul, and my sister, Aparna, for their love and best wishes; and for sharing beautiful memories that I will cherish forever. It is beyond words to express my gratitude for my family for always being there for me and giving me the purpose of my life. I have always been fortunate to have so many considerate and trustworthy friends. My life wouldn't have been the same without them. I want to thank one of my dearest friends, Harsh Pareek, for sharing the best memories

from college days, for always believing in me and encouraging me in all of my endeavors and efforts.

I would like to take this opportunity to acknowledge all the teachers and mentors, from my school days to the time that I spent at Georgia Tech, for their teachings and guidance; and for making me a better person in every aspect of life. I will forever be indebted to them for their contributions.

TABLE OF CONTENTS

Page

ACKNOWLEDGEMENTS…….....iv

LIST OF TABLES…….. x

LIST OF FIGURES……..xiii

LIST OF SYMBOLS AND ABBREVIATIONS……..xv

SUMMARY……..xvi

CHAPTERS

1 - INTRODUCTION……...1

Cancer is a genetic disease…….1

Cancer genomes are characterized by somatic mutations……..1

Genomic-rearrangements are a prevalent class of mutations that give rise to gene-fusions.……..3

Genomic rearrangements and gene-fusions are non-random and cancer specific mutations……..5

Gene-fusions are employed as biomarkers and therapeutic targets in cancer...6

High-throughput DNA sequencing has accelerated the discovery of gene-fusions and their global patterns in cancer…….....8

2 - R-SAP: A MULTI-THREADING COMPUTATIONAL PIPELINE FOR THE TRANSCRIPTOMICS STUDIES USING HIGH-THROUGHPUT RNA-SEQUENCING……..11

Abstract……11

Introduction……..11

Materials and Methods…….14

Overview of the pipeline……14

Implementation and requirements……..21

Methods……..23

Results and Discussion……24

Demonstration of the applicability of R-SAP using the MAQC dataset...24

R-SAP's performance compares favorably with currently popular pipelines……37

Evaluation of RNA expression level quantification……..41

Evaluation of the chimer-detection module……...44

Evaluation of R-SAP's run time performance....……...44

Summary and Conclusion……46

Acknowledgements……..48

3 - *DE NOVO* ASSEMBLY AND CHARACTERIZATION OF BREAST CANCER TRANSCRIPTOMES IDENTIFIES LARGE NUMBERS OF NOVEL FUSION-GENE TRANSCRIPTS OF POTENTIAL FUNCTIONAL SIGNIFICANCE….49

Abstract……49

Introduction……..50

Methods……51

Data pre-processing……...52

Transcriptome assembly……53

Chimeric transcript detection and filtering……53

Expression quantification……...56

Results……..57

An average of 35 chimeric transcripts per sample were detected in cancerous and normal breast tissue samples……..57

Chimeric transcripts were classified based on structural and functional criteria……60

Some fusion-protein transcripts recur across cancer patient samples……67

Seventy-nine cancer-specific fusions encode protein-coding domains where the ORFs are maintained……68

Fusions that place protein-coding genes under novel regulatory control are frequent in breast cancer samples……..72

A number of chimeric transcripts include sequences from gene desert regions of the genome……76

Comparative analysis of chimeric transcripts in normal and cancer samples identifies potential pro-neoplastic genes……..78

Discussion……81

Acknowledgements……..83

4 - IDENTIFICATION AND EXPRESSION ANALYSIS OF GENE FUSIONS AND OTHER STRUCTURAL VARIANTS IN OVARIAN CANCER USING HIGH-THROUGHPUT SEQUENCING……...84

Abstract……84

Introduction……..84

Materials and Methods……86

Sequencing data acquisition ……..86

Genomic SV Detection using WGS ……..87

Fusion transcript detection using RNA-Seq ……91

Gene-expression analysis ……..92

Results……..92

More than 10,000 structural variants (SVs) identified in six ovarian cancer patient samples……...92

Ovarian Cancer SVs can be divided into 3 groups based upon the location of chromosomal breakpoints ……96

Inter-genic SVs encompass multiple classes of fusion-genes ……100

The breakpoints of most intra-genic SVs map to introns ……...103

Many of the SVs map to gene desert regions ……103

A minority of gene fusions is transcribed ……...103

Only somatically derived coding sequence gene fusions are expressed..104

Microarray analysis …….109

Chromosomal translocations are most frequently associated with changes in gene expression ……...109

Discussion……..113

Acknowledgements……115

5 - CONCLUSIONS…….116

APPENDIX A: SUPPLEMENTARY INFORMATION FOR CHAPTER 2……...121

APPENDIX B: SUPPLEMENTARY INFORMATION FOR CHAPTER 3……...135

APPENDIX C: SUPPLEMENTARY INFORMATION FOR CHAPTER 4……...142

REFERENCES……148

LIST OF TABLES

Page

Table 2.1. Results of initial mapping and alignment screening of MAQC Reference Human RNA-seq data using R-SAP……..24

Table 2.2. Number (%) of high-scoring reads (obtained from MAQC Reference Human dataset) partitioned by R-SAP into sub-categories……25

Table 2.3. Number (%) of chimeric transcripts detected by R-SAP from MAQC Reference Human dataset and represented RefSeq transcripts……..36

Table 2.4. Comparison between R-SAP and Trans-ABySS characterization sub-categories for the high-scoring reads from MAQC Reference Human dataset…….39

Table 2.5. Comparison between R-SAP characterizations and Cuffcompare's novel-isoforms classification from transcripts assembled by Cufflinks using ENCODE Gm12878 cell line RNA-Seq dataset…….40

Table 3.1. Distribution of breast cancer specific chimeric transcript across multiple structural and functional classes……65

Table 4.1. Summary of the number of the various types of SVs detected in the DNA sequencing analysis and their expression as detected by RNA seq or microarray studies ……..108

Table 4.2. Summary of the number of various functional classes of SVs across multiple structural classes of SVs..……110

Table A.1. Data sources and types of datasets that were used for the demonstration of R-SAP's application as well as its performance assessment and testing…….128

Table A.2. GenBank accession IDs for the 206 EST and mRNA sequences that were used as the high confidence test dataset for testing the chimer-detection module of R-SAP..129

Table A.3. Intron-retention events detected in MAQC Reference Human dataset using R-SAP from high-scoring reads that were also characterized as internal-exon-extension……130

Table A.4. Distribution of "multiple-annotations" reads that were detected in MAQC Reference Human dataset using R-SAP…….....130

Table A.5. Distribution of Trans-ABySS characterized reads that were also classified as "high-scoring" by R-SAP previously using MAQC Human Reference RNA-Seq data.131

Table A.6. Distribution of transcripts that were assembled from ENCODE Gm12878 RNA-Seq data using Cufflinks and then characterized by R-SAP……..132

Table A.7. Distribution of transcripts that were assembled from ENCODE Gm12878 RNA-Seq data using Cufflinks and then classified by Cuffcompare into structurally variant classes of RefSeq transcripts (hg18)……133

Table A.8. Comparison between R-SAP's characterizations and Cuffcompare's classification of transcripts that were previously assembled from ENCODE Gm12878 RNA-Seq dataset using Cufflinks……134

Table A.9. Sequencing reads, reference genome alignment and R-SAP characterization statistics for the ENCODE RNA-seq data for Gm12878 cell line……...134

Table A.10. New intronic-exons detected in human RefSeq transcripts (hg18) by R-SAP from intron-only reads in MAQC Reference Human RNA-Seq dataset…….134

Table B.1. Summary statistics on raw and processed RNA-Seq data from the 55 breast samples used in this study……137

Table B.2. Detailed alignment and annotation information on 1959 filtered chimeric transcripts from 55 samples analyzed in the study……..137

Table B.3. Distribution of structural and functional classes for chimers found only in normal tissue samples…….138

Table B.4. Distribution of structural and functional classes for chimeras found in both normal and in cancer tissue samples……138

Table B.5. Recurrence of chimeric transcripts across cancer samples……139

Table B.6. Cancer specific in-frame fusions where at least one protein domain from each (5' and 3') of the participating genes is covered by the ORFs involved in the chimera formation……..139

Table B.7. Cancer specific in-frame fusions where 3' partner gene is up-regulated by > 2X relative to the intact gene in normal tissue samples……...140

Table B.8. Cancer specific chimeric transcripts with fused 5' or 3' UTRs and having the ORF of the coding gene intact and displaying > 2X change in expression relative to the intact gene's expression in normal tissue……140

Table B.9. Detailed information for gene-desert-I and gene-desert-II chimeric transcripts…….141

Table B.10. Chimeric transcripts comprised of in-frame fusion gene transcripts present in both normal and cancer samples……..141

Table C.1. Summary statistics on processed whole genome sequencing data and detected structural variants from 12 samples (6 control (whole blood), 6 cancer patient samples)……...144

Table C.2. Table describing read-groups in the ovarian WGS data and various cutoffs used for the SV detection ……144

Table C.3. Summary of the ovarian samples used to perform the microarray gene-expression by TCGA ……...145

Table C.4. Detailed alignment and annotation information on 14,719 validated SVs from 12 ovarian samples (6 control (whole blood) and 6 ovarian cancer patient samples) analyzed in the study ……...145

Table C.5. Table summarizing the potential functional impacts each class of inter-genic SV ……...146

Table C.6. Distribution of somatically and germline derived SVs that were characterized as intra-genic SVs ……...146

Table C.7. Somatically and germline derived inter-genic SVs that were detected by RNA-Seq or resulted in differential gene-expression as measured by microarray……..147

Table C.8. Detailed distribution of functional classes of inter-genic SVs among various structural classes of SVs ……147

LIST OF FIGURES

Page

Figure 2.1. Architecture of R-SAP and data flow in the pipeline……..14

Figure 2.2. Characterization strategy of R-SAP for high-scoring reads……18

Figure 2.3. Schematic diagram of the detection and annotation of chimeric transcripts by R-SAP using fragmented genomic alignments……..20

Figure 2.4. Distribution of the high-scoring reads from MAQC Reference Human dataset onto RefSeq transcripts.....26

Figure 2.5. Frequency of exon skipping in high-scoring reads from MAQC Reference Human dataset……27

Figure 2.6. Examples of various sub-categories characterized by R-SAP from the test MAQC Reference Human dataset as they are displayed in the UCSC genome browser (hg18) snap-shots……...35

Figure 2.7. Distribution of RefSeq transcripts detected by R-SAP using MAQC Reference Human dataset…….....37

Figure 2.8. Comparison of R-SAP estimated RPKM vs. Affymetrix microarray and TaqMan qRT-PCR expression values……41

Figure 2.9. Correlation plots of RefSeq transcripts (hg18) quantification estimates from ENCODE Gm12878 RNA-Seq data using three different methods: R-SAP, Cufflinks and RSEM…….43

Figure 2.10. Benchmarking of R-SAP's running time as compared with Cufflinks…….45

Figure 3.1. Computational workflow for chimeric transcript discovery……...52

Figure 3.2. Chimeric transcript detection and characterization by R-SAP……54

Figure 3.3. Re-confirmation of chimeric transcripts……..56

Figure 3.4. Sequencing coverage distribution across samples……...58

Figure 3.5. Chimeric transcript distribution across samples before and after filtering…..59

Figure 3.6. Distribution of chimeric and associated reference transcripts…….59

Figure 3.7. Hierarchical classification system for chimeric transcripts…….61

Figure 3.8. Relative distribution of inter-genic, gene-desert-I and gene desert-II in (A) cancer samples, (B) in normal tissue samples, and (C) in both cancer and normal tissue samples……...63

Figure 3.9. Structure based functional classification of chimeric transcripts……64

Figure 3.10. Relative distribution of functional classes of chimeric transcripts……66

Figure 3.11. Recurrence of breast cancer associated chimeric transcripts across patient samples……...68

Figure 3.12. Structure of in-frame gene-fusion mutations resulting in gain of signaling protein domains (trans-membrane and/or signal peptide domains) from another participating gene……...72

Figure 3.13. Gene-expression change due to fusion with heterologous UTRs……..75

Figure 3.14. Detection of transcription factor binding sites (TFBS) in proximity to gene-desert regions involved in chimera formation……...77

Figure 3.15. Potential pro-neoplastic gene-fusions that are functionally suppressed in normal breast tissues but activated in cancer tissues…….80

Figure 4.1. Integrative data analysis workflow for structural variants ……87

Figure 4.2. Validation and breakpoint detection ……...91

Figure 4.3. Comparison between germline and cancer SVs …….93

Figure 4.4. Comparison between germline and cancer SVs for individual patient samples ……94

Figure 4.5. Distribution of SVs across structural categories ……95

Figure 4.6. Multiplicity of SVs across samples ……96

Figure 4.7. Structural classification scheme for SVs ……98

Figure 4.8. Characterization of SVs ……..99

Figure 4.9. Distribution SVs across functional characterization classes ……..99

Figure 4.10. Distribution SVs across functional characterization classes ……..102

Figure 4.11. Structure of the six transcribed SVs resulting in in-frame gene-fusions....107

Figure 4.12. Genomic distribution of inter-genic SVs ……112

LIST OF SYMBOLS AND ABBREVIATIONS

Blast	Basic local alignment search tool
BLAT	Blast like alignment tool
BP	Base-pair
BRCA	Breast invasive carcinoma
CDS	Protein coding sequence
ENCODE	Encyclopedia of DNA Elements
Kb	Kilobases
lincRNA	Large intergenic non-coding RNA
lncRNA	Long non-coding RNA
NGS	Next-generation sequencing
RNA-Seq	RNA-Sequencing
R-SAP	RNA-Seq analysis pipeline
SMART	Simple molecular architecture analysis tool
SSAHA2	Sequence search and alignment by hashing algorithm
SV	Structural variant
TCGA	The Cancer Genome Atlas
TFBS	Transcription factor binding site
TM	Trans Membrane
UTR	Untranslated Region
WGS	Whole-genome sequencing

SUMMARY

Gene-fusions are a prevalent class of genetic variants that have been implicated in the onset and progression of variety of cancer types (Mitelman et al. 2007). Gene-fusions often lead to oncogenic activation by creating fusion-protein or resulting in transcriptional deregulation of cancer genes (Rabbitts 1994; Tomlins et al. 2005). Recurrent gene-fusions, in particular, considered as 'driving' or causal mutations that have often been employed as cancer biomarkers (Mitelman 2000; Laxman et al. 2008)and, in some cases as, potential therapeutic targets (Baselga et al. 1996; Druker et al. 2001).

In recent years, rapid advances in high-throughput DNA sequencing (also known as next-generation sequencing, NGS) technologies have enabled the detection of chromosomal aberrations and fusion-genes at single base-pair resolution (Campbell et al. 2008; Maher et al. 2009a; Stephens et al. 2009). Massively parallel RNA sequencing (RNA-Seq) of the cellular transcriptome has emerged as a promising approach for the identification of previously uncharacterized fusion-gene or "chimeric" transcripts of potential functional significance (Maher et al. 2009a; Ozsolak and Milos 2011; Wang et al. 2013). Despite these technological advancements, our knowledge about the global patterns and complete functional consequences of fusion-genes in cancer is still rudimentary. In recent years, the discovery of novel functional and regulatory elements in the previously considered 'gene-desert' regions of the human genome (Consortium et al. 2007; Cabili et al. 2011; Prensner et al. 2011) poses the question if these regions can also contribute to the formation of gene-fusions. This dissertation describes studies that characterize gene-fusions and resulting chimeric transcripts in breast and ovarian cancer using high-throughput transcriptome and whole genome sequencing. I also address the bioinformatics challenges associated with the analysis of the massive volumes of

sequencing data by developing bioinformatics pipelines and more applied integrated computational workflows.

Research advance 1: Chapter 2 presents the bioinformatics pipeline called R-SAP (RNA-Seq analysis pipeline) that systematically analyze and characterize cancer transcriptomes. Multi-threading capability of R-SAP allows rapid analysis. A systematic hierarchical characterization R-SAP allows accurate detection of complex fusion structures and novel splice-variants as well.

Research advance 2: Chapter 3 and Chapter 4 describes the design and application of computational workflows that integrate R-SAP with specialized set of tool in order to perform qualitative as well as quantitative analysis of gene-fusions and underlying genomic rearrangements using RNA-Seq and whole genome sequencing data.

Research advance 3: Analysis of 45 breast invasive carcinoma and 10 healthy breast samples using RNA-Seq based transcriptome assembly resulted in the findings indicating that an unexpectedly large number of chimeric transcripts are present in both cancerous and normal breast tissues and that many of these variants may play a significant role in breast cancer onset and development. The study also finds that the 'gene-desert' regions can also participate in chimeric transcript formation and result in transcriptional de-regulation of protein-coding genes.

Research advance 4: Whole-genome sequence analysis of six ovarian cancer and six matched controls (whole blood) revealed that the structural variants can be of germline or somatically derived, and very few of them have potential to form gene-fusions. RNA-Seq and gene-expression microarray based analysis indicate that the transcriptional de-repression of gene-fusions determines their biological and clinical significance in cancer.

CHAPTER 1

INTRODUCTION

Cancer is a genetic disease

Cancer is a group of diseases that is characterized by unregulated cell growth and spread of abnormal cells in the body. Cancer is one of the most lethal diseases and is responsible for 580,350 deaths per year (1600 per day) alone in the US, and an additional 1,660,290 new cases are expected to be diagnosed this year (ACS 2013). Research efforts for more than a century have established that the genome plays a central role in the development of cancer. David von Hansemann, in 1890, found an asymmetric distribution of chromosomes as a result of multipolar mitosis or aberrant cell divisions in 13 carcinoma samples (von Hansemann 1890). Working with sea urchin eggs, in 1902, Theodor Boveri suggested that an "incorrect combination of chromosomes" can enable cells to have "unlimited growth" potential and become malignant (Boveri 1914). Subsequent work by Robert Schimke showed genome instability and chromosomal aberrations resulting in gene amplifications that can render cancer cells drug resistant (Schimke et al. 1978). These findings from the late 19th and early 20th century laid the foundation for the theory that cancer is caused by abnormalities in the hereditary material. The theory was further supported by the demonstration that agents that damage DNA and cause chromosomal alterations cause cancer (Loeb and Harris 2008).

Cancer genomes are characterized by somatic mutations

Chromosomal aberrations and DNA level changes are collectively called 'mutations'. Depending upon the origin, DNA mutations can be classified as 'germline' or 'somatic'. Germline mutations are inherited mutations that may increase susceptibility to cancer and lead to familial forms of cancer. For example, mutation in *BRCA1* (breast cancer 1, early onset) and *BRCA2* (breast cancer 2, early onset) genes can increase risk of

breast cancer by 20 fold (Harris and McCormick 2010) and nearly 15% of ovarian cancers can be attributed to such mutations (Risch et al. 2006). Somatic mutations, on the other hand, are DNA level changes acquired during the lifecycle of the cell and passed along from the progenitor cells through mitotic division (Stratton et al. 2009). DNA damage in cells is caused by exposure to mutagens such as radiation (including UV light), tobacco smoke, naturally occurring chemicals such as aflatoxins (Lengauer et al. 1998), and oxidative stress within the cell (Cooke et al. 2003). Most of the damage caused by mutagens is repaired by the cell; however some may become fixed somatic mutations due to inefficient repair mechanisms in the cell and result in cancer. Moreover, intrinsic errors in DNA replication can accelerate the rate of somatic changes (Lengauer et al. 1998; Stratton et al. 2009). The first cancer causing somatic mutation was reported in the *HRAS* gene (Harvey rat sarcoma viral oncogene homolog) in a human bladder cancer cell line (Reddy et al. 1982). Since then, three decades of research have resulted in the discovery of nearly 300 genes that are causatively mutated in cancer (Futreal et al. 2004; Forbes et al. 2011) and comprise ~1% of all known human genes. Somatic mutations are a more prominent cause for cancer progression than inherited mutations. 90% of cancer genes are somatically mutated, 20% show germline mutations and 10% show both [(Futreal et al. 2004) and http://www.sanger.ac.uk/genetics/CGP/Census/]. Cancer genomes may harbor hundreds to thousands of somatic alterations but only a few of them confer a selective clonal growth advantage and are causally implicated in oncogenesis. Such mutations are called ‘driver’ mutations (Greenman et al. 2007; Vogelstein et al. 2013) . The remainders of the alterations are called ‘passenger’ or ‘bystander’ mutations and may not contribute to cancer development (Futreal et al. 2004). However, passenger mutations may be the result of causal mutational mechanisms in cancer and hence they can also provide useful insight into the pathogenesis of cancer (Pleasance et al. 2010).

DNA mutation can encompass a variety of nucleotide changes including point mutations that are single base pair substitutions; insertions and deletions of base pairs (indels) and genomic rearrangements (also known as large structural variants) involving hundreds to millions of base pairs (Lupski and Stankiewicz 2005; Pleasance et al. 2010). Genomic rearrangements are gross DNA alterations that collectively represent mutational changes including deletion, insertion, inversion, translocation and transposition (Lupski and Stankiewicz 2005). Cancer genomes are also subjected to loss or amplification of large genomic segments that are collectively referred to as 'copy number alterations'.

Genomic-rearrangements are a prevalent class of mutations that give rise to gene-fusions

Genomic rearrangements (also known as large structural variants) are among the most common mutations in cancer (Futreal et al. 2004; Edwards 2010). Cytogenetic based research over the last 25 years has resulted in more than 600 registered cases of somatic chromosomal rearrangements in cancer (Mitelman 2000). Over 50,000 cases of rearrangements in cancer have been reported in more than 11,500 published articles (Mitelman et al. 2007). Prevalence of genomic rearrangements can be estimated by the fact that every known tumor type contains at least one documented case of rearrangement, although the prevalence may vary from 0-100% among patients (Mitelman et al. 2007). The most frequent mutation in cancer causing genes is chromosomal translocation that results in oncogenic activation (Futreal et al. 2004; Stratton et al. 2009). The current catalogue (Forbes et al. 2008) of cancer 16213703mutations includes 317 out of 522 genes that are mutated by translocation. Currently there are 267 known in acute myeloid leukemia, 155 in acute lymphoblastic leukemia and 75 in solid tumors.

Genomic rearrangements typically join normally distant genomic loci and can result in fusion-gene structures. Gene-fusions exert their action via transcription where

transcribed mRNA is called a “fusion transcript” or “chimeric RNA”. A fusion transcript may encode for a fusion protein with oncogenic activity (Rabbitts 1994; Rowley 2001). For example, in chronic myeloid leukemia (CML), a reciprocal translocation between chromosomes 9 and 22 results in *BCR-ABL* gene-fusion (Nowell 1962). As a result the coiled-coil (CC) oligomerization domain from *BCR* (breakpoint cluster region) activates the tyrosine kinase domain from *ABL* (Abelson murine leukemia viral oncogene homolog 1) that drives CML (McWhirter et al. 1993; Ren 2005). Gene-fusions can aberrantly appose enhancer or promoter elements of one gene to another gene without disrupting the protein-coding sequence and result in transcriptional deregulation of the latter gene (Look 1997; Xia and Barr 2005). For example, a deletion on chromosome 21 results in the oncogenic activation of *ERG* gene (ETS-related gene) due to its juxtaposition to *TMPRSS2* (Transmembrane protease, serine 2**)** gene’s promoter in prostate cancer (Tomlins et al. 2005). Cancer genomes may harbor several genomic rearrangements that may or may not be functional. Although, functional rearrangements give rise to fusion RNA by transcription, investigation of genomic aberrations at the transcriptome level is very important (Ju et al. 2012).

Apart from genomic rearrangements, recent studies have discovered two additional RNA level mechanisms that can result in gene-fusion transcripts. Co-transcription or read-through transcription (also known as ‘transcription induced chimera’ or TIC), describes two neighboring genes in the genome that are transcribed into a single RNA. Inter-genic regions between the two genes and introns are spliced out so that the resulting mRNA encodes for a new fusion protein (Akiva et al. 2006; Parra et al. 2006). Fusion-gene transcripts can also be generated at the post-transcription level by *trans*-splicing of multiple simultaneously processed pre-mature RNAs from different genes where the spliceosome ligates exons from two pre-mature RNA molecules in to a single mRNA (Sullenger and Gilboa 2002; Garcia-Blanco 2003).

Genomic rearrangements and gene-fusions are non-random and sometimes cancer-specific

Genomic rearrangements were initially considered to be random events that occur by chance and when selected, lead to oncogenesis (Savage 1993; Mitelman et al. 2007). But recent studies have suggested that genomic rearrangements are triggered by factors such as chemical and radiation exposure, faulty DNA repair pathways and DNA replication errors that are also responsible for cancer initiation.

Influences that trigger the genesis of genomic rearrangements are well known now and can be divided them into four categories that work synergistically in cancer (Aplan 2006; Mani and Chinnaiyan 2010). First, spatial proximity in the nucleus where rearranged genes are brought in close proximity in a cell-type and cell division-stage specific manner, and close proximity correlates to the frequency of translocation (Roix et al. 2003). Second, cellular stress, including genotoxic stress (chemical and radiation exposure) (Fugazzola et al. 1995), oxidative stress (Barzilai et al. 2002) and replicative stress (Tuduri et al. 2009) that cause double strand breaks and set off the formation of genomic rearrangements (Richardson and Jasin 2000)(10864328). Third, inefficient DNA damage response and faulty repair mechanisms of DNA breaks result in genomic rearrangements (Boboila et al. 2010; Simsek and Jasin 2010). And fourth, DNA sequence features such as the presence of repetitive sequences, palindromic sequences, CpG dinucleotide, and epigenetic modifications, are also known to increase the probability of genomic rearrangement (Ng et al. 2003; Tsai et al. 2008; Huang et al. 2010).

There are three known cellular mechanisms underlying genomic rearrangements: Non-allelic homologous recombination (NAHR) where low-copy repeats cause recombination between two otherwise un-related genomic regions; non-homologous end-joining (NHEJ) is the faulty double strand DNA break repair that ligates distant genomic loci; and third, replication fork stalling and template switching (FoSTeS) where the lagging DNA strand is switched during replication (Aplan 2006; Gu et al. 2008). Insights

into the genesis and cellular mechanisms underlying genomic rearrangements and gene-fusions suggest that the onset of cancer is accompanied by genomic rearrangements since they share common factors of initiation. The causal role of gene-fusions and their specificity to cancer further underscores their potential as biomarkers of cancer onset and progression.

Gene-fusions are employed as biomarkers and therapeutic targets in cancer

Gene-fusions represent the most common class of mutations that are detected in almost every tumor type (Rowley 2001). Recurrent gene-fusions, in particular, considered as 'driving' or causal mutations are perceived as potential biomarkers and therapeutic targets in cancer (Mitelman 2000; Laxman et al. 2008). The first consistent chromosomal rearrangement, known as the 'Philadelphia chromosome', was discovered in chronic myeloid leukemia (CML) by Nowell and Hungerford in 1962 (Nowell 1962). This rearrangement results in the *BCR-ABL* gene-fusion resulting in oncogene activation and is observed in 95% of CML patients. CML patients with this disorder are administered a tyrosine kinase inhibitor drug, imatinib, to treat the disease. Similarly, the proto-oncogene, c-MYC, is activated in 90% of the Burkitt's lymphoma as a result of translocation to immunoglobulin genes (Cory 1986). Gene-fusions have been predominantly observed in hematological malignancies, mainly leukemias and lymphomas, and soft tissue sarcomas, but their application in solid tumors has been limited (Kumar-Sinha et al. 2008). For example, all solid tumors and epithelial carcinomas account for 80% of the cancer related deaths but they make up only 27% of the known cases of karyotypic abnormality and rest is attributed to hematological disorders[(Kumar-Sinha et al. 2006; Mitelman et al. 2007), http://cgap.nci.nih.gov/Chromosomes/]. This discrepancy may seem to indicate that genomic rearrangements are rare in solid tumors. In reality, chromosomal aberrations in solid tumors underrepresented due to the poor chromosomal morphology, presence of

cytogenetically unrelated clones and presence of very complex karyotypes in solid tumor samples that make them less amenable to the traditional karyotyping methods (Gorunova et al. 1998; Kumar-Sinha et al. 2006). Despite technological barriers, advancement in biological assays and high-throughput genomics has led to major discoveries of several recurrent fusion genes in solid tumors and other epithelial carcinomas (Edwards 2010). The first breakthrough was achieved by (Tomlins et al. 2005) when they discovered the presence of *TMPRSS2-ERG* (Transmembrane protease, serine 2 and ETS-related gene) gene-fusion in more than 50% of localized prostate cancers. The *ERG* gene is an oncogenic transcription factor that becomes overexpressed as a result of fusion with the 5'UTR from *TMPRSS2*. Other examples of well documented gene-fusion biomarkers in solid tumors include *ETV6-NTRK3* (ets variant gene 6 and neurotrophic tyrosine-kinase receptor type 3) that was originally detected in congenital fibrosarcoma and later detected in secretory breast carcinoma (Knezevich et al. 1998; Tognon et al. 2002). A gene fusion between echinoderm microtubule-associated protein-like 4 (*EML4*) and anaplastic lymphoma kinase (*ALK*) was first discovered in non-small cell lung carcinoma and it is observed in 3-13% of the lung cancer patients (Soda et al. 2007). Another example is the gene-fusion *RET-NTRK1* (receptor tyrosine kinase and neurotrophic tyrosine kinase receptor) that is detected in as many as 50% of thyroid papillary carcinomas (Bongarzone et al. 1998; Pierotti 2001). Other solid tumors that have at least one reported biomarker gene-fusion include breast, pancreatic, colon, ovarian and brain tumors (Kumar-Sinha et al. 2006). Although, the current list of gene-fusion biomarkers for solid tumors is not as comprehensive as hematologic malignancies, advancement in the sensitivity of the analytical genomics assays will reveal more widespread occurrences of recurrent gene fusions in other cancer types.

High-throughput DNA sequencing has accelerated the discovery of gene-fusions and their global patterns in cancer

Early methods to identify genomic rearrangements and gene fusions were high resolution cytogenetic-based, such as spectral karyotyping followed by fluorescent *in situ* hybridization (FISH) or noncytogenetic-based methods such as the modified NIH 3T3 transformation foci assay (Kaye 2009). Development in biological assays led to the application of array based methods such as aCGH (array comparative hybridization) for the detection of gene-fusions but these methods are limited in their throughput and resolution of detection. In recent years, rapid advances in high-throughput DNA sequencing (also known as next-generation sequencing, NGS) technologies have enabled the detection of chromosomal aberrations and fusion-genes at single base-pair resolution (Campbell et al. 2008; Maher et al. 2009a; Stephens et al. 2009) . NGS allows sequencing of the fragments of target molecules such as DNA or RNA in a massively parallel way that generates millions to billions of short (50 – 150 bp) reads. The sequencing protocol typically follows the clonal amplification of the target sequences so that the output provides a multi-fold coverage (Metzker 2010). Currently available NGS technologies such as Illumina Hi-Seq, Ion torrent and Pacific Biosciences also allow sequencing of the cellular transcriptome that harbors expressed fusion genes known as fusion-gene transcripts or chimeric transcripts (Martin and Wang 2011). Sequencing of the transcriptome is called RNA-Sequencing or RNA-Seq (Wang et al. 2009). Since functional mutations in cancer are manifested through transcription, investigation of genomic aberrations at the transcriptome level becomes very important in isolating functional or potential driver mutations from the non-functional mutations (Ju et al. 2012).

Deep coverage RNA-Seq provides a comprehensive view of the transcriptome that enables researchers to systematically analyze cancer cell transcriptomes and uncover novel and potentially oncogenic fusion-gene transcripts (Maher et al. 2009a; Ozsolak and

Milos 2011; Wang et al. 2013). For instance, Maher et al. applied short and long read RNA-Seq to rediscover *BCR-ABL1* in CML cell lines, *TMPRSS-ERG* in prostate cancer and additionally, reported multiple novel fusion transcripts associated with prostate cancer. Targeted sequencing of prostate cancer using artificial exon-exon junctions uncovered six recurrent TIC (transcription induced chimeras) or read-through gene-fusion events including *SLC45A3-ELK4* that is already a known frequent erythroblast transformation-specific fusion in prostate cancer (Nacu et al. 2011). Studies involving RNA-Sequencing of large number of cancer samples have begun to reveal global patterns and the underlying molecular mechanisms of fusion-genes in solid tumors. For example, transcriptome sequencing of 24 breast cancer samples resulted in the detection of 15 primary breast tumor subtype specific fusion-gene transcripts (Asmann et al. 2012). These fusion-gene transcripts can serve as potential biomarkers for breast-cancer stratification for further targeted therapy. Recently, sequencing of 89 samples (79 breast cancer and 10 normal samples) discovered gene fusions that were recurrent in 4-6% of the patients and involved *MAST1* and *MAST2* genes, and NOTCH-family genes that also increased the proliferation of benign breast cancer cells (Robinson et al. 2011).

The increasing feasibility and the rapidly decreasing cost of sequencing have already paved the way for its routine application in cancer research (Voelkerding et al. 2009). Although, unprecedented amounts of data from cancer transcriptomes provides a new opportunity to uncover novel gene-fusions, it comes with bioinformatics challenges that need to be addressed. The cancer transcriptome is inherently complex as it contains novel RNA species such as fusion transcripts and splice-variants generated as a result of genomic mutations and transcriptional deregulation (Carninci et al. 2008; Costa et al. 2010). Hence the massive amounts of RNA-Seq data from cancer transcriptomes requires systematic analysis using high-performance bioinformatics tools that can address both complexity and massiveness of the sequencing data at the same time. In order to address this challenges we developed and automated multi-threading RNA-Seq analysis pipeline

(R-SAP; described in CHAPTER 2; (Mittal and McDonald 2012)) that follows a systematic and hierarchical characterization scheme to qualitatively and quantitatively analyze RNA-Seq data from cancer cell transcriptomes. In CHAPTER 3, we apply R-SAP to analyze 45 breast cancer transcriptomes in order to uncover global patterns of chimeric transcripts in cancer. In this chapter we create an integrated analysis workflow using R-SAP and currently available bioinformatics tools for with highly specialized functionality such as transcriptome assembly, RNA expression estimation and reference genome alignment. In CHAPTER 4, we expand the applicability of R-SAP to discover genomic rearrangements using whole genome sequence data from six ovarian cancer genomes and perform a comparative analysis with the gene-fusions detected in the transcriptome of the same patients.

CHAPTER 2

R-SAP: A MULTI-THREADING COMPUTATIONAL PIPELINE FOR THE TRANSCRIPTOMICS STUDIES USING HIGH-THROUGHPUT RNA-SEQUENCING

Abstract

The rapid expansion in the quantity and quality of RNA-Seq data requires the development of sophisticated high-performance bioinformatics tools capable of rapidly transforming this data into meaningful information that is easily interpretable by biologists. Currently available analysis tools are often not easily installed by the general biologist and most of them lack inherent parallel processing capabilities widely recognized as an essential feature of next-generation bioinformatics tools. We present here a user-friendly and fully automated RNA-Seq analysis pipeline (R-SAP) with built-in multi-threading capability to analyze and quantitate high-throughput RNA-Seq datasets. R-SAP follows a hierarchical decision making procedure to accurately characterize various classes of transcripts and achieves a near linear decrease in data processing time as a result of increased multi-threading. In addition, RNA expression level estimates obtained using R-SAP display high concordance with levels measured by microarrays.

Introduction

The cellular transcriptome is the complete set of protein coding mRNAs, non-coding RNAs and other regulatory RNAs present in a cell (Velculescu et al. 1997). In eukaryotes, the complexity of the cellular transcriptome is enhanced by the presence of alternatively spliced RNAs, fusion and other types of chimeric transcripts and transcripts encoded within previously uncharacterized genomic regions (Carninci et al. 2008; Costa

et al. 2010). The complexity of the transcriptome of cancer and other diseased cells can be even more complex due to deregulation of the cellular splicing machinery, and the transcription of various genomic mutations that contribute to aberrant cell function (Skotheim and Nees 2007; Ritchie et al. 2008). For these reasons, transcriptome profiling has become an important tool, not only in the diagnosis of cancer and other diseases, but additionally for the identification of putative molecular targets for therapeutic intervention (Aparicio et al. 2000; Sutherland et al. 2011).

While transcriptomics was first heralded by the introduction of microarray technologies over two decades ago (Kulesh et al. 1987; Maskos and Southern 1992), the field is currently undergoing revolutionary expansion by virtue of the application of deep-sequencing technologies to the quantitative and qualitative characterization of cellular transcripts (Morozova and Marra 2008). Commonly referred to as "RNA-Seq", these high-throughput methodologies involve the massively parallel sequencing of millions of copies of fragments of cellular transcripts (Wang et al. 2009). Contemporary sequencing platforms can generate megabytes to gigabytes of data in a single sequencing run (Morozova and Marra 2008). This magnitude of data not only allows for the characterization of moderate to high abundant transcripts, it also provides sufficient coverage and depth to characterize rare and potentially novel low abundant transcripts that went undetected by earlier methodologies.

The rapid expansion in the quantity and quality of RNA-Seq data requires the development of sophisticated high-performance bioinformatics tools capable of rapidly transforming this data into meaningful information that is easily interpretable by biologists. Current approaches to the analysis of RNA-Seq data involve the alignment of sequencing reads to a reference genome and subsequent association of these genome mappings with established transcript models to quantify expression levels and detect

mRNA isoforms, fusion genes and other novel transcript structures (e.g., (Mortazavi et al. 2008; Pan et al. 2008; Sultan et al. 2008; Guffanti et al. 2009; Maher et al. 2009b; Berger et al. 2010; Robertson et al. 2010)). Despite their obvious utility, currently available analysis tools are not easily installed by the general biologist and most of them lack inherent parallel processing capabilities widely recognized as an essential feature of next-generation bioinformatics tools (McPherson 2009; Richter and Sexton 2009).

We present here an automated RNA-Seq analysis pipeline (R-SAP) with built-in multi-threading capability to analyze and quantitate high-throughput RNA-Seq datasets. R-SAP is easy to install and follows a hierarchical decision making procedure to characterize various classes of transcripts. It compares reference genome alignment of sequencing reads with sets of well-annotated transcripts in order to detect novel isoforms. Reads that map completely within known exon boundaries are used for gene expression quantification. Fragmented alignments of sequencing reads are used to detect chimeric transcripts such as fusion genes. Novel exons detected within previously annotated inter-genic and intronic regions are also reported. R-SAP modules can be customized by a user-adjustable set of parameters for particular applications. R-SAP generates output files that contain transcript assignments for the sequencing reads, gene expression levels, lists of aberrantly spliced genes and data statistics. The computational outputs can be viewed with online genome browsers by uploading the R-SAP generated browser compatible output file. To demonstrate the applicability of the pipeline, we analyzed publically available RNA-Seq data generated from the Roche 454 and the Illumina GA platforms. We achieved a linear decrease in the data processing time as a result of increased multi-threading. RNA expression level estimates obtained using our pipeline displayed high concordance with levels measured by microarrays. R-SAP program is publicly available at www.mcdonaldlab.biology.gatech.edu/r-sap.htm.

In the following sections, we describe the architecture of the pipeline and results from the analysis of the test data to evaluate various modules of the pipeline.

Materials and Methods

Overview of the pipeline:

R-SAP compares reference genome mappings of RNA-Seq reads with the genomic coordinates of known and well-annotated transcripts (reference transcripts or known transcript models) in order to detect known and new RNA isoforms and, chimeric transcripts. There are four core modules in R-SAP's workflow (Figure 2.1): (i) initial alignment screening, (ii) characterization with reference transcripts (iii) chimeric transcript detection and (iv) RNA expression quantification. A main wrapper script controls the flow of data to these core modules (Figure 2.1).

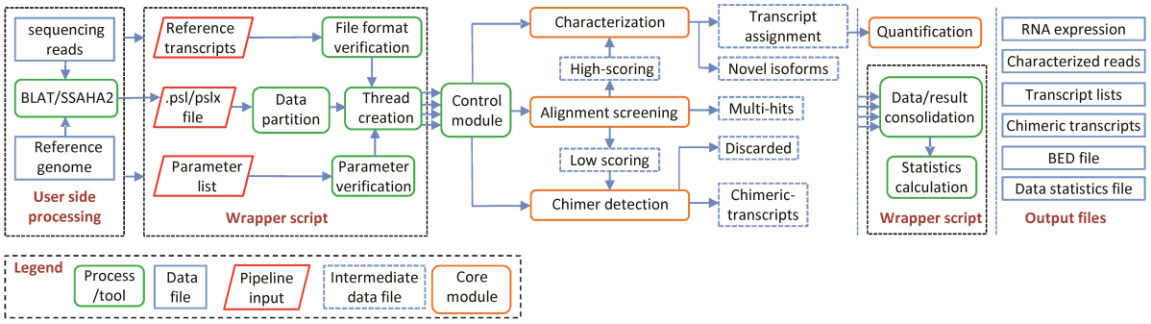

Figure 2.1. Architecture of R-SAP and data flow in the pipeline. Wrapper script begins the execution of the pipeline and divides the data in to smaller sub-sets. Multiple threads are created and each core module in each thread is run under the "Control-module". Output files are merged by the wrapper script and corresponding output files are written to the disk.

To initiate analyses using R-SAP, the user provides two required inputs for the pipeline: the sequence alignment file and known transcripts' coordinate file. Currently R-SAP accepts alignment files only in psl format that are generated by mapping RNA-Seq reads to the reference genome using BLAT (Blast like alignment tool) (Kent 2002) or SSAHA2 (Sequence search and alignment by hashing algorithm) (Ning et al. 2001).

RNA-Seq reads mapping to the genome may result in the alignments scattered across multiple exons separated by introns. We chose psl as the alignment format for the pipeline because the scattered alignments are precisely stitched together and reported as a large single alignment. As a result, for each sequencing read the most likely alignment and corresponding genomic locus can be readily found in the alignment files. Moreover, the psl format preserves the orientation of alignment blocks originating from the contiguous genomic loci enabling their accurate re-mapping to the annotated exons and determination of associated reference structural variants.

R-SAP is also configured to work with two of the currently available transcript assemblers: Cufflinks (Trapnell et al. 2010) and Scripture (Guttman et al. 2010). Assembled transcripts can be supplied to R-SAP either in GTF (Gene Transfer Format) or in BED (Browser Extensible Data) format. GTF and BED are default output formats from Cufflinks and Scripture respectively.

Known transcript model files for the reference genome can be obtained from the UCSC genome database (Fujita et al. 2011), the UCSC table browser (Karolchik et al. 2004) or the Ensembl database (Hubbard et al. 2002). R-SAP accepts known transcript model file formats in standard table browser format, GTF or BED. The analysis stringency can be adjusted using a set of cutoff and threshold values (described in Supplementary Methods) provided by the user at the beginning of the pipeline.

R-SAP begins with the parsing of input data files for the format check and verification of the input parameters using the main wrapper script. The same wrapper script then divides the input alignment file into the number of parallel threads specified by the user (default is one thread). Each part of the input file is supplied to the set of core

modules, in parallel. At the completion of each thread run, the main wrapper script merges the intermediate output files and creates the final set of output files.

(a) Alignment screening:

The first step in the pipeline is to select the most likely alignment for each of the sequencing reads as reads may have multiple genomic hits. Alignment hits with the highest alignment identity, alignment score and read coverage among all the genomics hits are selected as the best alignments (top-scoring) on the genome (see Supplementary Methods). Top-scoring alignments are then classified as high-scoring if they have only one best possible alignment with identity and read coverage values above the cutoff (default 95% and 90%, respectively). Reads that map to multiple genomic loci with equivalent alignment identity and read coverage are classified as multi-hit reads. Those reads that produce low quality alignments with identity and/or read coverage below the threshold values are further analyzed by a separate module of the pipeline to detect chimeric transcripts (see below). The remaining reads that are low quality alignments are classified as "discarded". Both "discarded" and multi-hits reads are excluded from the further analysis and reported separately.

(b) Characterization with reference transcripts:

High-scoring reads from the alignment module are subjected to the characterization module where genome mapping coordinates of the sequencing reads are precisely compared with the transcriptional and exons boundaries of the well annotated transcripts. Mapping of a read within the known exon boundaries is considered as indicative of normal splicing whereas out of exon or partial exon mapping is indicative of aberrant splicing or the presence of a novel isoform. The characterization strategy is outlined in Figure 2.2. Read alignments that skip exonic bases because of discontinuous blocked alignment on the reference genome are characterized as exon-deletions in that

reference transcript (Figure 2.2B, C). Small deletions (10 bp by default) are permitted in the alignment in order to tolerate small gaps due to the sequencing errors. Read mappings, that span multiple exons are used to detect exon-skipping events (Figure 2.2D).

Partial mapping of the sequencing reads onto known exons results in either gene boundary expansion (Figure 2.2E,F) or extension of exons into introns (Figure 2.2G,H). Slight extensions in the alignment beyond the exon boundary are tolerated by applying minimum exon extension cutoff (2 bp default).

Sequencing reads that extend 5' terminal exons (5'UTR) into upstream promoter regions (Figure 2.2E) are considered the result of potential new transcription start sites (alternative TSS). Similarly, reads that extend 3' terminal exons (3'UTR) into downstream regions are characterized as potential alternative polyadenylation site variants (Figure 2.2F). Intron-retentions (or complete intron inclusion) are detected when a read alignment completely spans an intron including at least part of flanking exons (Figure 2.2H). Such events are included in the internal-exon-extensions characterizations. Reads mapping completely within introns are characterized as intron-only reads (Figure 2.2I). Sequencing reads that do not map to any known transcript and fall within a pre-specified gene -radius (5 kb default setting), on either side of the transcript, are characterized as neighboring-exons (Figure 2.2J). Clusters of such reads may represent the existence of new transcriptional boundaries and can be aggregated with the known transcript models. Reads falling outside the gene-radius are designated as gene-desert reads (Figure. 2.2K). Some of the high-scoring reads may exhibit multiple characterizations with the reference transcripts. For example, a read may exhibit internal-exon-extension simultaneously with a 5' UTR expansion. Such reads are sub-characterized as multiple-annotation reads. We apply one additional stringency criterion during the characterization step to further filter out possible sequencing artifacts.

Sequencing reads that expand the transcript boundary by more than 100 kb or have alignment blocks separated by more than the cutoff distance value (100 kb default setting) are conservatively reported as uncharacterized and excluded from the further analysis.

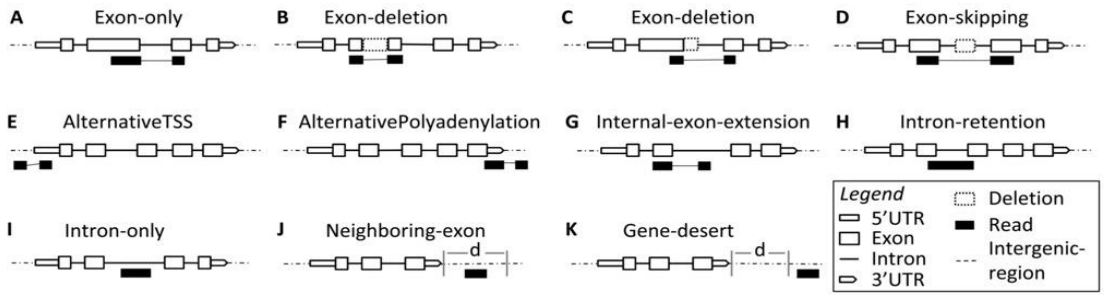

Figure 2.2. Characterization strategy of R-SAP for high-scoring reads. Read mappings (black boxes) are compared with the known exon (empty boxes) and intron (black lines). The larger empty boxes represent coding regions while the smaller empty boxes represent untranslated regions. **A.** Read mapping within the known exon. **B,C.** Discontinuous blocked alignment resulting in exonic base skipping (dashed-line box). **D.** Skipping of third exon. Exon skipping is also characterized as exon-deletion. **E.** Extended 5'UTR. **F.** Extended 3'UTR. **G,** Exon extended into intron. **H.** Intron retention . **I.** Read mapping completely within the intron. **J.** Read mapping outside the permissible (d) gene-radius **K.** Read mapping outside the permissible (d) gene-radius.

As a default setting, the pipeline characterizes each read with only one best fitting reference transcript. The best fitting transcript is the one with maximum exon overlap and minimum non-exonic regions (intron and intergenic) overlap with the read. Reference transcripts with protein-coding potential are selected over the non-protein-coding transcripts. In cases where multiple transcripts are equally likely, the best fitting transcript is selected randomly. The pipeline provides the user with the option to inactivate all of these defaults settings in which case all possible reference transcript associations will be displayed.

(c) Chimeric transcript detection:

Chimeric transcripts may be due to genomic rearrangements such as translocations and inversions, or transcriptional processes such as co-transcription, trans-splicing or aberrant intra-genic (within the same gene) splicing (Flouriot et al. 2002; Mitelman et al. 2005; Guffanti et al. 2009; Maher et al. 2009b). Sequencing reads from chimeric transcripts are very likely to produce discrete alignments to distant or close genomic loci. In order to detect candidate chimeric reads, all the reads with top-scoring alignments displaying low query coverage (below the cutoff coverage value, default 90%) and an alignment identity greater than the cutoff value (default 95%) are selected. These reads are considered potential chimeric reads only if the region not covered in the top-scoring alignment of the read is at least 20 bp (default gap threshold). Twenty bp was selected as the default setting because alignment algorithms will not produce a significant alignment for the relatively short remaining part of the read. Once the above criteria are met, alignments are parsed to obtain the alignment pair for the top-scoring alignment (Figure 2.3A).

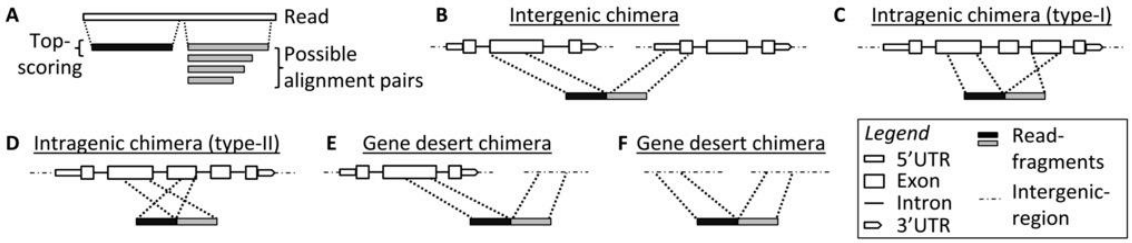

Figure 2.3. Schematic diagram of the detection and annotation of chimeric transcripts by R-SAP using fragmented genomic alignments. A. Best possible alignment pairs are selected for the reads displaying significant sequence similarity to the reference genome. Alignment fragments are then individually compared with known transcript models. **B.** Alignment pairs belong to two different genes (inter-chromosomal or intra-chromosomal). **C.** Alignment pairs mapped to the same gene but in opposite orientation on the reference genome. **D.** Both pairs mapped within the same gene but their order on the sequencing read is opposite of their alignment order on the corresponding gene. **E, F.** At least one alignment pair mapped to the genomic region with no known gene from the reference gene set.

Alignments are filtered out if the alignment identity is less than the cutoff identity value (default 95%). The alignment with the highest coverage on the remaining part of the read and with highest alignment identity is selected as the best possible pairing alignment. In addition, intra-chromosomal pairing is preferred over inter-chromosomal pairing. Small overlaps (less than one third of alignment pair's coverage on remaining part of the read) and gaps (not more than the gap-threshold, 20 bp default) between the two read segments corresponding to alignment pairs are allowed. To ensure the validity and significance of the alignment, chimeric read segments are required to be at least 25 bp long. Thus, chimeric reads shorter than 50 bp are rejected. False positives are further minimized by excluding chimeric reads that produce alignments from repetitive genomic regions. If more than one hit are identified for any part of a chimeric read with identity above the cutoff value and with more than 90% coverage on the same region of read sequence, the candidate chimeric transcript is rejected as a false positive. The remaining alignment pairs are associated with reference transcripts and categorized in various

chimeric read structures according to the genic or intergenic regions to which they map (Figure 2.3B-F).

(d) Expression level quantification:

Reference transcript assignment information for exon-only and intron-only reads is consolidated from multiple threads into a single file. Expression levels are quantified using the RPKM (reads per kilobase of exon model per million mapped reads) method proposed by Mortazavi *et al.* (Mortazavi et al. 2008). Transcript level RPKM values are calculated using exon-only reads and similarly the RPKM value for each individual intron is calculated using intron-only reads. R-SAP estimates expression values only if the input alignment file is provided in psl format. Since, assembled transcript files do not contain read level mapping information, expression estimation is not possible using these files.

Once each of the above modules are run, annotation and data statistics are collected from various intermediate output files and merged to generate the final output files. The final set of output files contains RNA level expression files, assignment of known transcripts to the high-scoring reads and their characterization, chimeric reads with annotation and data statistics files with distribution of reads over the various classes. Finally, browser compatible out-put files containing annotation information of all the reads are generated that can be uploaded to web based genome browsers (such as UCSC and Ensembl) for the visualization purposes.

Implementation and requirements:

R-SAP was implemented using Perl 5.8.0 (also the minimum version of perl required to run the pipeline) enabled with multi-threading and is compatible with all UNIX and Windows based systems. Disk space required during the pipeline run is ~1.5 X the size of the input alignment file.

Test datasets

MAQC Universal Reference Human data: The MAQC Universal Reference Human Poly-A+ selected RNA-Seq data compiled from Mane *et al.* (Mane et al. 2009) was obtained from Short Read Archive (SRA accession SRX002934). The data consisted of 881,555 of Roche's 454 sequencing reads with an average length of 258 bp from five 454 GS-FLX sequencing runs. 878,275 of those reads were retained after low-complexity repeat trimming and short read (<20 bp) exclusion (see Supplementary Methods). Raw microarray data (Affymetrix Human U133Plus2.0) was downloaded from the Gene Expression Omnibus (GEO accession: GSM589512). Four replicates of TaqMan qRT-PCR measurements for the same sample were also obtained from Gene Expression Omnibus (GEO accessions: GSM129641, GSM129640, GSM129639 and GSM129638) that consisted of expression values for 1044 probes.

ENCODE lymphoblastoid cell line data:

As a short read ultra high-throughput data set, RNA-Seq data for Gm12878 (lymphoblastoid cell line) from ENCODE project (Birney et al. 2007) was downloaded from hgdownload.cse.ucsc.edu /goldenPath/hg19/encodeDCC/wgEncode CaltechRnaSeq/wgEncodeCaltechRnaSeqGm12878R2X75N aIl200FastqRd1Rep1.fastq.gz. The data file contained a total of 87929372 paired-end Illumina GA reads of read length 75-bp. Microarray intensities (Affymetrix Human Exon 1.0 ST chip) for the same sample were obtained from GEO (accession: GSM472901).

NCBI nucleotide data:

We searched ChimerDB 2.0 (Kim et al. 2010) to obtain the GenBank accession IDs of the publicly available sequences that are considered chimeric transcripts. Because these chimeric transcripts were computationally detected, we limited the dataset to the high confidence set of chimeric transcripts by choosing only those chimeric transcripts

that also represented fusion gene pairs in the literature based annotation from ChimerDB 2.0. In this way, we obtained 206 accessions IDs whose sequences were drawn from the NCBI's nucleotide database. Test datasets are also summarized in Table A.1-A.2 and Supplementary Methods.

Methods

All RNA-Seq reads and GenBank sequences were mapped to the reference human genome (hg18) using BLAT with the default parameters settings for the DNA sequence alignment in BLAT. We used RefSeq (Pruitt et al. 2007) transcripts (hg18) as our reference set and the corresponding genomic coordinates were downloaded using UCSC Table browser.

To demonstrate the applicability of R-SAP, a complete pipeline run was performed on the MAQC Reference Human RNA-Seq dataset. For the evaluation of pipeline's expression estimation and isoform detection performance, we employed the ENCODE Gm12878 cell line RNA-Seq dataset in addition to MAQC RNA-Seq dataset. The high confidence chimeric transcript dataset obtained from Chimer DB 2.0 and NCBI was used for testing R-SAP's chimer-detection module. To evaluate R-SAP's RNA-seq quantifications, the output was compared with the results of microarray gene expression analyses and TaqMan qRT-PCR measurements carried out on the same cells. R-SAP's expression estimation performance was benchmarked using the same RNA-Seq datasets against Cufflinks (Trapnell et al. 2010) and RSEM (Li and Dewey 2011) while isoform predictions were compared with those from Trans-ABySS (Robertson et al. 2010) and Cufflinks. Data analyses and comparison methods used for the different platforms and programs are summarized in Supplementary Methods.

We performed R-SAP test runs using the default parameter settings (described in Supplementary Methods) of the pipeline. These default values were previously derived

and optimized empirically during the development of R-SAP by running core modules individually on various RNA-Seq datasets (data not shown here).

Results and Discussion

Demonstration of the applicability of R-SAP using the MAQC dataset

Sequencing tags from the test MAQC Reference Human RNA-Seq dataset were initially mapped to the human reference genome. We mapped 855,159 (97.3% of the 878,275 cleaned reads, Table 2.1) and analyzed these alignments using R-SAP. More than half (491,117/855,159 or 57.43%) of the mapped reads were high-scoring (Table 2.1) and were further characterized with the RefSeq transcripts (Table 2.2).

Table 2.1. Results of initial mapping and alignment screening of MAQC Reference Human RNA-seq data using R-SAP.

Description	Reads
Total raw sequencing reads	881,555
Cleaned reads	878,275
Genome mapped reads	855,159
Classification	**Reads (% genome mapped reads)**
High-scoring	491,117 (57.43%)
Chimers	8,458 (0.99%)
Multi -hits	29,279 (3.42%)
Discarded	326,305 (38.16%)

Table 2.2. Number (%) of high-scoring reads (obtained from MAQC Reference Human dataset) partitioned by R-SAP into sub-categories. Also, shown is the number of RefSeq transcripts represented in each sub-category.

Sub-categories (characterization)	Reads (% high-scoring)	Represented RefSeq transcripts
Exon-only	267,279 (54.42%)	24,461
Exon-deletion	6,786 (1.38%)	4,850
AlternativeTSS	1,210 (0.25%)	1,078
Alternative Polyadenylation	2,759 (0.56%)	2,042
Internal-exon-extension	18,419 (3.75%)	7,648
Multiple-annotations	3,020 (0.61%)	1,973
Intron-only	104,824 (21.34%)	22,383
Neighboring-exons	17,935 (3.65%)	5,929
Gene-desert	66,694 (13.58%)	
Uncharacterized	2,191 (0.45%)	
Total high-scoring:	491,117	

As expected from the RNA-Seq data, the majority (299,473/491,117 or 61%) of the high-scoring reads mapped to the exons (Figure 2.4, Table 2.2). Slightly more than half (54.42%; 267,279/491,117) of high-scoring reads were exon-only reads that could be attributable to 24,461 RefSeq transcripts (Table 2.2). RPKM values (expression levels) for these RefSeq transcripts are presented in Table A.10. R-SAP identified a wide spectrum of expression values RPKM values) ranging from a minimum of 0.046 for the *TTN* (titin or connectin) gene to a maximum of 2,112 for the *MTRNR2L2* (humanin- like protein 2) gene. More than 1% (1.38%; 6,786/491,117) of the high-scoring reads were found to be associated with exon-deletion events among the 4,850 of the RefSeq transcripts (Table 2.2). Relatively few (840/6,786 or 12.37%) of the events characterized by R-SAP as exon deletions were attributable to exon-skipping events corresponding to 620 RefSeq transcripts. While skipping of a maximum of 20 exons was observed, the majority of the exon skipping events involved skipping of only one exon (Figure 2.5). It is important to note that the power and accuracy of R-SAP to detect splice variants

depends completely upon the length of the sequencing reads. For instance, exon-skipping events are detected when the read spans the flanking exons of the skipped exon. Short reads from such new splice junctions will not produce significant alignments on the genome and hence will go undetected. Previously published RNA-Seq studies detect exon skipping by mapping the short reads to synthetically created library of new splice junctions (Sultan et al. 2008).

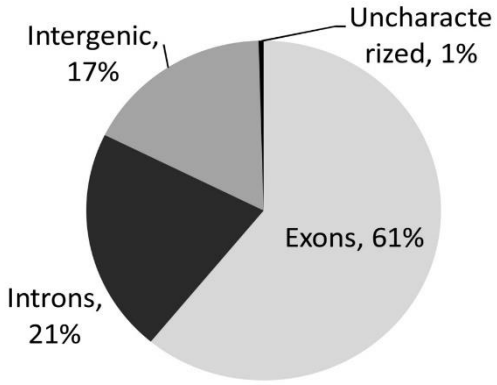

Figure 2.4. Distribution of the high-scoring reads from MAQC Reference Human dataset onto RefSeq transcripts. "Exons" includes those reads characterized as Exons-only, Exon-deletion, Alternative TSS, AlternativePolyadenylation, Internal-exon-extension and Multiple-annotations. "Intergenic" includes those reads characterized as gene-desert or neighboring-exon, "Introns" represent reads mapping completely within introns and "Uncharacterized" are those reads that cannot be characterized with any RefSeq transcript (distribution is presented in Table 2.2).

We observed that internal-exon-extension (3.75%, Table 2.2) accounted for more than the extension of known transcription boundaries (AlternativeTSS and AlternativePolyadenylation) combined (0.25% + 0.56%, Table 2.2). These transcriptional events can be further examined in the follow-up analysis.

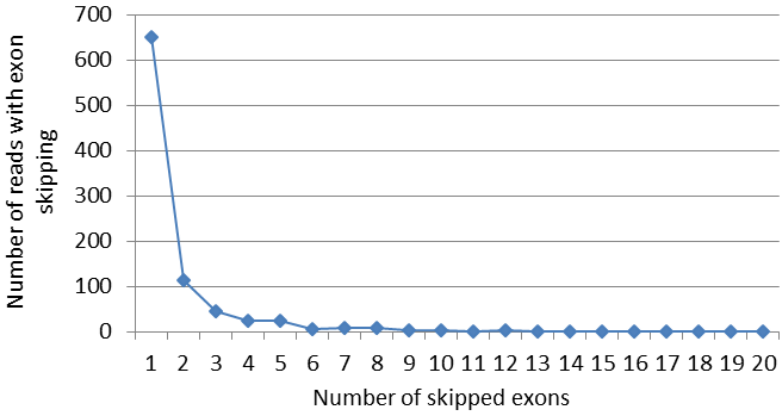

Figure 2.5. Frequency of exon skipping in high-scoring reads from MAQC Reference Human dataset. A total of 893 sequencing reads resulted from the skipping of 1191 exons corresponding to 645 Hg18 RefSeq known transcripts.

For example, internal-exon-extension in the last intron or extension of 3'end of the transcript is indicative of the potential alternative polyadenylation site. Presence of poly-A tail or poly-T prefix on the reads may confirm the presence of polyadenylation site (Nagalakshmi et al. 2008). Internal-exon-extension reads also included 361 reads that showed retention of 305 introns in 275 of the RefSeq transcripts (Table A.3).

The second most frequent category of high-scoring reads identified by R-SAP (21.34%, Table 2.2) was intron-only reads. While intron-only reads may occasionally result from the presence of premature mRNAs containing un-spliced introns in sequencing samples, intron-only reads that are in high abundance may be indicative of yet-to-be annotated exons. In an effort to separate these potentially new "intronic exons" from un-spliced introns, RPKM values for each intron is calculated using intron-only reads. Introns with RPKM values of the same order of magnitude as the RPKM value of the corresponding annotated transcript are reported by R-SAP as potentially new intronic-exons. Our pipeline reported 9,707 introns containing potentially new exons that correspond to 5,890 of the RefSeq transcripts (presented in Supplementary File S3).

About 3% (17,935/491,117) of the high-scoring reads were characterized as neighboring-exons (Table 2.2). Further examination revealed that the distribution of neighboring-exons was biased downstream of 3'end of the RefSeq transcripts relative to the 5' end (70% 3'end and 30% 5' end)

Gene-desert was the third most abundant category (13.58%, 66,694/491,117) of the high-scoring reads (Table 2.2). The remaining ~1% of the high-scoring reads were delegated to either the multiple-annotations (0.61%, Table A.4) or uncharacterized (0.45%) category (Table 2.2). Uncharacterized were those that could not be associated with any known reference transcript by the pipeline. Examples for each type of characterization from the MAQC Reference Human dataset are displayed in Figure 2.6 (A-M).

A. **Exon-only**

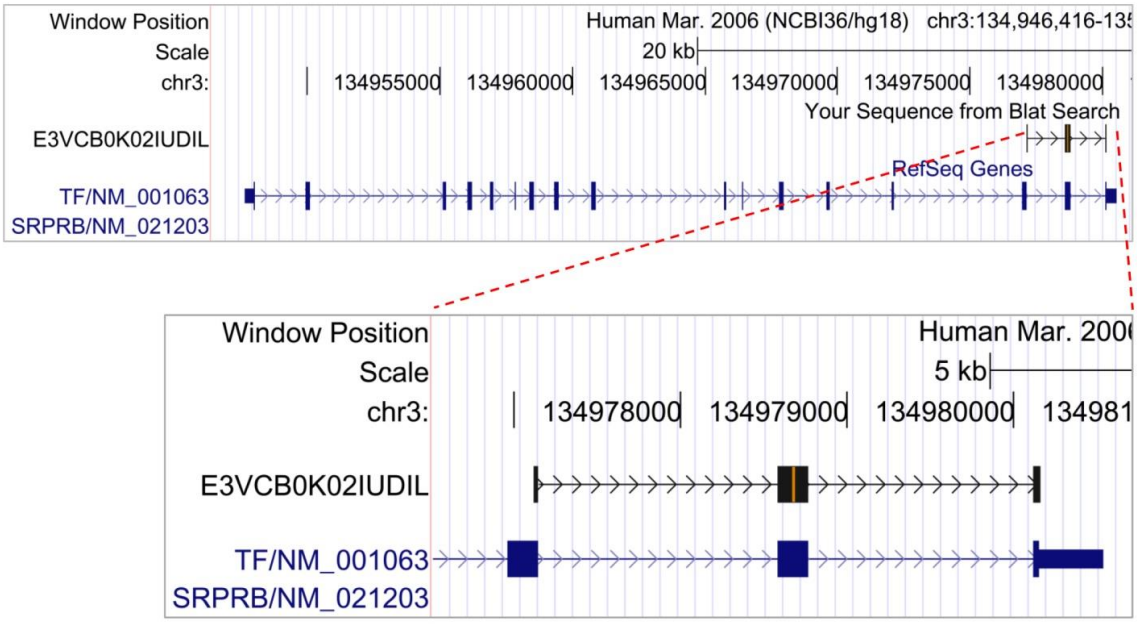

B. **Exon-deletion**

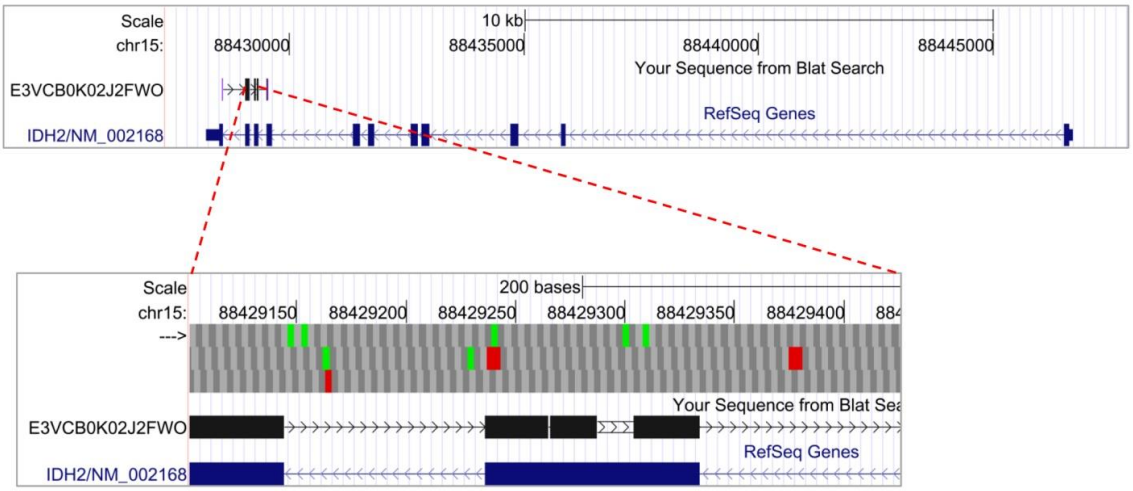

C. **Exon-deletion**

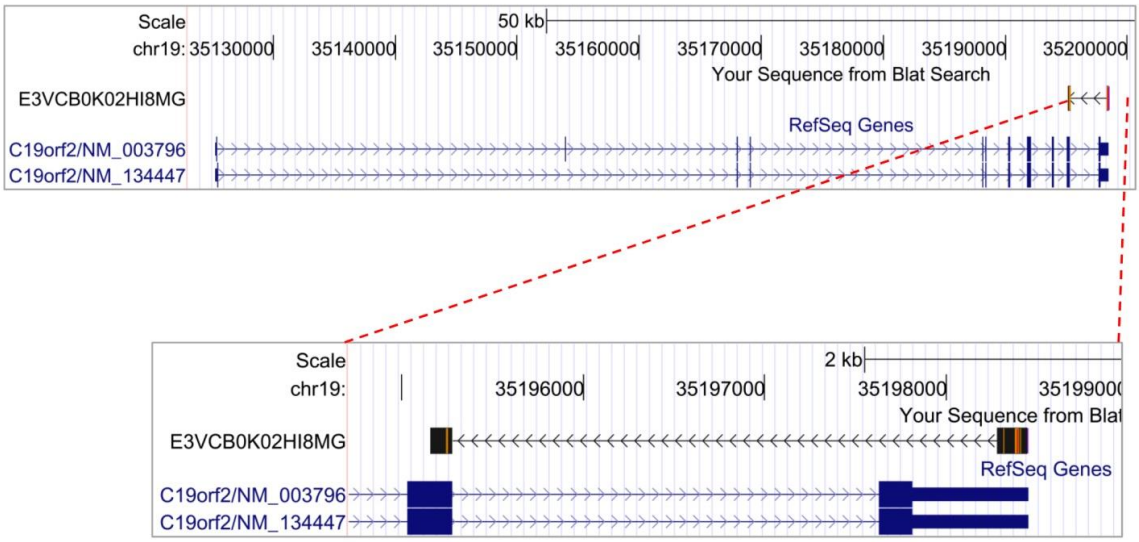

D. **Exon-skipping**

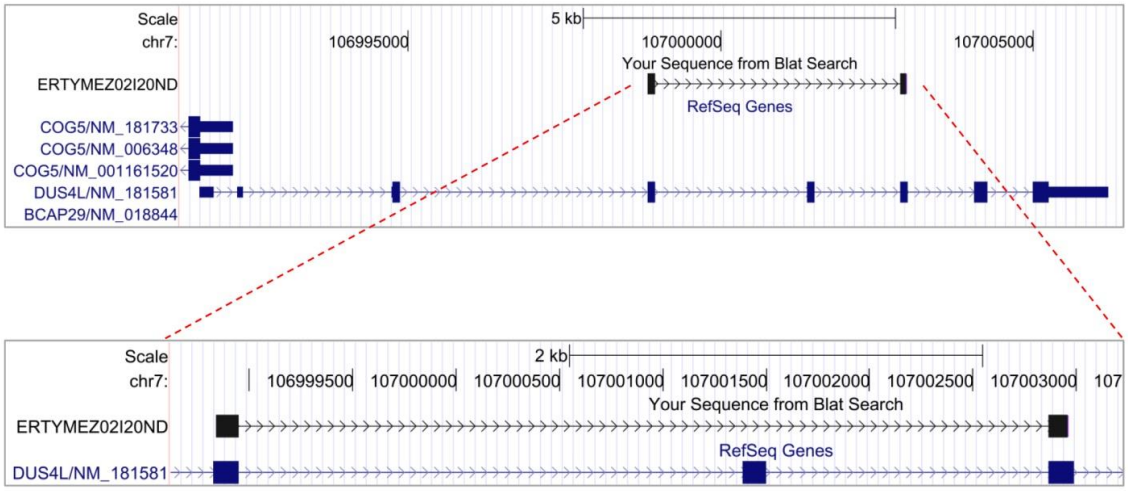

E.

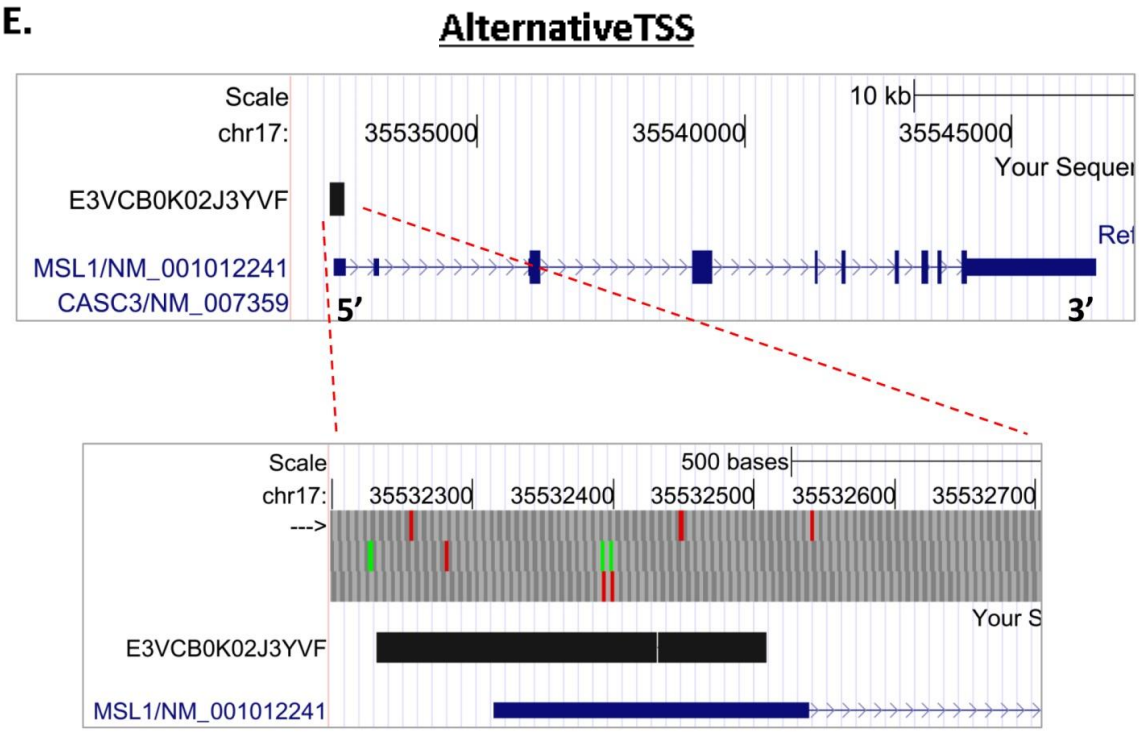
AlternativeTSS
Scale
chr17:
35535000
35540000
35545000
10 kb
Your Sequer
E3VCB0K02J3YVF
MSL1/NM_001012241
CASC3/NM_007359
5'
3'
Scale
chr17:
500 bases
35532300
35532400
35532500
35532600
35532700
--->
Your S
E3VCB0K02J3YVF
MSL1/NM_001012241

F.

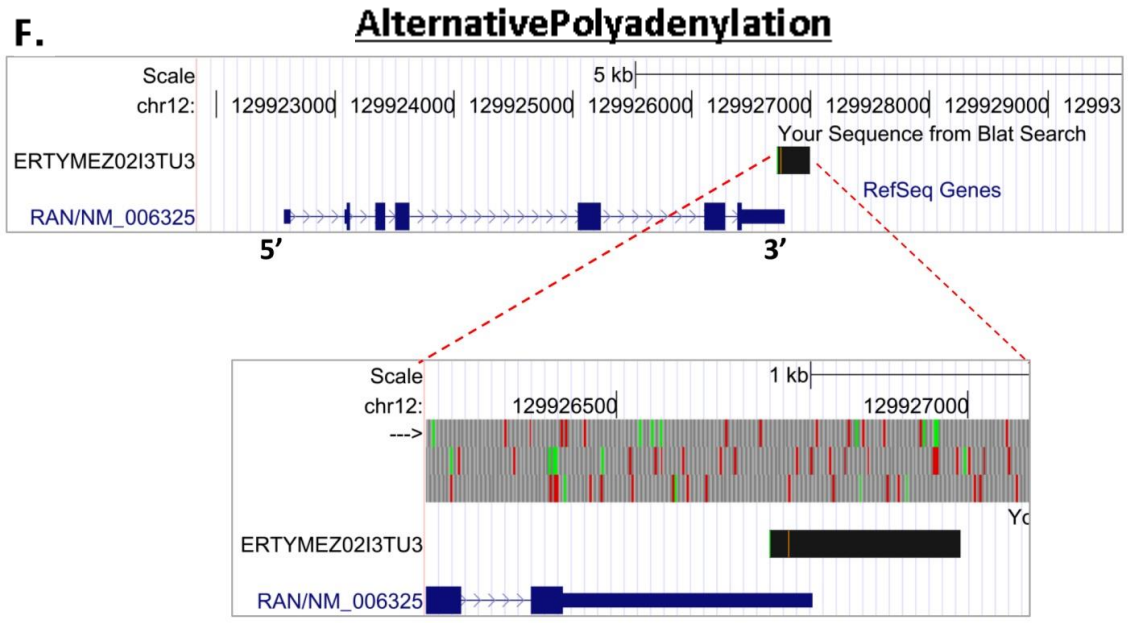
AlternativePolyadenylation
Scale
chr12:
5 kb
129923000
129924000
129925000
129926000
129927000
129928000
129929000
12993
Your Sequence from Blat Search
ERTYMEZ02I3TU3
RefSeq Genes
RAN/NM_006325
5'
3'
Scale
chr12:
1 kb
129926500
129927000
--->
Yc
ERTYMEZ02I3TU3
RAN/NM_006325

G. **Internal-exon-extension**

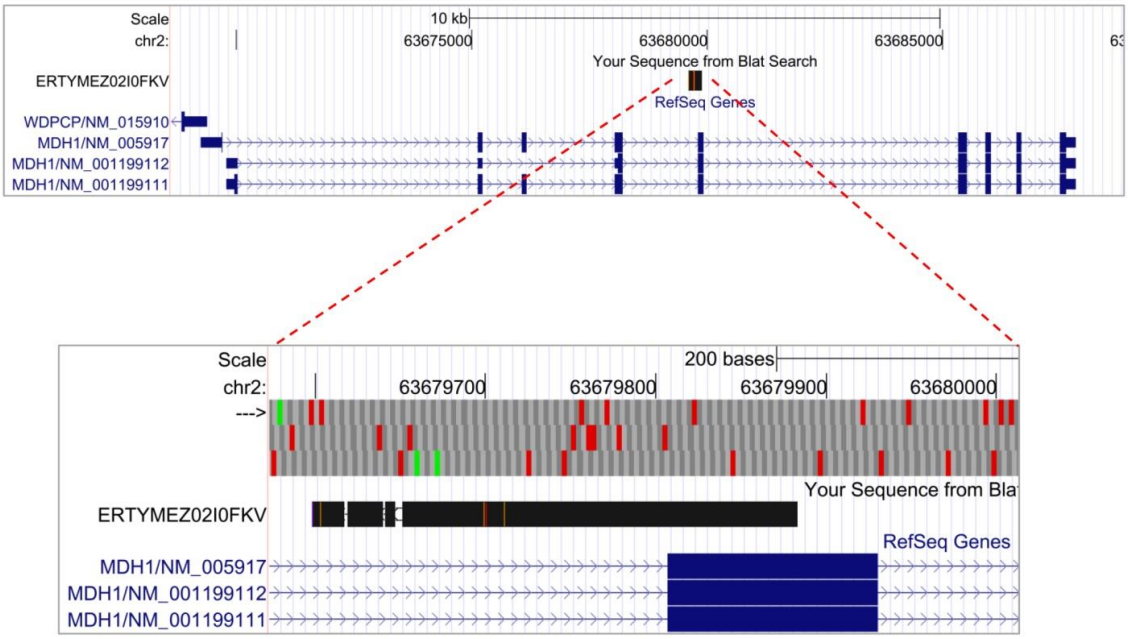

H. **Intron-retention**

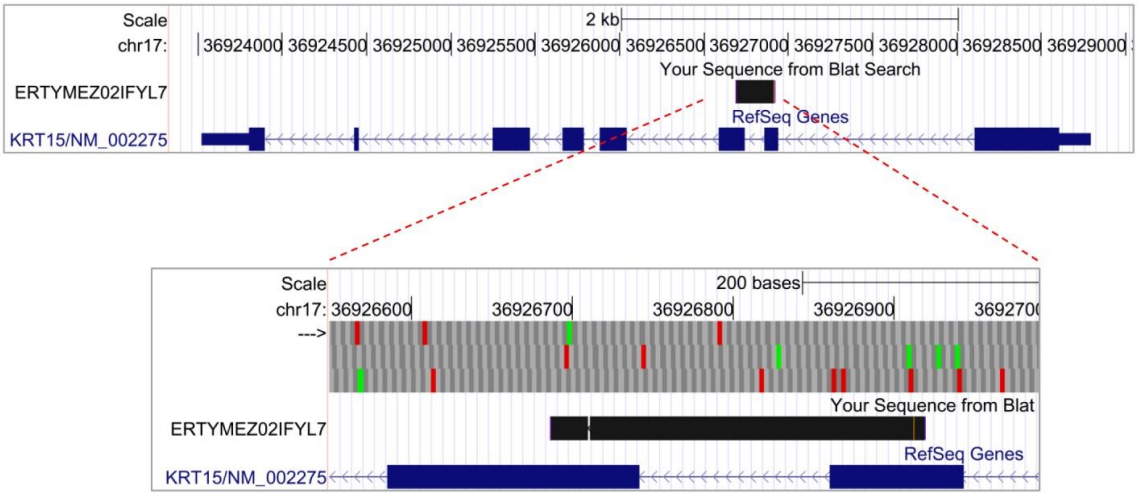

I. **Intron-only**

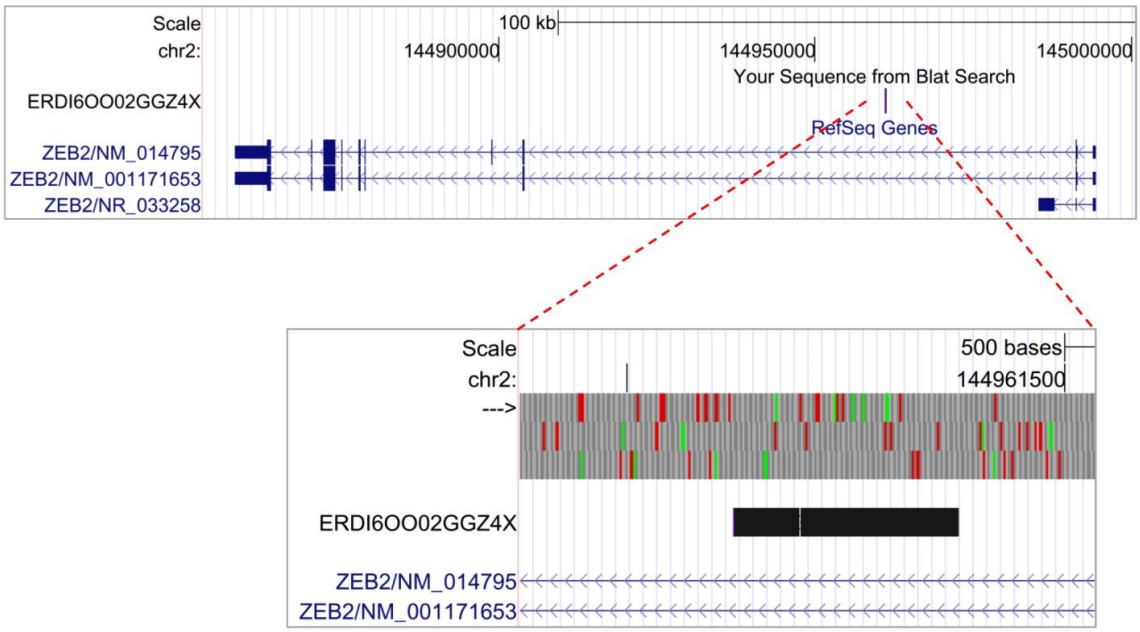

J. **Potential new intronic-exon**

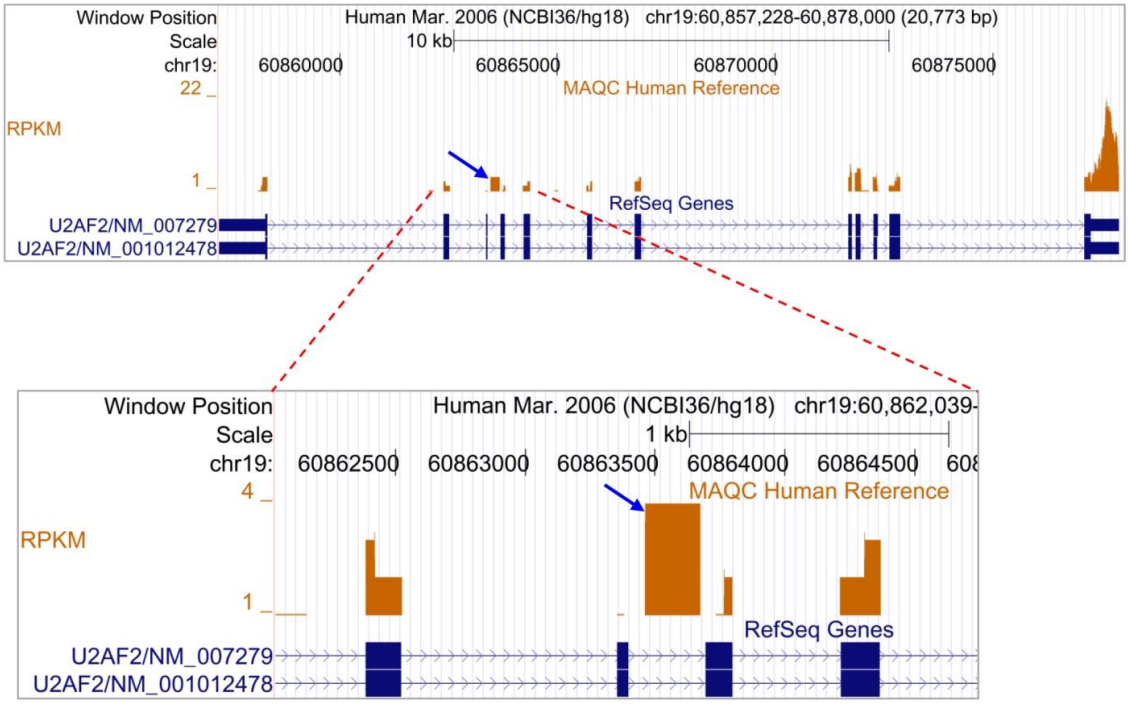

K. **Neighboring-exon**

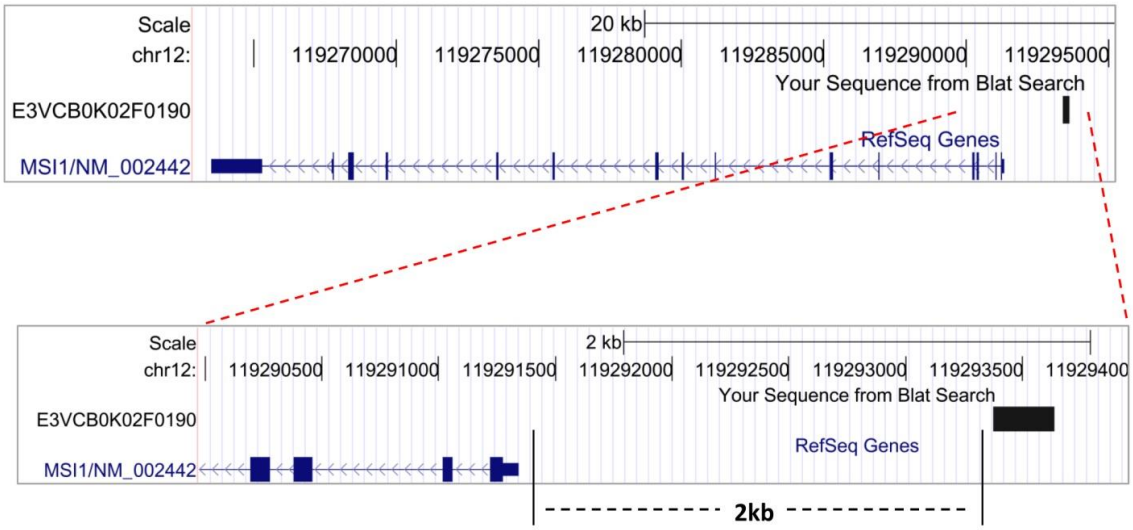

L. **Gene-desert**

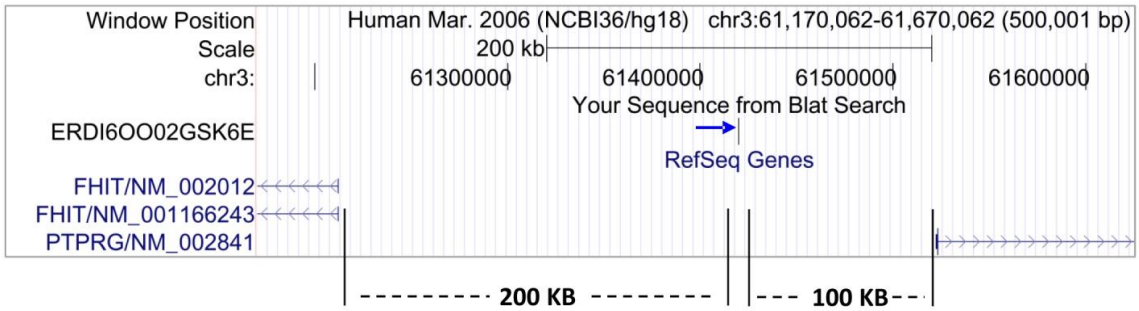

M. **Uncharacterized**

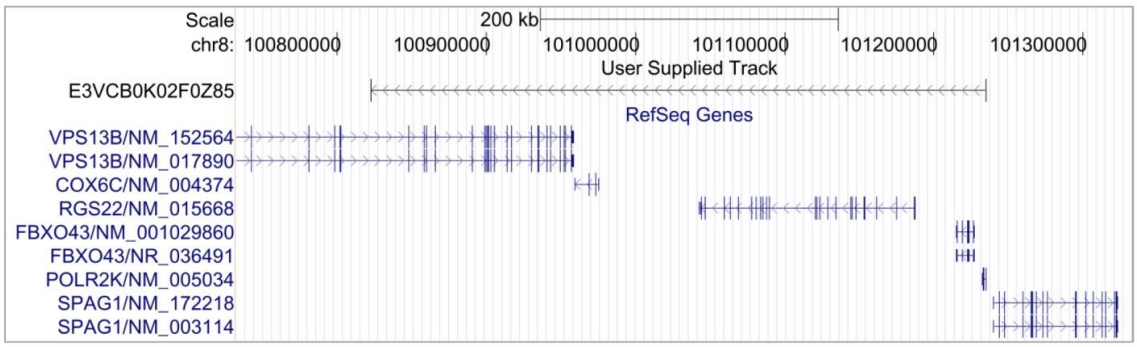

Figure 2.6. Examples of various sub-categories characterized by R-SAP from the test MAQC Reference Human dataset as they are displayed in the UCSC genome browser (hg18) snap-shots. Reference genome alignment of the sequence is shown under the track "Your Sequence from Blat search" (in black). RefSeq gene tracks are displayed under "RefSeq genes" track (in blue). (**A)** Exon-only. (**B-C)** Exon-deletion events in RefSeq transcripts resulting from the skipping of exonic bases and detected from the discontinuous blocked alignment of sequencing read. (**D)** Exon-skipping event. (**E)** Gene boundary expansion event at 5'UTR (alternativeTSS) **(F)** Gene boundary expansion event at 3'UTR (alternativePolyadenylation) , respectively. **(G)** Internal-exon-extension. **(H)** Intron-retention. **(I)** Intron-only. **(J)** Intron-only read sequences were further used for the detection of potential new "intronic-exon" events that had comparable (same order of magnitude) expression value (estimated with as RPKM) with the expression value (RPKM) value of the transcript itself. 3rd intron of gene *U2AF2* is shown in the figure with a potential new exon (pointed by blue arrow). RPKM values are displayed under the track "MAQC Human Reference" (in orange). **(K-L)** Sequencing reads that do not fall within any of the RefSeq transcript boundaries but map within the pre-specified gene radius ('d', 5kb default) are characterized as neighboring-exon **(K)** while reads that map outside gene-radius are characterized as gene-desert reads **(L). (M)** Shows an "uncharacterized" read (under "Use Supplied Track") where alignment blocks of the read are separated by more than the cutoff value (100kb default). Such reads could not be associated or characterized with any RefSeq transcript and very likely be resulting from cDNA library or sequencing artifact, or alignment artifact.

As MAQC Reference Human sample was obtained from a pool of cancer cell lines (Supplementary Materials of (Shi et al. 2006)) and since cancer cells have been previously reported to harbor chimeric transcripts (Mitelman et al. 2005), we expected to observe such transcripts in our test dataset. R-SAP characterized 8,458 reads (~ 1% of the 855,159l mapped reads) as the chimeric transcripts (Table 2.1). This relative low abundance of chimeric transcripts is consistent with the fact that prevalence of such RNA-species is reported to be typically low (37,38). These designated chimers were further characterized by R-SAP as inter-chromosomal (51.1%) or intra-chromosomal (48.9%) based on the target genomic regions of the alignment pairs in the chimeric transcripts (Table 2.3). Nearly 40% of the detected chimeras were intra-genic (type -1

and type-2), i.e., chimeras likely generated by deletions resulting from loop formation or other restructurings of the precursor transcript (Table 2.3). Only 13.18% of the detected chimeras were designated inter-genic chimeras, i.e., chimeras resulting from the potential fusion of heterologous gene transcripts (Table 2.3). The remainder of the aligned reads was comprised of "discarded" reads (38.16%, Table 2.1) and multi-hits reads (3.42%, Table 2.1).

Table 2.3. Number (%) of chimeric transcripts detected by R-SAP from MAQC Reference Human dataset and represented RefSeq transcripts

Chimer type	**Reads (% total chimers)**	
Inter-chromosomal	4,327 (51.16%)	
Intra-chromosomal	4,131 (48.84%)	
Chimer type	Reads (% total chimers)	RefSeq transcripts
Intragenic (type-1)	2,896 (34.24%)	1,677
Intragenic (type-2)	524 (6.20%)	114
Gene-desert	3,923 (46.38%)	253
Inter-genic	1,115 (13.18%)	480
Total chimers	8,458	

In summary, the MAQC Reference Human RNA-Seq data mapped to 30,074 of the RefSeq transcripts (27,068 protein coding and 3,006 non-protein coding). R-SAP classified these detected reference transcripts as either normally or aberrantly spliced (Figure 2.7).

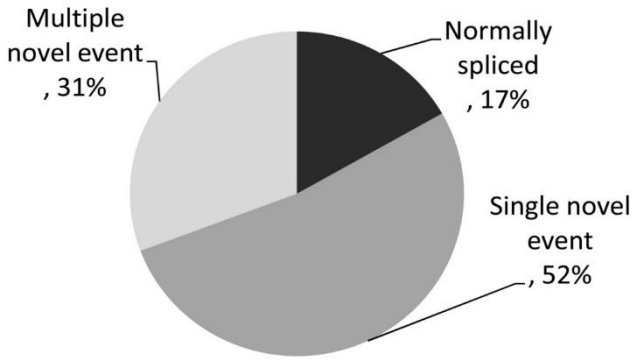

Figure 2.7. Distribution of RefSeq transcripts detected by R-SAP using MAQC Reference Human dataset. "Normally spliced" RefSeq transcripts (5,039 transcripts) showed no novel transcriptional events. "Single novel event" transcript (15,796 RefSeq transcripts) and "Multiple novel event" transcripts (9,239 RefSeq transcripts) were detected to have only one type and more than one type of novel transcriptional event, respectively.

R-SAP's performance compares favorably with currently popular pipelines

Comparison with Trans-AbySS:

To evaluate the performance of R-SAP against existing pipelines, we compared R-SAP's characterization results for the MAQC Reference Human dataset with the output from another commonly used pipeline, Trans-ABySS. Trans-ABySS is a highly respected RNA-Seq data analysis pipeline used to detect novel transcriptional events using the reference genome alignments of contigs obtained after performing a *de novo* assembly on short RNA-Seq reads. Since we already had 454 reads that were long enough to be treated as assembled contigs, we skipped the assembly step and directly ran the intermediate step of the Trans-ABySS that compares reference genome BLAT alignment of contigs (long reads) with the known transcript models. We used the reference genome alignment of 491,117 high-scoring reads (already classified by R-SAP, Table 2.1) from the MAQC test dataset and RefSeq transcripts (hg18) as reference transcript models. Out of 491,117 high-scoring reads, Trans-ABySS associated 127,913

(26%) reads with known exons while R-SAP associated more than twice as many (299,473 or 61%, Figure 2.2 Table 2.2) high-scoring reads with known exons. Of 127,193 exon-associated reads, Trans-ABySS classified 4847 (0.98% of the 491,117 high-scoring) reads as novel transcriptional events (exon-skipping, alternative splice sites, intron-retention, UTR expansion and new exons) (Table A.5) and the remaining 123,066 (25.05% of the 491,117 high-scoring) reads as those mapping completely within the known exons. Overall, Trans-ABySS reported a lower number of novel transcriptional events compared with R-SAP's characterizations (4,847 v/s 32,194; exon-deletion, AlternativeTSS, AlternativePolyadenylation, internal-exon-extension, multiple-annotations; Table 2.2). The lower number of novel transcriptional events detected by Trans-ABySS may be due to the filtering of all the reads/contigs that have single block alignments with the reference genome before novel transcriptional events are detected. Table 2.4 displays the overlap between the characterization categories that were comparable between R-SAP and Trans-ABySS outputs. R-SAP predictions included 91% to 100% of the Trans-ABySS predictions (Table 2.4).

Table 2.4. Comparison between R-SAP and Trans-ABySS characterization sub-categories for the high-scoring reads from MAQC Reference Human dataset (R-SAP characterizations include reads from "multiple-annotations" category) (Table 2 and Supplementary Table S4).

R-SAP characterization	Trans-AbySS characterization	Number of associated reads		Characterization overlap		
		R-SAP	Trans-ABySS	#Reads	%Trans-ABySS	%R-SAP
Exon-skipping	Exon-skipping	1419	768	757	98.56%	53.1%
Alternative TSS + PolyAdenylation	Alternative UTR (5′ and 3′)	5314	357	327	91.59%	5.9%
Intron-retention	Intron-retention	374	2	2	100%	0.53%
Exon-deletion	New-intron	9675	259	259	100%	2.7%

Comparison with Cufflinks/Cuffcompare:

Cufflinks is a widely used a*b initio* assembler that reconstructs full transcript structures using genomic alignments of RNA-Seq fragments. Cufflinks also includes a module, called Cuffcompare that compares the assembled transcripts to reference or annotated transcripts in order to build transcript structural equivalence classes and also to detect novel isoforms (Trapnell et al. 2010). In order to compare Cuffcompare classifications with R-SAP's characterizations, we used our ENCODE lymphoblastoid cell line RNA-Seq test data from which 38,524,540 reads were aligned to the human reference genome (hg18) using TopHat (Trapnell et al. 2009) (see Supplementary Methods). Transcript assembly on the genomic alignments was performed using Cufflinks (see Supplementary Methods) that resulted in 76,101 transcripts of length varying from 73 to 38,345 bp. Assembled transcripts were reported in a GTF file that contains genomic coordinates of assembled transcripts and their exons. The GTF file was then used as the input for R-SAP and Cuffcompare. Since TopHat reports only high-quality alignments, we considered Cufflinks assembled transcripts as high-scoring

alignments for R-SAP's characterization module. RefSeq transcripts (hg18) were used as a reference annotation set for R-SAP and Cuffcompare (Table A.6 and A.7).

Based on the classification definitions provided in Cuffcompare's manual (see also (Trapnell et al. 2010)), we selected those classifications that were comparable with R-SAP's characterizations (comparisons are displayed in Table 2.5). Cuffcompare reported 24,752 (32% of 76,101 assembled transcripts) as novel-isoforms while R-SAP detected 40,025 (52.6% of 76,101) novel transcripts. 86% of Cuffcompare's novel-isoforms were also reported by R-SAP as either exon-skipping (~97%), exon-deletion (~87%), internal-exon-extension (~58%), intron-retention (~33%), alternativeTSS (~62%) or alternativePolyA (~57%) (Table 2.5). While Cuffcompare reported exon-associated novel transcriptional events as a generic category "novel-isoform", R-SAP provided a more comprehensive characterization of novel-transcriptional events. Other R-SAP characterization classes such as exon-only, intron-only, neighboring-exon and gene-desert showed even higher overlap of 62%, 99.9% and 100% respectively with Cuffcompare' comparable classifications (Table A.8).

Table 2.5. Comparison between R-SAP characterizations and Cuffcompare's novel-isoforms classification from transcripts assembled by Cufflinks using ENCODE Gm12878 cell line RNA-Seq dataset (R-SAP characterizations include reads from "multiple-annotations" category) (Supplementary Table S6).

R-SAP characterization	Cuffcompare classifications	Number of associated assembled transcripts		Overlap		
		R-SAP	Cuffcompare	#Reads	%Cuffcompare	%R-SAP
Exon-skipping	Novel-isoform	7184	24752	6961	28.12%	96.9%
Exon-deletion		3233		2809	11.3%	86.9%
Internal-exon-extension		24652		14428	58.3%	58.2%
Intron-retention		5735		1870	7.5%	32.6%
AlternativeTSS		6952		4292	17.5%	61.7%
AlternativePolyA		9358		5380	21.73%	57.5%
Total novel transcriptional events		40025		21365	86.3%	53.3%

Evaluation of RNA expression level quantification

MAQC Human Reference sample:

Comparison between R-SAP's RPKM values from MAQC Human Reference sample and gene expression values determined from Affymetrix U133 Plus2.0 resulted in a significant correlation (Spearman correlation = 0.67, $p < 0.0001$) (Figure 2.8A) that is in agreement with the similar correlations previously reported in (Fu et al. 2009; Griffith et al. 2010). We further evaluated our expression estimates by comparing with TaqMan qRT-PCR measurements that is generally considered a more accurate abundance estimation than microarrays. After initial filtering, we retained 962 expressed RefSeq transcripts from TaqMan qRT-PCR data, of which 727 were also present (RPKM > 0) in the RPKM estimates from R-RAP. With TaqMan qRT-PCR estimates, we observed a better correlation of (Spearman correlation = 0.88, $p<0.001$, Figure 2.8B) of our RPKM values than those with microarray estimated values.

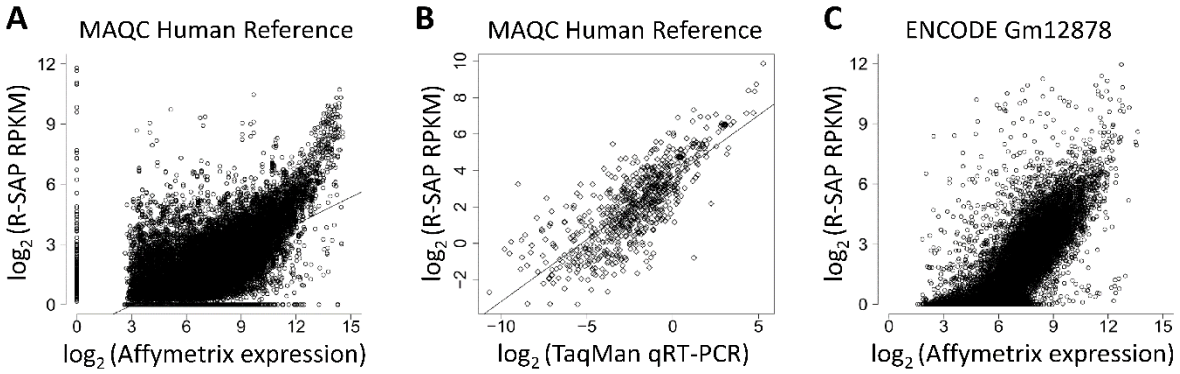

Figure 2.8. Comparison of R-SAP estimated RPKM vs. Affymetrix microarray and TaqMan qRT-PCR expression values. A. Correlation of 0.67 (Affymetrix microarray) and **B.** 0.88 (TaqMan qRT-PCR) (B.) were obtained using the MAQC Human reference sample **C.** A higher correlation of 0.78 (Affymetrix microarray) was obtained using the Gm12878 reference cell line from the ENCODE project.

ENCODE lymphoblastoid cell line sample:

To explore the possibility that expression estimates may be further improved by using higher throughput RNA-Seq data than are available in the MAQC Human Reference dataset, we used R-SAP to quantify expression levels using RNA-Seq data of a lymphoblastoid cell line, Gm12878, obtained from ENCODE (Birney et al. 2007) and compared the results with microarray data (Affymetrix Human Exon 1.0 ST arrays) generated from the same cell line. We mapped ~54 million sequencing tags to the reference human genome (alignment details are presented in Table A.9) resulting in a highly significant correlation (Spearman correlation = 0.77, $p < 0.0001$) between the RPKM values and the microarray generated expression values (Figure 2.8C).

In order to benchmark R-SAP's RNA expression accuracy, we further compared R-SAP's RPKM values with those estimated from Cufflinks and RSEM using ENCODE RNA-Seq dataset. Reference genome alignments for Cufflinks were generated using TopHat (mapped ~38 million reads) while reference transcript (RefSeq hg18) sequence alignments were generated by RSEM using BowTie (Langmead et al. 2009) (mapped ~26 million reads). Cufflinks was run in isoform abundance estimation mode in order to generate FPKM values for RefSeq transcripts. Parameter setting for TopHat, Cufflinks and RSEM runs are describe in Supplementary Methods. RSEM generated TPM (transcripts per million) values as abundance measures that were further converted to comparable RPKM values using the conversion formula described in (Li et al. 2010a).

Since expression values are observed to be robust at 1.0 RPKM for ~40 M mapped RNA-Seq reads (Mortazavi et al. 2008) and our ENCODE RNA-Seq dataset is comparable to that, we used only reference transcripts with RPKM ≥ 1 for comparing expression values between different methods. With Cufflinks RPKM estimates, we observed a high correlation of 0.84 ($p<0.0001$). Surprisingly, RSEM's expression values

showed relatively low correlation with RPKM values from R-SAP (Spearman correlation 0.65, $p < 0.0001$) and from Cufflinks (Spearman correlation 0.40, $p<0.0001$) (See Figure 2.9 for correlation plots).

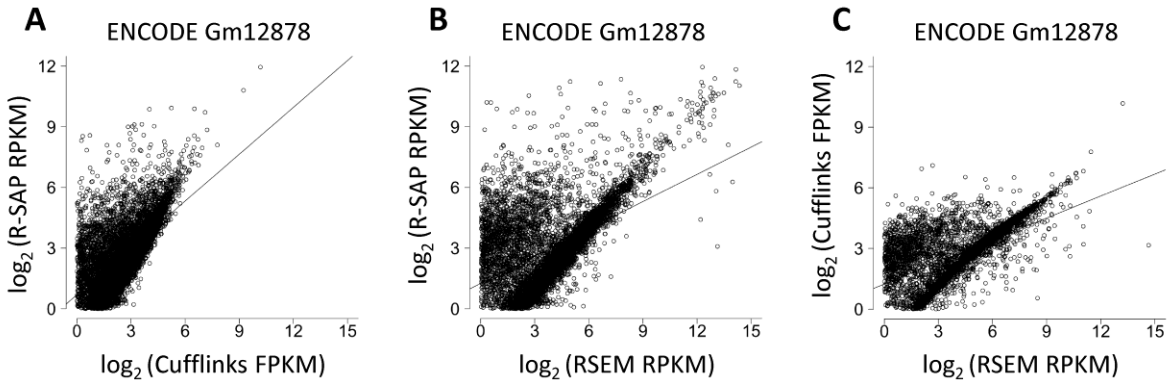

Figure 2.9. Correlation plots of RefSeq transcripts (hg18) quantification estimates from ENCODE Gm12878 RNA-Seq data using three different methods: R-SAP, Cufflinks and RSEM. Log2 transformation expression estimates shown here. A Spearman correlation of **A.** 0.84 ($p<0.0001$) and **B.** 0.65 ($p<0.0001$) was observed when R-SAP's expression estimates (Y-axis) were compared with those from Cufflinks **(A.)** and RSEM **(B.)** (X-axis). **C.** Shows a correlation of .040 ($p<0.0001$) expression estimates from Cufflinks and RSEM.

The low concordance of RSEM with the R-SAP and Cufflinks expression quantifications may be due to the fact that only uniquely mapped reads were allowed to be used for quantification. Also, RSEM inherently uses BowTie as an aligner and Bowtie is not a gapped or spliced aligner like BLAT, SSAHA2 and TopHat. Hence, reads with INDELs larger than few base pairs, or those resulting from novel splicing events such as exon-skipping or exon-extension may fail to map to the transcript sequence. Both of these factors may have lowered the total number of mapped reads that in-turn may affect the detection power and quantification accuracy of RSEM. In our ENCODE RNA-Seq dataset, TopHat mapped nearly 38 million reads where as RSEM mapped only ~26 million reads.

Evaluation of the chimer-detection module

In order to assess the accuracy of the chimer-detection module of R-SAP, we compared R-SAP's chimeric predictions with those 206 high-confidence chimeric transcripts generated by ChimerDB 2.0. We observed a ~79.6% (164/206) overlap with the ChimerDB 2.0 predictions (Table A.2). Manual inspection indicated that the 42 chimeric transcripts un-classified by R-SAP had multiple hits on the reference genome and were thus rejected as false positives by R-SAP during the filtering step in the chimer-detection module. Although R-SAP's filtering criteria was designed to minimize false positives, it should be noted that, RNA-Seq data may inherently contain some chimeric cDNA artifacts that are generated by template switching during reverse transcription, and/ or amplification and ligation reactions (Ozsolak and Milos 2011). Further experimental methods such as RT-PCR followed by re-sequencing should be used to validate the putative chimeric transcripts generated from RNA-Seq data (Guffanti et al. 2009; Maher et al. 2009b).

Evaluation of R-SAP's run time performance

We benchmarked R-SAP's runtime performance and effect of parallelization against Cufflinks. For the test run purposes, we selected reference genome alignments of 20 million reads from our ENCOE RNA-Seq test dataset that was aligned to the reference genome (hg18) previously using BLAT and TopHat. These 20 million reads were selected from high-scoring reads previously classified by R-SAP. In order to make the comparison between R-SAP and Cufflinks fair, we ran Cufflinks only in its quantification mode while R-SAP was allowed to run only characterization and transcript expression estimation modules. RefSeq transcripts (hg18) were used as reference annotation set. Running time for R-SAP and Cufflinks with varying number of parallel threads is shown

in Figure 2.10. Although we observed a near linear scalability in R-SAPs performance, Cufflinks performed better than R-SAP for any given number of threads.

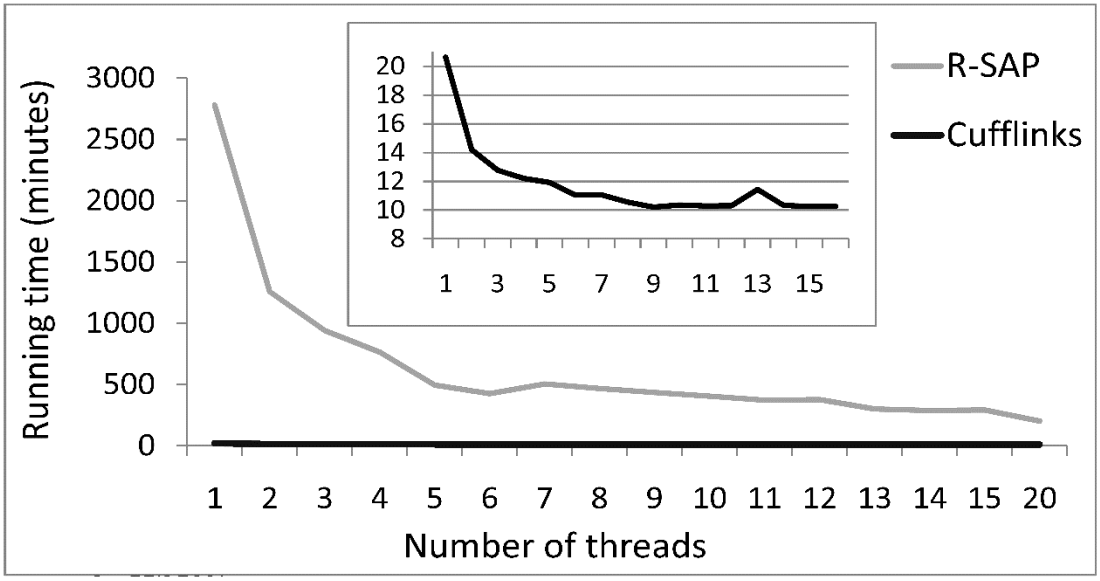

Figure 2.10. Benchmarking of R-SAP's running time as compared with Cufflinks. R-SAP (gray line) and Cufflinks (black line) running time (Y-axis) for the quantification of 20 million reads from ENCODE Gm12878 RNA-Seq dataset was compared. R-SAP shows near linear scalability as the number of parallel threads (X-axis) are increased. Inset shows the same plot magnified on of Cufflinks running time.

Cufflinks was implemented in C while R-SAP was implemented using Perl. It has been previously shown that Perl performs five to ten times slower than C (Prechelt 2000). Therefore, the relatively slower performance of R-SAP may be attributed to its implementation in Perl. Also, R-SAP was designed to generate multiple output files to provide detailed annotation information and data statistics. Writing multiple files involves extensive number of disk operations that may create high volumes of system-overheads for large datasets and may ultimately lower the running time of the program. We also compared the performance of R-SAP with Trans-ABySS by comparing the time required to perform the characterization of high-scoring reads on MAQC RNA-Seq data.

Since Trans-ABySS cannot be run on multiple threads for the characterization step, we noted processing time on single thread only. R-SAP was observed to be almost twice as fast as Trans-ABySS (R-SAP: 319.29 minutes, Trans-ABySS: 728.58 minutes). Overall we observed that R-SAP performs slower than Cufflinks but faster than Trans-ABySS. It is known that the absolute running time is not an accurate measure of an algorithm's performance. More accurate evaluation of the performance is only possible if other factors such as time and space (memory) complexity, number of instructions and frequency and duration of function calls are taken into consideration (Cormen et al. 2001) which is currently beyond the scope of this study.

Summary and Conclusion

R-SAP is a bioinformatics tool for the processing and analyses of the high-throughput RNA-Seq data that integrates reference genome alignments of sequencing reads with known transcripts models.

Using three publically available datasets (MAQC, ENCODE and ChimerDB 2.0) to evaluate different modules of the pipeline, we have shown that R-SAP can systematically detect novel transcriptional events including various classes of RNA isoforms and other transcript structures such as intra-genic and inter-genic chimeras. R-SAP's performance in categorizing transcripts represents a significant improvement over currently available pipelines as exemplified by Trans-ABySS and Cufflinks/Cuffcompare. Moreover, R-SAP's RNA expression level estimates are highly correlated with independent gene expression microarray analyses and experimentally derived qRT-PCR measurements. Currently, R-SAP simply excludes multi-hit reads from further analysis because they cannot be assigned to unique genomic loci. We expect a significant improvement in R-SAP's expression estimates once bias-correction and multi-hit read re-distribution methods are included in R-SAP's future releases.

R-SAP's ability to accurately detect alternative splicing and chimeric transcripts is optimal for sequencing reads longer than 40-50 bp. We do not consider this to be a significant shortcoming given that most current and envisioned sequencing methodologies do or soon will generate read lengths well above this threshold (Metzker 2010). R-SAP's characterizations of sequencing reads are also dependent on the choice of the reference set of the transcripts. In our test analyses, we conservatively used RefSeq transcripts as our reference set. We believe that characterization can further be improved by using a more informative, non-redundant and inclusive set of all established transcript models such as UCSC, Ensembl, RefSeq and AceView (Thierry-Mieg and Thierry-Mieg 2006; Robertson et al. 2010).

One of our major goals in constructing R-SAP was to develop a pipeline that can be fine-tuned according to the nature of the data. We sought to achieve this goal by incorporating various user adjustable cutoffs in the workflow that can be used to alter the stringency of each analysis. For example, in case of poor quality of the reference genome or lower quality sequencing reads, a high rate of mismatches and small gaps can be compensated for by lowering the coverage, identity and/or deletion cutoff values. Similarly, for poorly annotated exon boundaries where alignments may extend slightly beyond the edge of the exon, the exon-extension, the cutoff can be increased accordingly to accommodate for alignment errors at exon boundaries.

The characterization of transcriptomes using RNA-Seq is a multi-facited problem that includes cataloguing of coding and non-coding transcripts, uncovering and characterization of novel RNA isoforms and chimeric transcripts, detection of new splice-sites, discovery of new transcriptional structures, measurement of RNA expression levels and estimation of RNA isoforms specific expression levels (Wang et al. 2009; Ozsolak and Milos 2011). We hope that R-SAP will prove useful as a user-friendly bioinformatics

tool to compliment more specialized programs in the quantitative and qualitative analysis of RNA-Seq data.

Acknowledgements

We thank Dr. Nathan J. Bowen for his insightful suggestions during the early stages of the pipeline development and the Office of Information Technology at Georgia Institute of Technology for providing access to computing clusters at "Partnership for an Advanced Computing Environment" (pace.gatech.edu). This work was supported by grant from Ovarian Cancer Institute, Ovarian Cycle, The Waterfall Foundation, Deborah Nash Harris Endowment Fund and Robinson Family Foundation.

CHAPTER 3

DE NOVO ASSEMBLY AND CHARACTERIZATION OF BREAST CANCER TRANSCRIPTOMES IDENTIFIES LARGE NUMBERS OF NOVEL FUSION-GENE TRANSCRIPTS OF POTENTIAL FUNCTIONAL SIGNIFICANCE

Abstract

Gene-fusion or chimeric transcripts have been implicated in the onset and progression of a variety of cancers. Massively parallel RNA sequencing (RNA-Seq) of the cellular transcriptome is a promising approach for the identification of chimeric transcripts of potential functional significance. We report here the development and use of an integrated computational pipeline for the *de novo* assembly and characterization of chimeric transcripts in 55 primary breast cancer and normal tissue samples. *De novo* assembly allowed for the accurate detection of 1959 chimeric transcripts to nucleotide level resolution and facilitated detailed molecular characterization and quantitative analysis. A number of the chimeric transcripts are of potential functional significance including 79 novel fusion-protein transcripts and 80 chimeric transcripts with alterations in their un-translated leader regions (UTRs). Over 300 chimeric transcripts in the cancer samples mapped to genomic regions devoid of any known genes. Several 'pro-neoplastic' fusions comprised of genes previously implicated in cancer are expressed at low levels in normal tissues but at high levels in cancer tissues. Collectively, our results underscore the utility of deep sequencing technologies and improved bioinformatics workflows to uncover novel and potentially significant chimeric transcripts in cancer and normal somatic tissues.

Introduction

Gene-fusions are a prevalent class of genetic variants that have been implicated in the onset and progression of a variety of cancers (Mitelman 2000; Mitelman et al. 2007). These variants may be generated on the DNA level by genomic rearrangements [*e.g*., large deletions or insertions, inversions and/or chromosomal translocations (Maher et al. 2009b)]. On the RNA level gene-fusion variants may be generated by co-transcription or transcriptional read-through of neighboring genes (Akiva et al. 2006; Parra et al. 2006), or by *trans*-splicing of multiple simultaneously processed pre-mature RNAs from different genes (Garcia-Blanco 2003). Recurrent gene-fusions in cancers have often been employed as cancer biomarkers (Mitelman 2000; Laxman et al. 2008) and, in some cases, as potential candidates for targeted gene therapy (Baselga et al. 1996; Druker et al. 2001).

In recent years, massively parallel RNA sequencing (RNA-Seq) of the cellular transcriptome has emerged as a promising approach for the identification of previously uncharacterized fusion-gene or "chimeric" transcripts of potential functional significance (Maher et al. 2009a; Ozsolak and Milos 2011; Wang et al. 2013). In cancer biology, for example, a recent RNA-Seq analysis of 24 primary breast cancer samples uncovered 15 subtype specific fusion-genes that may serve as useful biomarkers of drug sensitivities (Asmann et al. 2012). In another study, analysis of 89 breast cancer and control samples identified several fusion transcripts involving MAST (microtubule associated serine-threonine) kinase and Notch-family genes that may be drivers of breast cancer onset and/or progression (Robinson et al. 2011).

Currently available computational methods for fusion-gene transcript discovery such as Tophat-Fusion (Kim and Salzberg 2011), SnowShoeFTD (Asmann et al. 2011) and FusionSeq (Sboner et al. 2010), typically rely upon reference genome mapping of short (50 -75 bp) paired-end reads generated by the sequencing of both ends (5'- and 3'-) of an RNA or cDNA fragment. While these methods are relatively rapid, the results can

be ambiguous due to the inherent imprecision associated with genome mapping of short reads (Li et al. 2010a; Li et al. 2010b). In this study, we take an alternative method of whole transcriptome *de novo* assembly to screen for fusion transcripts in The Cancer Genome Atlas (TCGA) RNA-Seq data of 45 primary breast cancer and 10 normal breast tissue samples. We developed an integrated computational workflow to generate significantly longer (>800 bp) contiguous sequences or "contigs". These longer contigs not only provide greater accuracy in reference genome mapping but also allow for more reliable identification of splice-variants because longer contigs typically extend across multiple exons (Martin and Wang 2011). We report here the detection of 1959 chimeric transcripts including 1535 that are specific to the breast cancer samples, 155 that are present only in the normal samples and 269 that are present in both the cancer and normal samples. We found that a number of these fusions are of potential functional significance including novel fusion-proteins and chimeric transcripts with alterations in their un-translated leader regions (UTRs). Over 300 breast cancer chimeras mapped to genomic regions devoid of any known genes. Finally, we identified several 'pro-neoplastic' chimers (Li et al. 2008) of potential significance that are suppressed in normal tissue but activated in cancer tissues. Collectively our findings indicate that an unexpectedly large number of chimeric transcripts are present in both cancerous and normal breast tissues and that many of these variants may play a significant role in breast cancer onset and development.

Methods

For the accurate detection, characterization and quantitative analysis of chimeric transcripts using RNA-Seq data, we designed a computational workflow (Figure 3.1) that integrates several existing bioinformatics tools including our previously published pipeline R-SAP (Mittal and McDonald 2012). The overall workflow is as follows:

1. Data pre-processing:

RNA-Seq data (see Supplemental Methods) may contain low-quality bases due to sequencing errors and fragments of sequencing adapters derived from failed or short cDNA inserts during the library preparation. Such low quality bases can reduce the efficiency of the assembler and lead to miss-assembly (Lindgreen 2012). We, therefore, trimmed low quality bases (quality score < 20) and sequencing adapters from the 3'-end of the reads using 'Trim Galore' (http://www.bioinformatics.babraham.ac.uk/projects/trim galore/). Subsequently the quality of the data were assessed using FastQC (http://www.bioinformatics.babraham.ac.uk/projects/fastqc/)

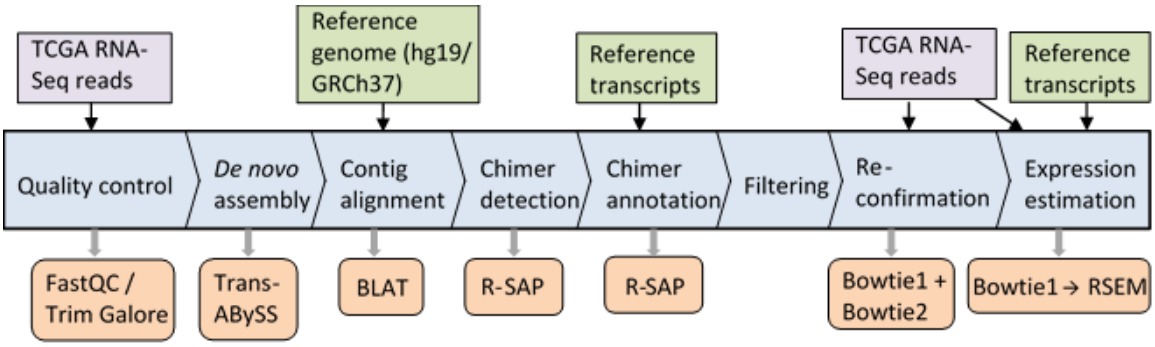

Figure 3.1. Computational workflow for chimeric transcript discovery. The central blue block shows the workflow, orange boxes represent the tools and programs integrated with the workflow, purple boxes represent RNA-Seq reads and green boxes represent datasets from the UCSC genome database. RNA-Seq reads (in fastq format) were trimmed and only paired-end reads were used for the assembly process. Assembled contigs (in fasta format) were then aligned to the reference genome and the resulting alignment files (in pslx format) were analyzed by R-SAP to detect potential chimeric transcripts. Chimeric transcripts were further characterized by comparing alignment coordinates with known reference transcripts (BED format) using R-SAP. Part of the filtering was done by R-SAP internally while additional filtering was done using in-house perl scripts. A re-conformation step includes alignment of RNA-Seq reads to chimeric transcript sequences and also to the reference genome using Bowtie1 and Bowtie2, respectively. Alignment files (in bam format) resulting from RNA-Seq reads to chimer transcript sequences were used to estimate the raw read-counts by expectation-maximization using RSEM.

2. Transcriptome assembly:

Since, a major objective of this study was to detect chimeric transcripts where two non-contiguous genomic loci are involved, a reference genome guided assembly approach could not be used. Hence, we performed *de novo* assembly (assembly without the reference genome) using ABySS that is a memory efficient de Bruijn graph construction based short-read assembler (Simpson et al. 2009). The *de novo* assembly process merges short DNA or RNA sequences that share terminal overlapping bases into a longer contiguous sequence (contig). The length of the terminal overlap or "k-mer length" is a critical parameter for assembly programs. Unlike genomic libraries, where a uniform representation of each base pair can be assumed, non-normalized transcriptome libraries contain a broad range of expressed transcripts and splicing isoforms. Therefore, complete coverage of the transcriptome cannot be achieved at a single k-mer value assembly (Robertson et al. 2010). To maximize coverage, we adopted previous recommendations (Robertson et al. 2010) and varied the k-mer length from half of the read length up to the full read length in the increments of two base pairs at a time. For example, for a library with 50bp long reads, we performed assembly for k-mer length of 25, 27, .. 49. Multiple k-mer assemblies were then merged into a single meta-assembly by using the Trans-ABySS pipeline (Robertson et al. 2010) that combines overlapping contigs by extension and removes duplicate contigs from the assembly.

3. Chimeric transcript detection and filtering:

Assembled transcripts were aligned to the human reference genome (hg19, GRCh37) using BLAT (Blast like alignment tool), (Kent 2002). Additional details are provided in Supplemental Methods. For potential chimeric transcript detection, we employed our previously developed pipeline R-SAP (Mittal and McDonald 2012) that efficiently detects gene-fusion events and filters potential false positives and alignment errors. Chimeric transcripts, representing a fusion-gene event, are very likely to produce

discrete alignments to distant or proximate genomic loci. These discrete alignments are also called as fragmented- or split-alignments. R-SAP performs the characterization of detected chimeric transcripts by associating the fragmented alignments with reference transcripts and categorizes various chimeric transcript structures according to the genic or inter-genic regions to which they map (Figure 3.2). We created a comprehensive set of 224,555 reference transcripts by merging Ensembl (Hubbard et al. 2002) and lincRNA (large intergenic non-coding RNAs, (Cabili et al. 2011)) annotations for hg19 available from the UCSC genome (Karolchik et al. 2014). These merged annotations were used as the known transcript set for analysis by R-SAP.

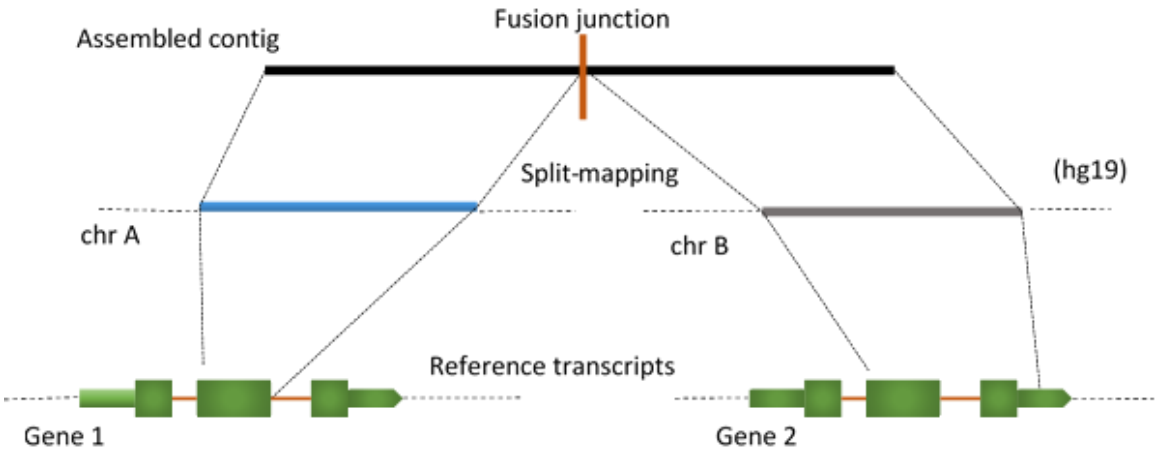

Figure 3.2. Chimeric transcript detection and characterization by R-SAP.
Assembled contigs (black box) representing chimeric transcripts will produce discrete or fragmented alignments (blue and grey boxes) when mapped to the reference genome. It will result in the alignment structure where fragments of the assembled contigs will map to the genomic locations (e.g. chrA and chrB) underlying the fusion-gene formation. This structure is also called as 'split-mapping' of the contig. R-SAP detects split-mapping and then compares the alignment coordinate of each fragment with the genomic coordinates of the known reference transcripts (shown in green boxes). Based on the fusion-point mapping (vertical orange bar on the top), R-SAP can determine the transcripts regions (such as CDS or UTRs) are involved in the gene-fusion.

Chimeric transcripts that were detected and characterized by R-SAP were subjected to additional stringent filtering in order to minimize potential assembly and alignment errors. First, to ensure the validity and significance of the alignment, chimeric transcript fragments were required to be at least 25 bp long and to have an alignment identity of >95%. Chimeric transcripts with fragments mapping to the same gene were discarded as potential library artifacts. Similarly, fusion-gene events between two paralogous genes [as determined using BioMart for Ensembl genes, see: (Flicek et al. 2014)] were also discarded because they may potentially represent alignment errors.

Additional potential chimeric transcripts were discarded if either component fulfilled at least one of the following filtering criteria: a) Maps to mitochondrial or Y chromosome; b) Overlaps with genome assembly gaps or maps within 100k bps of centromere or telomeres (assembly gaps, centromere and telomere coordinates were obtained from UCSC genome database); c) Maps to genomic region containing ribosomal RNAs (defined by UCSC genome database); d) Has >50% overlap with the genomic low-complexity or simple repeat regions (determined by RepeatMasker track in the UCSC genome table browser).

In order to further filter potentially miss-assembled chimeric contigs, we aligned the original RNA-Seq reads to the chimeric transcripts using Bowtie (Langmead et al. 2009) in single-end mode and retained only those contigs that had support of at least two sequencing reads at the fusion breakpoint (Figure 3.3). We also aligned sequencing reads to the reference genome using Bowtie2 (Langmead and Salzberg 2012) and defined a chimeric transcript to be supported by mate-pairs if both mates of the same pair map to the genomic locations involved in the fusion event. We required that each chimeric transcript be supported by at least two sets of mate-pairs.

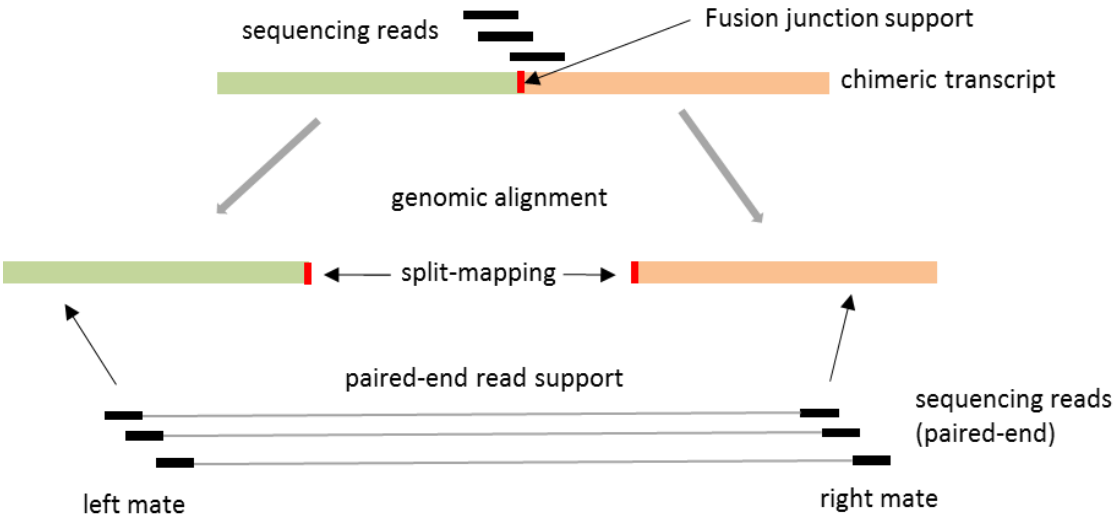

Figure 3.3. Re-confirmation of chimeric transcripts. In order to remove chimeric transcripts resulting from potential mis-assemblies, we looked for the support for chimeric transcripts (green-orange boxes) in the original RNA-Seq reads (black boxes). RNA-Seq reads were mapped to the chimeric transcripts and reads spanning the fusion-junction (vertical red box) were counted. Reads were also mapped to the reference genome and the occurrence of mate-pairs mapping to the genomic locations underlying the gene-fusions confirmed. We consider a chimeric transcripts as 'confirmed' if there are at least two reads supporting the fusion-junction and at least two mate pairs supporting the genomic alignment of the chimeric transcript.

Chimeric transcripts are generally considered to be in low abundance in the human transcriptome (Frenkel-Morgenstern et al. 2012). Ninety-five percent (52/55) of our samples exceeded the sequencing depth of 100 million reads recommended for optimal detection of low abundance transcripts (Robertson et al. 2010). In addition, the correlation between the number of reads in the RNA-Seq library and the number of filtered chimeric transcripts was insignificant ($R=0.24$, p-value > 0.05) further indicating our estimates of chimeric transcripts are independent of depth of sequencing coverage.

4. Expression quantification:

RNA-Seq reads were mapped to the transcript sequences using Bowtie and abundance estimation (raw read counts for each assembled contig) was carried out using

RSEM ((RNA-Seq by Expectation Maximization) (Li and Dewey 2011). In order to compare the expression across the samples, raw read counts were normalized using the 'Upper Quartile' normalization method proposed by Bullard *et al* (Bullard et al. 2010). For additional details see Supplemental Methods.

Results

An average of 35 chimeric transcripts per sample were detected in cancerous and normal breast tissue samples

We analyzed RNA-Seq data from 45 breast adenocarcinoma primary tumors and 10 normal breast tissue samples downloaded from the TCGA project database (https://tcga-data.nci.nih.gov/tcga/). The RNA-Seq data (Table B.1) were generated by sequencing total RNA libraries on the Illumina HiSq2000 system in paired-end mode. The raw data consisted of 50 bp long paired-end reads with an average of 170 million (from 47 million minimum to 374 million maximum; see Figure 3.4). We developed an integrated computational workflow that included the ABySS (Simpson et al. 2009) and Trans-ABySS (Robertson et al. 2010) algorithms to generate long (>800 bp) contiguous sequences or "contigs". *De novo* assembly (see Methods) of 7.8 billion 50 bp long reads from the 55 RNA-Seq libraries resulted in 12.8 million contigs (an average of 233,000 contigs per samples) with an average length of 860 bps (Table B.1). The R-SAP algorithm (Mittal and McDonald 2012) was incorporated into the workflow to identify and characterize chimeric transcripts (Figure 3.1).

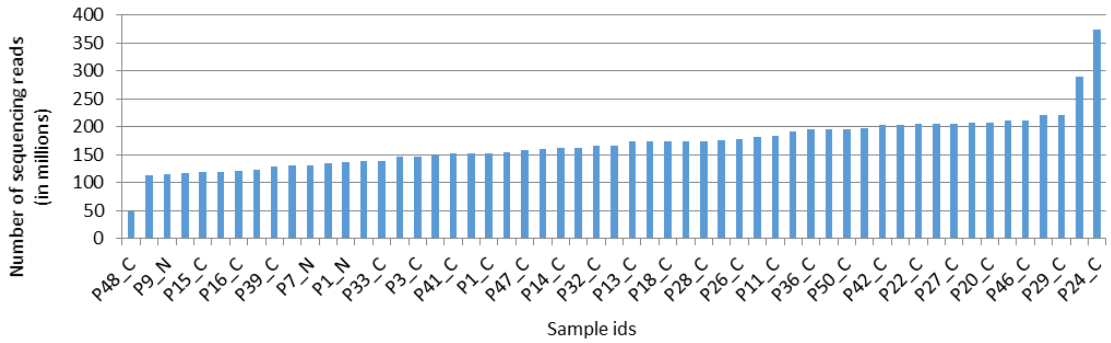

Figure 3.4. Sequencing coverage distribution across samples. The X-axis displays the 55 breast tissue samples analyzed in the study and y-axis presents the number of reads in millions in each sample.

After subjecting the putative chimeric transcripts to a stringent set of filtering criteria (see Methods), 2461 high-confidence chimeric transcripts remained. Of these, nearly 21% were Immunoglobulin (Ig) gene fusions likely due to infiltrating T-cells in breast tissue and were excluded from further analysis. After this additional filtering, 1959 chimeric transcripts remained with an average of 35 chimeric transcripts per sample (3 minimum to 121 maximum) (Figure 3.5). We compared chimeric transcripts across all normal and cancer samples by comparing the genomic alignment coordinates of each partner fragment of the chimeric transcript and allowing up to six base pairs to vary around the breakpoint. Out of the 1959 identified chimeric transcripts, 1535 were detected only in the cancer samples, 155 were detected only in the normal samples and 269 were detected in both the normal and cancer samples (Figure. 3.6A).

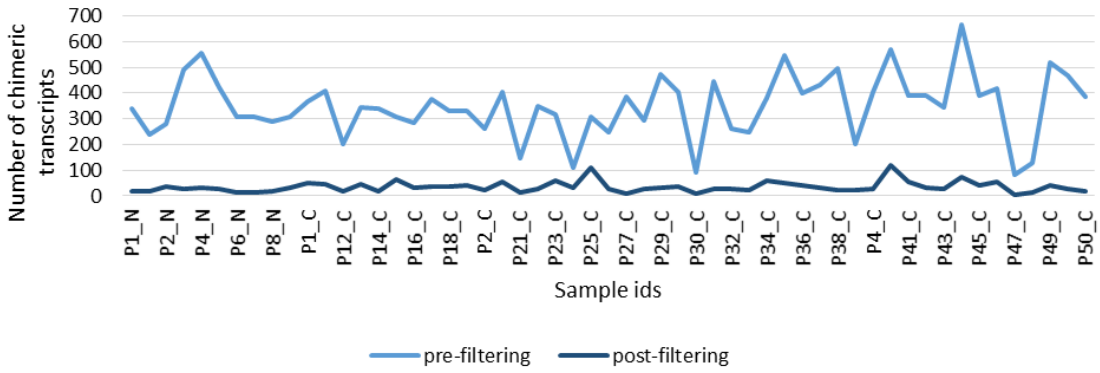

Figure 3.5. Chimeric transcript distribution across samples before and after filtering. The X-axis displays the 55 breast tissue samples analyzed in this study; the y-axis displays the number of chimeric transcripts per tissue sample. Pre-filtered chimeric transcripts (light blue line) are those that were detected by R-SAP while post-filtered chimeric transcripts (dark blue line) are those that were retained after initial filtering, re-confirmation and removal of immunoglobulin (Ig) genes associated chimers (see Methods for details).

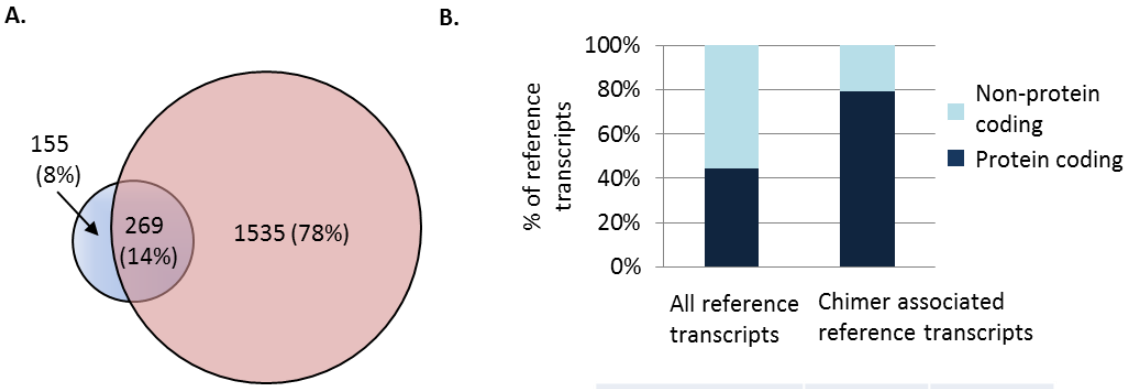

	All reference transcripts	chimeric associated reference transcripts
Non-protein coding	124403	413
Protein coding	100152	1599

Figure 3.6. Distribution of chimeric and associated reference transcripts. A) Venn diagram representing the distribution of chimeric transcripts in 10 normal (blue) and 45 cancer (red) breast tissues. Two-hundred and sixty-nine chimeric transcripts were found in both normal and cancer samples. B) Relative distribution of protein coding (black) and non-protein coding (blue) reference transcripts associated with all annotated human transcripts vs. the relative distribution associated with chimeric transcripts detected in this study. Table insert displays the total numbers of transcripts in each category.

Chimeric transcripts were classified based on structural and functional criteria

A detailed characterization of all chimeric transcripts identified in this study was carried out using the R-SAP algorithm (Mittal and McDonald 2012) and employing a comprehensive set of 224,555 reference transcripts (Ensembl version 73 and lncRNAs, see Methods). Most (98.82%) of the cancer-specific chimeric transcripts overlapped with at least one reference transcript. Overall 2,012 reference transcripts (corresponding to 1,917 genes) were associated with chimeric transcripts across all breast cancer samples (Table B.2). Interestingly, the proportion of protein coding reference transcripts associated with chimeric transcripts was significantly greater (Fisher's exact test $p < 0.0001$) than the proportion associated with the entire reference annotation set (Figure 3.6B). This suggests that protein-coding transcripts may be preferentially selected in the formation of chimeric transcripts.

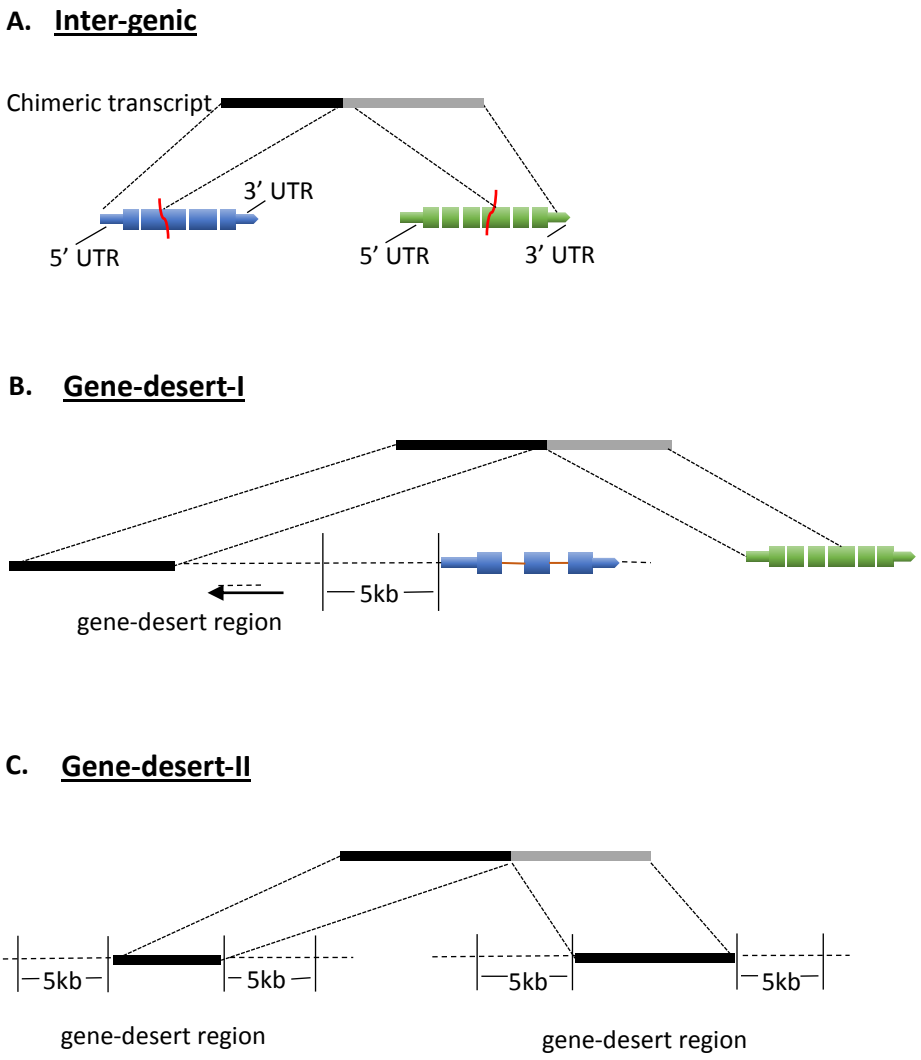

Figure 3.7. Hierarchical classification system for chimeric transcripts. Chimeric transcripts are depicted as a black-grey box, reference transcripts are represented by blue and green boxes where thick boxes represent open-reading-frames and thin boxes represent 5' and 3 UTRs. An **Inter-genic chimera** (**A**) is defined as a chimeric transcript where components map independently to annotated genes; A **'gene-desert-I' chimera** (**B**) is defined as a chimeric transcript where one component maps to a gene-desert region (black box) while the other maps to an annotated gene (green); A **'gene-desert-II' chimera** (**C**) is defined as a chimeric transcript where both components map to gene-desert regions. A gene-desert region is defined as the genomic region devoid of any annotated genes within 5kb of the transcript.

To more accurately characterize chimeric transcripts and infer potential functional significance, we first established a hierarchical classification system (Figure 3.7) where the chimeric transcripts were divided into three major classes: inter-genic-where the chimera is composed of two annotated genes; gene-desert-I where the chimera is composed of one annotated gene and a sequence from an un-annotated or "gene desert" region (lacking any annotated gene within a 5kb radius); and gene-desert-II where the chimera is comprised of sequences from two distant 'gene-desert' regions. Overall, the vast majority (>80%) of chimeric transcripts were inter-genic while <18% were gene-desert-I chimers. Only ~1% of the chimers were comprised of two un-annotated transcripts (gene desert-II) (Figure 3.8).

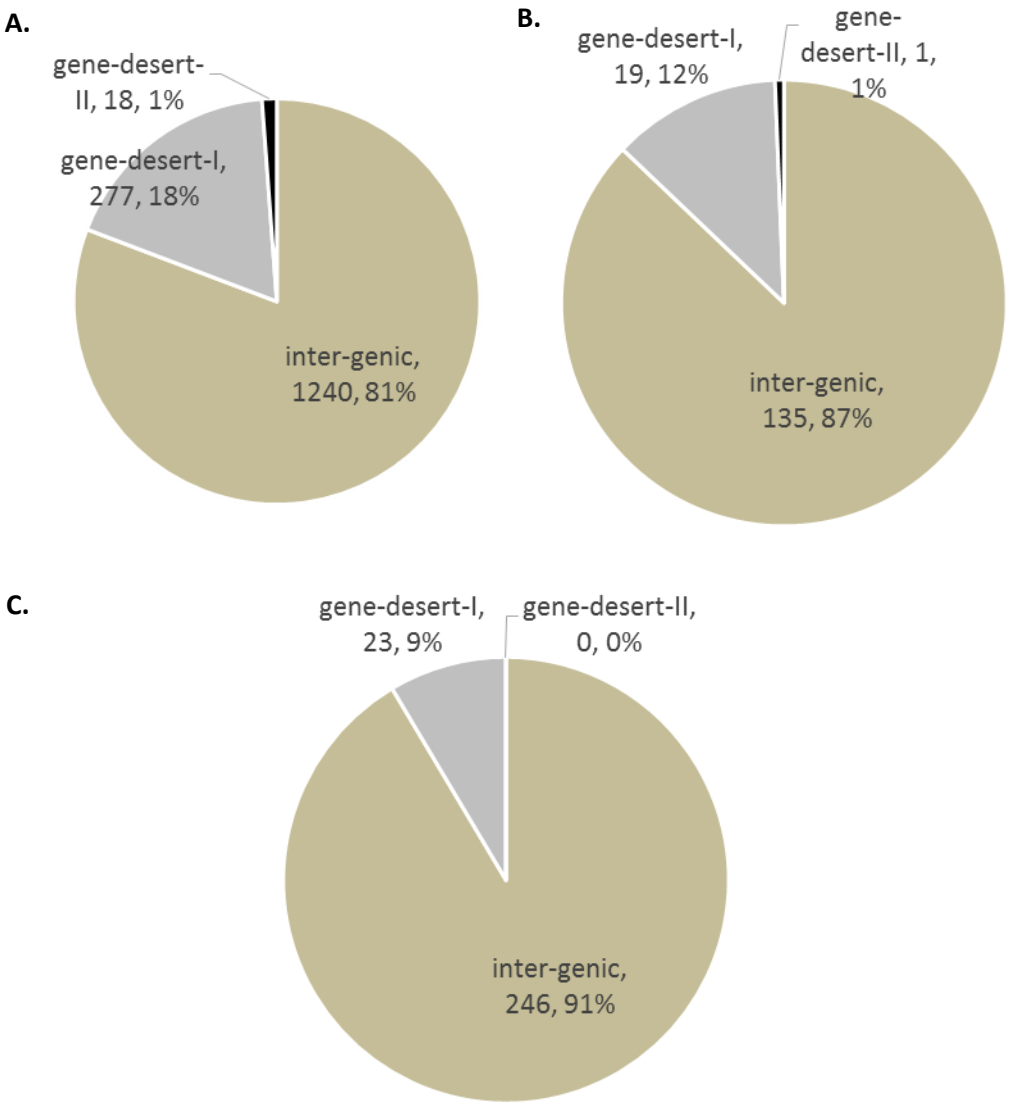

Figure 3.8. Relative distribution of inter-genic, gene-desert-I and gene desert-II in (A) cancer samples, (B) in normal tissue samples, and (C) in both cancer and normal tissue samples. Classification scheme is described in Supplementary Figure 3.3.

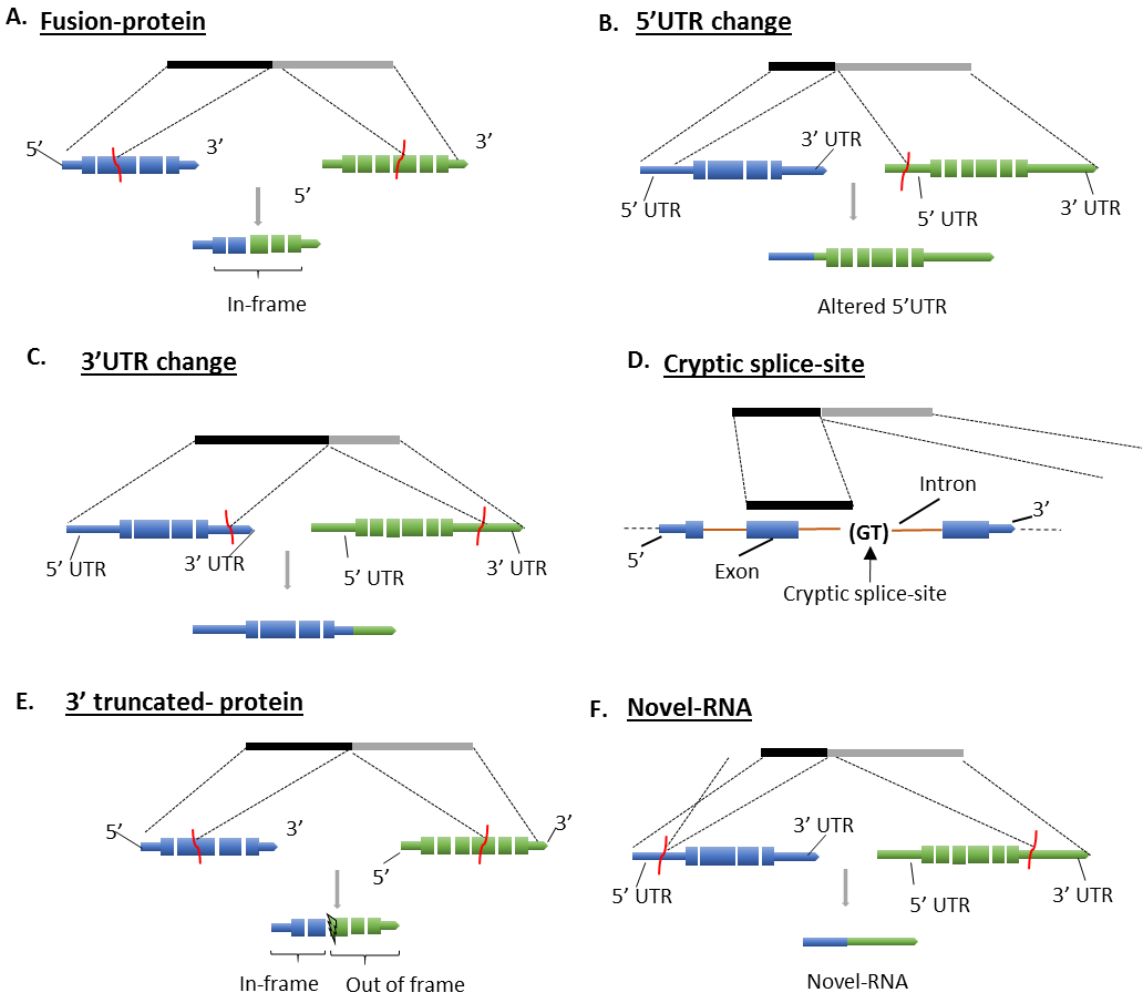

Figure 3.9. Structure based functional classification of chimeric transcripts. Chimeric transcripts are represented by black and grey boxes; reference transcripts are represented by blue and green boxes where thick boxes represent exons, gaps represent introns and thin boxes represent the 5' and 3' UTRs. Functional classifications are established by comparing the reference genome alignment coordinates of chimeric transcript regions (5'UTR, coding regions or 3'UTR) of the reference transcripts involved in the fusion (spanned by the chimeric transcript). A) Fusion-protein- Fusion of protein coding sequences from two different annotated genes where open-reading frames remain intact; B) 5' UTR- Fusion of 5' UTR from a gene or gene-desert region with protein coding region of another gene keeping the open-reading frame intact; C) 3' UTR – Fusion of a 5' and protein coding region of a gene with the 3' UTR of another gene or gene-desert region keeping the open-reading frame intact; D) Cryptic splice-site- A novel splice-variant chimera where the breakpoint lies within a known intron. This group may include inter-genic and gene-desert-I chimeras; E) 3' truncated-protein- Fusion transcript where the 5' and coding (in frame) region of one gene is combined with an out-of-frame coding region of another gene or with the 3' region of a gene desert region; F) Novel-RNA- Non-canonical chimeric transcript formation where the potential function of the transcript, if any, is unknown (e.g., 5'UTR-3'UTR fusions). This group also includes out-of-frame truncated fusion-protein transcripts.

We further classified the detected chimeras into 5 functional sub-categories (Figure 3.9): A) Fusion-protein- Chimeric transcripts that combine protein coding sequences (CDS) from two different annotated genes while keeping the open-reading frames intact; B & C) 5' or 3' UTR- UTR exchange from another gene or gene-desert region in such a way that the original protein-coding region of the chimera remains intact. This group may include inter-genic and gene-desert-I type chimeras (Figure 3.7); D) Cryptic splice-site- A novel splice-variant chimera where the breakpoint lies within a known intron. This group may include inter-genic and gene-desert-I chimeras; E) 3' truncated-protein- The in-frame coding sequence of the upstream (5') gene in the chimera is partially included (truncated) while the coding region of the 3' gene is not in frame. This group may include inter-genic and gene-desert-I chimeras; and F) Novel-RNA- Non-canonical chimeric transcript formation where the potential function of the transcript, if any, is unknown (*e.g.*, 5'UTR-3'UTR fusions). This group also includes out-of-frame truncated fusion-protein transcripts. The distribution of the identified cancer specific chimeras in each of these functional groups is displayed in Figure 3.10A, Table 3.1; see also Tables B.3, B.4).

Table 3.1. Distribution of breast cancer specific chimeric transcript across multiple structural and functional classes.

	inter-genic	gene-desert-I	gene-desert-II	**Total**
fusion-protein	79	NA	NA	79
3' truncated-protein	286	133	NA	419
5' UTR-change	41	4	NA	45
3'UTR-change	145	21	NA	166
cryptic splice-site	289	78	NA	367
novel RNA	400	41	18	459
Total	1240	277	18	

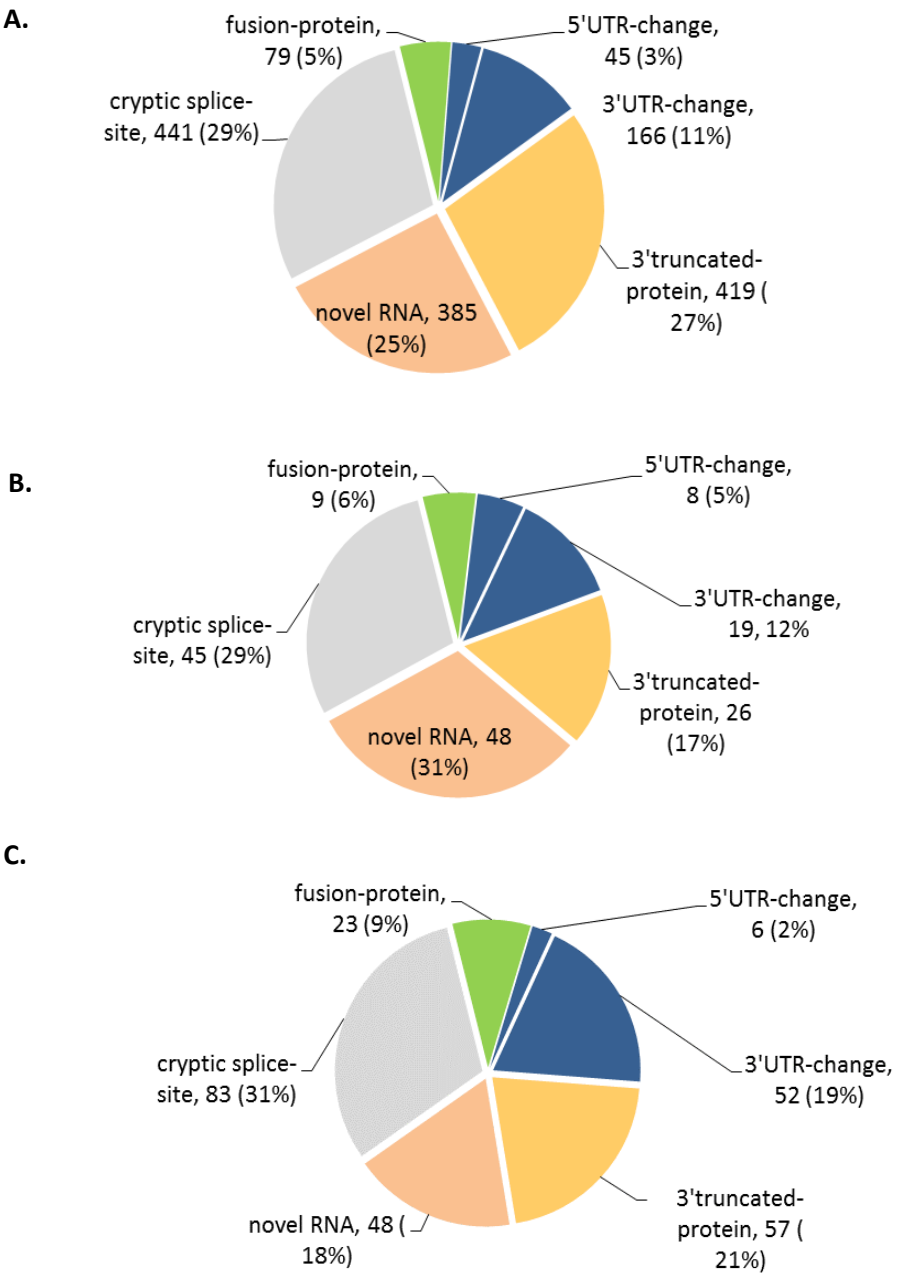

Figure 3.10. Relative distribution of functional classes of chimeric transcripts present. A) only in cancer tissue samples; B) only in normal tissue samples; and C) in both normal and cancer samples.

Out of 1535 cancer specific chimers, 5% (79/1535) are fusion-proteins, 3% (45/1535) are 5' UTR changes and 11% (166/1535) are 3' UTR changes. Cryptic splice-site chimeras are the most abundant class of fusion transcripts (29%, 441/1535). The next most frequent classes were the 3' truncated-protein (27%, 419/1535) and novel-RNAs (25%, 385/1535) (Figure 3.10A). These relative proportions were generally maintained in the normal specific and overlap class of chimeras (Figure 3.10B, C).

Some fusion-protein transcripts recur across cancer patient samples

Although the functional significance of chimeric transcripts cannot be unambiguously determined without experimental validation, the recurrence of chimeric transcripts across multiple patients is sometimes taken as tentative indication of biological significance (Mitelman 2000). For example, the *KRI1-ATRX* chimeric transcript is the most frequently observed chimeric transcript in our study (present in nine cancer and one normal samples). It involves a fusion between a partial ORF associated with the *KRI1* (KRI 1 homolog) gene and the DEAD helicase domain from the *ATRX* (ATP-dependent helicase ATRX) gene. The DEAD box helicases are a family of proteins involved in ATP hydrolysis dependent DNA and RNA unwinding that, in-turn, regulates RNA expression and its translational efficiency (*e.g.*, (Tanner and Linder 2001). The frequency of recurrent chimeric transcripts across cancer samples is shown in Figure 3.11 and Table B.5.

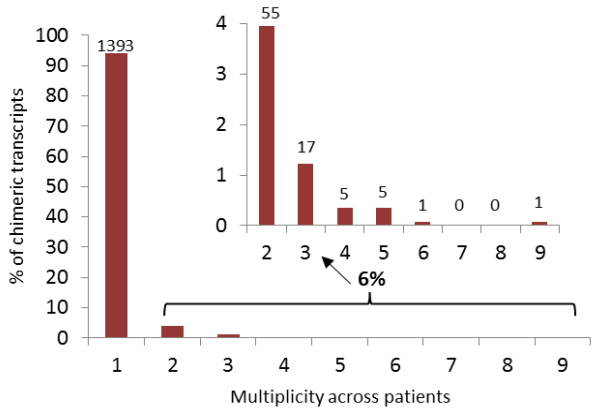

Figure 3.11. Recurrence of breast cancer associated chimeric transcripts across patient samples. Shown is the percentage of all cancer chimeric transcripts detected in one or more cancer patient samples. The vast majority of chimeric transcripts are specific to individual patients. Inset details the distribution of transcripts found in more than one sample.

Seventy-nine cancer-specific fusions encode protein-coding domains where the ORFs are maintained

We identified 79 breast cancer specific chimeric transcripts where the fusion occurs within the protein coding regions of the two participating genes and the open-reading frames are maintained (Figure 3.10A; Table 3.1). We analyzed the protein coding domains in these 79 fusion-protein chimeric transcripts using the SMART [simple modular architecture research tool; (Letunic et al. 2012)] . We found that 38% (30/79) of the fusion-protein chimers contained functional domains for both genes involved in the chimera formation (Table B.6). Interestingly, 50% (15/30) of these protein coding fusion-chimeras involved the novel joining of a signal peptide (2/15) or a trans-membrane domain (13/15) with a protein coding domain not previously associated with these functional groups. Signal peptide sequences are components of proteins that are normally secreted from cells (von Heijne 1985). Trans-membrane (TM) domains are signaling, transport and subcellular localization components of proteins that are critical to a variety of inter- and intracellular interactions (Deutsch et al. 2008; Roth et al. 2008; Gui

and Hagenbuch 2009). Mutations resulting in the gain or loss of TM domains are known to have a significant effect on cellular functions and molecular interactions (Maeda et al. 2005). Of the 15 chimers associated with signal peptide/TM domain sequences, 12 are fusions with protein coding sequences (*COL27A1*, *IGFBP4*, *KDM5A*, *MDM1*, *NAP1L2*, *NHP2L1*, *NMT2*, *PAXIP1*, *RP11-433C9.2*, *SMARCA4*, *STXBP6* and *TRIO)* not previously associated with these signaling functions (Figure 3.12).

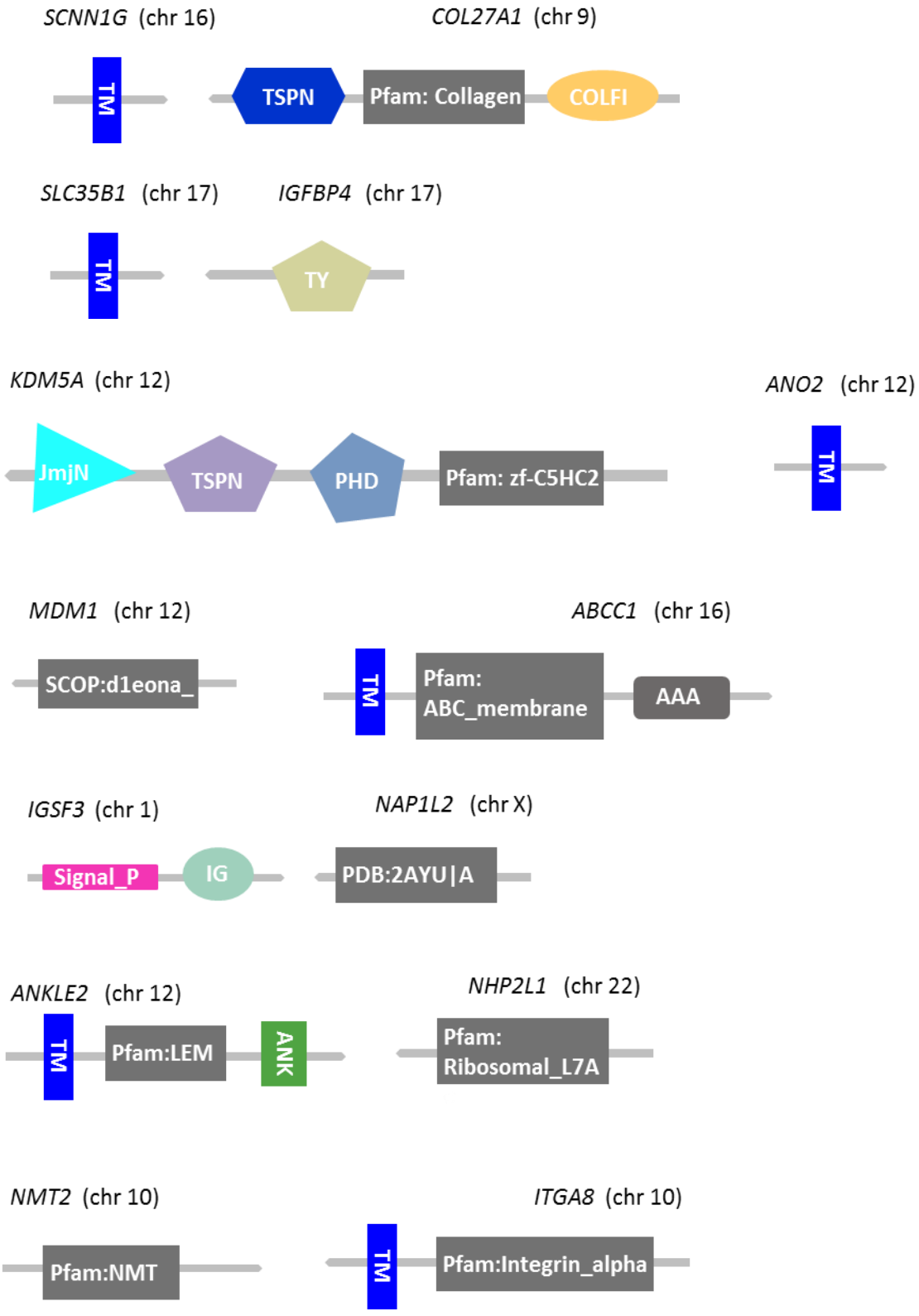
SCNN1G (chr 16)
TM
COL27A1 (chr 9)
TSPN
Pfam: Collagen
COLFI
SLC35B1 (chr 17)
TM
IGFBP4 (chr 17)
TY
KDM5A (chr 12)
JmjN
TSPN
PHD
Pfam: zf-C5HC2
ANO2 (chr 12)
TM
MDM1 (chr 12)
SCOP:d1eona_
ABCC1 (chr 16)
TM
Pfam: ABC_membrane
AAA
IGSF3 (chr 1)
Signal_P
IG
NAP1L2 (chr X)
PDB:2AYU|A
ANKLE2 (chr 12)
TM
Pfam:LEM
ANK
NHP2L1 (chr 22)
Pfam: Ribosomal_L7A
NMT2 (chr 10)
Pfam:NMT
ITGA8 (chr 10)
TM
Pfam:Integrin_alpha

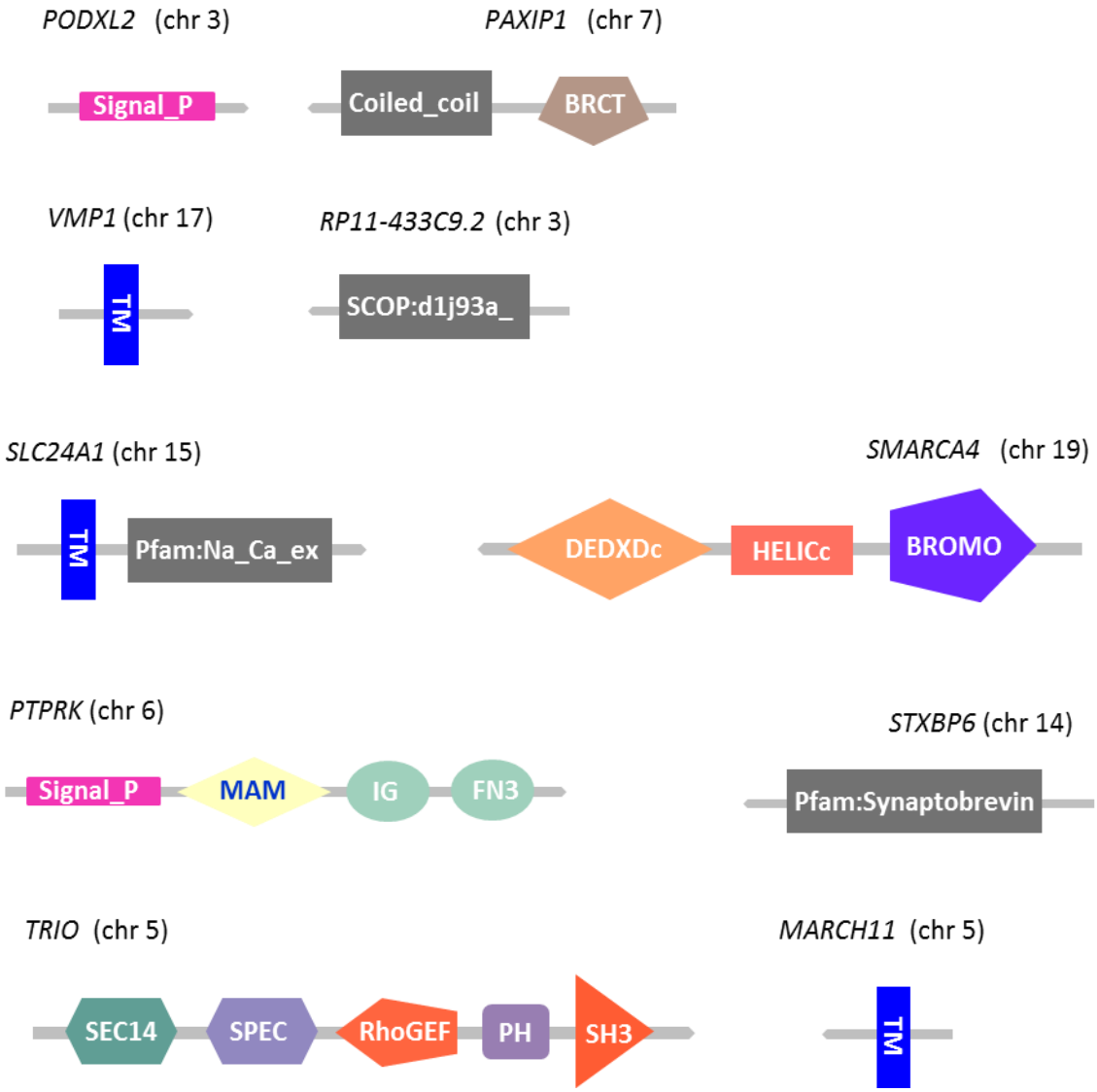
PODXL2 (chr 3)
Signal_P
PAXIP1 (chr 7)
Coiled_coil
BRCT
VMP1 (chr 17)
TM
RP11-433C9.2 (chr 3)
SCOP:d1j93a_
SLC24A1 (chr 15)
TM
Pfam:Na_Ca_ex
SMARCA4 (chr 19)
DEDXDc
HELICc
BROMO
PTPRK (chr 6)
Signal_P
MAM
IG
FN3
STXBP6 (chr 14)
Pfam:Synaptobrevin
TRIO (chr 5)
SEC14
SPEC
RhoGEF
PH
SH3
MARCH11 (chr 5)
TM

Figure 3.12. Structure of in-frame gene-fusion mutations resulting in gain of signaling protein domains (trans-membrane and/or signal peptide domains) from another participating gene. Depicted are 12 of 15 detected fusion events where genes were not previously associated with the signaling functions. Gene symbols and corresponding chromosomes (in parenthesis) are shown above of each gene fusion structure). Gene symbols are defined as follows: *SCNN1G*: Sodium Channel, Non-Voltage-Gated 1, Gamma Subunit; *COl27A1L*: Collagen, Type XXVII, Alpha 1; *SLC35B1*: Solute Carrier Family 35, Member B1; *IGFBP4*: Insulin-Like Growth Factor Binding Protein 4; *KDM5A*: Lysine (K)-Specific Demethylase 5A; *ANO2*: Anoctamin 2; *MDM1*: Mdm1 Nuclear Protein Homolog (Mouse); *ABCC1*: ATP-Binding Cassette, Sub-Family C (CFTR/MRP), Member 1; *IGSF3*: Immunoglobulin Superfamily, Member 3; *NAP1L2*: Nucleosome Assembly Protein 1-Like 2; *ANKLE2*: Ankyrin Repeat And LEM Domain Containing 2; *NHP2L1*: NHP2 Non-Histone Chromosome Protein 2-Like 1 (S. Cerevisiae); *NMT2*: N-Myristoyltransferase 2; *ITGA8*: Integrin, Alpha 8; *PODXL2*: Podocalyxin-Like 2; *PAXIP1*: PAX Interacting (With Transcription-Activation Domain) Protein 1; *VMP1*: Vacuole Membrane Protein 1; *RP11-433C9.2*: Clone based putative protien coding gene on chromosome 3; *SLC24A1*: Solute Carrier Family 24 (Sodium/Potassium/Calcium Exchanger), Member 1; *SMARCA4*: SWI/SNF Related, Matrix Associated, Actin Dependent Regulator Of Chromatin, Subfamily A, Member 4; *PTPRK*: Protein Tyrosine Phosphatase, Receptor Type, K; *STXBP6*: Syntaxin Binding Protein 6 (Amisyn); *TRIO*: Trio Rho Guanine Nucleotide Exchange Factor; *MARCH11*: Membrane-Associated Ring Finger (C3HC4) 11.

Fusions that place protein-coding genes under novel regulatory control are frequent in breast cancer samples

A gene fusion between two different genes often puts one gene (downstream or 3' partner gene) under the transcriptional regulatory elements (promoter or enhancer) of the other gene (upstream or 5' partner gene). Such fusion-based regulatory variants have often been associated with the activation of the 3' proto-oncogene in cancer cells. For example, it has been previously reported that the oncogenic transcription factor *ERG* (ETS-related gene**)**, is up regulated in prostate cancer due to the fusion with the 5' region of the *TMPRSS2* (Trans-membrane protease, serine 2) gene that contains an androgen responsive promoter element (Tomlins et al. 2005).

For the 79 fusion-protein chimeric transcripts in cancer, we estimated the fold-change in gene expression of the 3' partner genes involved in the fusion relative to their expression in their normal configurations (*i.e.*, non-chimeric) by comparing the expression of each of the 3' partners with the expression of each corresponding non-chimeric reference transcript in a reference expression database (see Methods). We found that 24% (19/79) of the 3' partners displayed a ≥ 2-fold expression increase in cancer for at least one protein coding domain (Table B.7). Several of the genes involved in these up-regulated fusions have been previously identified as either cancer biomarkers or as potential therapeutic targets. For example, the *B4GALNT2 (*Beta-1,4 N-acetylgalactosaminyltransferase 2*)* gene, the 3' partner in the *THRA* (Thyroid Hormone Receptor, Alpha)-*B4GALNT2* fusion, has been previously proposed as a prognostic biomarker of breast cancer (Patani et al. 2008) and is reported to be up regulated in colorectal and metastatic prostate cancer (Kudo et al. 1998; Barthel et al. 2008). The *ABCC3* (canalicular multispecific organic anion transporter 2) gene, the 3' partner in the *MED1* (Mediator Complex Subunit 1)-*ABCC3* fusion, is known to efflux therapeutic compounds resulting in multidrug resistance in cancer cells (Dean 2009; Fletcher et al. 2010).

Another class of fusions that may be expected to alter patterns of gene expression involves the exchange of 5' or 3' un-translated leader regions (UTRs) of intact protein coding sequences. For example, alteration in the poly-A tail attached to 3'UTR and removal of 5' cap (7-methyle guanosine) may promote mRNA decay and hence overall turnover in the cell (Mignone et al. 2002). Additionally, fusions involving the exchange of a 5'UTR may place a gene under the control of a novel promoter. For example, chromosomal rearrangements involving UTRs that result in high level expression of *ETS* (E26 transformation-specific) gene family members are common events in human prostate cancer (Tomlins et al. 2005). Similarly, changes in the 3'UTR can alter microRNA target binding sites leading to changes in the gene expression. For example, in

glioblastoma, the *FGFR3* (fibroblast growth factor receptor 3) gene has been shown to escape regulation by the miR-99a microRNA due to a fusion with the 3'UTR of the *TACC3* (Transforming, Acidic Coiled-Coil Containing) gene (Parker et al. 2013).

In our analysis, 14% (211/1535) of chimeras detected in our breast cancer samples consisted of un-disrupted protein coding sequences fused with heterologous UTRs. Nearly 21% (45/211) of these are 5'UTR fusions while 79% (166/211) are fusions with 3'UTRs (Figure 3.10A, Table 3.1). Most (88%, 186/211) of the UTRs were interchanged between two known genes but 12% of the chimers involved the UTRs of known coding sequences with sequences from un-annotated 'gene-deserts' regions of the genome (Table 3.1).

We estimated the effects of 5' and 3' UTR changes on gene expression by measuring the fold-change in the expression level of each UTR-protein coding gene fusion in the cancer samples relative to the protein-coding gene's average level of expression in our normal samples (see Methods and Supplemental Methods). The results indicate that 54 of the UTR-protein coding fusion genes are $\geq$ 2-fold up-regulated relative to their wild-type counterparts in normal cells (Figure 3.13; Table B.8). Several of the up-regulated genes encode transcription factors previously implicated in cancer. For example, the epigenetic transcriptional regulator proteins *CBX3* (chromobox homolog 3) and *CBX4* (chromobox homolog 4) were up regulated in our cancer samples due to alternative 3'UTRs obtained by gene-fusion. *CBX3* has been previously identified as a potential biomarker for tumor stem cells in osteosarcoma (Saini et al. 2012), while *CBX4* has been reported to induce hypoxia-mediated activation of *VEGFA* (vascular endothelial growth factor A) and angiogenesis in hepatocellular carcinomas (Li et al. 2014). Another chimeric transcript up regulated in our cancer samples is a fusion of the transcriptional regulator-encoding gene, *RARA* (retinoic acid receptor, alpha), with the 3' UTR from the *PSME3* (proteasome activator subunit 3) gene. Interestingly, an analogous reciprocal translocation between the *RARA* with *PML* (promyelocyctic leukemia) genes has been

previously associated with the primary cytogenetic abnormality leading to acute promyelocytic leukemia (Reiter et al. 2004).

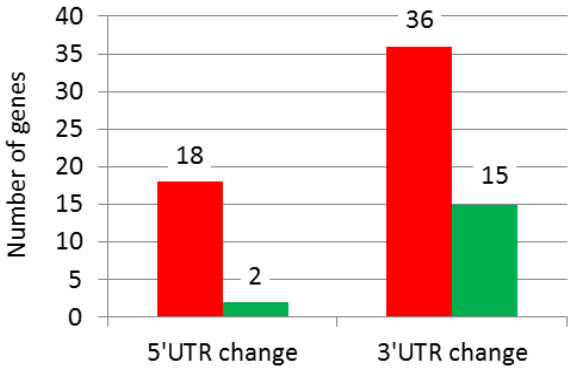

Figure 3.13. Gene-expression change due to fusion with heterologous UTRs. Chimera formation can result in the altered 5'UTR or 3'UTR while keeping the original ORF intact. Histograms display the number chimeric transcripts where the protein-coding genes are up-regulated (red) or down-regulated (green) by >2 fold in breast cancer samples relative to the protein-coding genes (native state) in normal breast tissue.

In our breast cancer samples, 17 genes were estimated to be ≥ 2-fold down-regulated due to the fusion with novel UTRs (Table 3.1, Figure 3.13, Table B.8). For example, a fusion between the *PTEN* (phosphatase and tensin homolog) and the 3' UTR of the *PIK3C2A* (Phosphatidylinositol-4-Phosphate 3-Kinase, Catalytic Subunit Type 2 Alpha) gene resulted in the down regulation of *PTEN* >2-fold in our cancer samples. *PTEN* is a well-known tumor suppressor gene that displays loss-of-function mutations in many cancers in (*e.g.*, (Chen et al. 2005b).

Other protein coding genes involved in UTR fusions in our cancer samples that have been previously associated with cancer onset and/or progression are the interferon gamma receptor 1 (*IFNGR1*) gene (Duncan et al. 2007), the period circadian clock 2 (*PER2*) gene (Chen et al. 2005a; Gery et al. 2007), the chloride intracellular channel 4 (*CLIC4*) gene (Suh et al. 2012), the sorbin and SH3 domain containing 2 (*SORBS2*) gene (Alsafadi et al. 2011) and the eukaryotic translation initiation factor 2-alpha kinase encoding (*EIF2AK2*) gene (Vorburger et al. 2004; Lee et al. 2013).

A number of chimeric transcripts include sequences from gene desert regions of the genome

Previous studies have shown that the human genome is more pervasively transcribed than previously thought (Consortium et al. 2007). For example, the recent ENCODE (Encyclopedia of DNA Elements) data release suggests that nearly 80% of the human genome displays transcriptional functionality in a cell type specific manner (Qu and Fang 2013). Although many of these transcripts are derived from annotated protein-coding genes, others may represent long non-encoding RNAs or other non-encoding regulatory RNAs of currently undetermined function. In our cancer samples, we identified 338 'gene-desert' chimeras where either one (319, gene-desert-I) or both components (19, gene-desert-II) of the chimeric transcript maps to the 'gene-desert' regions of the genome (Figure 3.9, Table B.9).

We obtained transcription factor binding site (TFBS) predictions based on Chip-Seq data from the ENCODE project [https://genome.ucsc.edu/ENCODE/; (Rosenbloom et al. 2013)] for five breast or mammary cell lines (HMEC, HMF, MCF-7, MCF10A-Er-Src, T-47D). We then searched for active TFBS in the ENCODE database at positions proximal to gene-desert regions involved in our chimeric transcripts. Since most TFBS are present within 8kb of the transcription start site of regulated genes (Koudritsky and Domany 2008), we considered only those TFBS mapping within 8kb of the gene desert transcripts (Figure 3.14A). Interestingly, all (100%, 319/319) of the gene-desert regions involved in chimer formation had at least one active TFBS within 8KB of the transcript. Also, we found that the gene-desert chimeric regions are distributed at distances form TFBS similar to that observed for annotated reference transcripts (Figure 3.14B). These findings support the contention that actively transcribed transcripts mapping to gene desert regions of the genome participate in chimera formation. However, since neither the structure nor the function of transcripts mapping to these gene-desert regions are currently known, the potential functional significance of gene-desert chimeras also

remains undetermined. Nevertheless, the fact that 9% (28/319) of gene desert chimeric transcripts involve the fusion of know protein coding sequences with UTRs from gene desert regions suggests that at least some of these chimeras may represent significant regulatory variants.

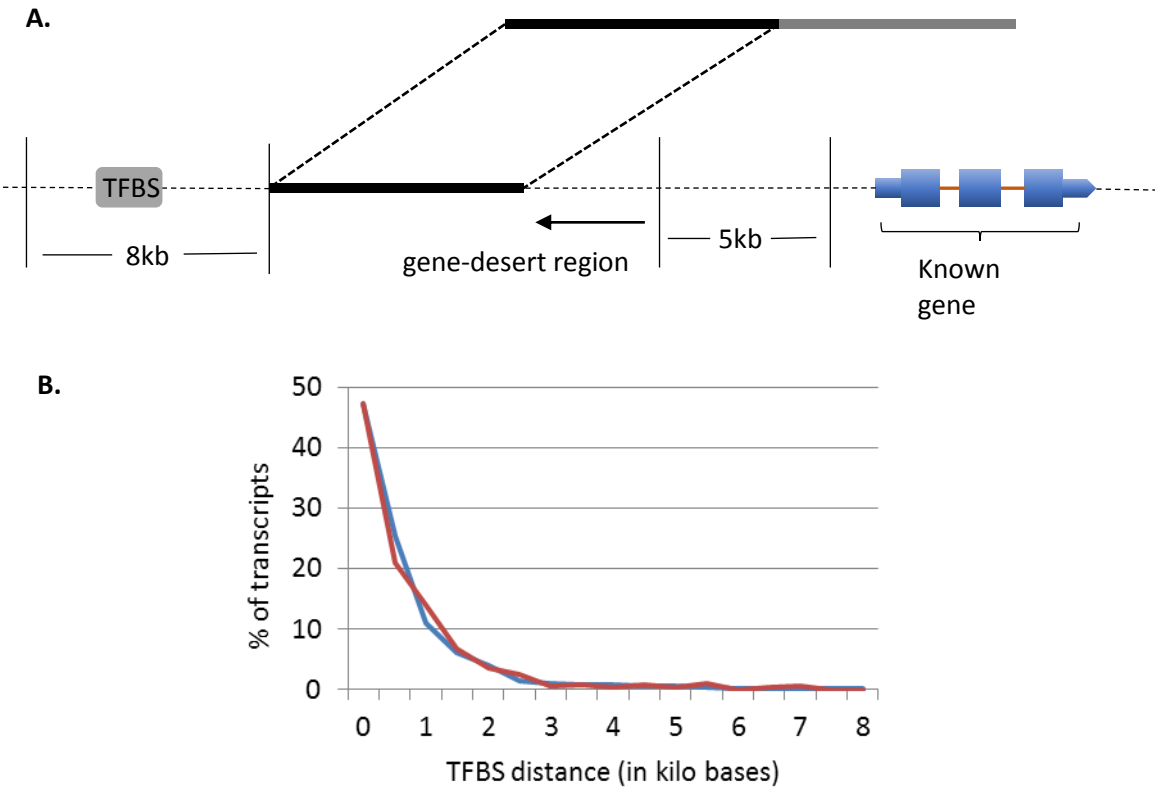

Figure 3.14. Detection of transcription factor binding sites (TFBS) in proximity to gene-desert regions involved in chimera formation. A. A search was carried out for documented transcription factor binding sites (TFBS; grey box) within 8kb from gene-desert transcripts (black box) involved in breast cancer gene fusions. **B.** At least one active TFBS is located within 8 KB of gene-desert transcripts involved in gene-fusions in cancer. The distribution of the locations of TFBS from the gene-desert transcripts (red line) is identical to that associated with annotated reference transcripts (blue line). The x-axis is the distance in kilobases of a TFBS detected from a transcript; the y-axis is the percentage of transcripts with a specific TFBS distance corresponding to X-axis.

Comparative analysis of chimeric transcripts in normal and cancer samples identifies potential pro-neoplastic genes

Comparison of chimeric transcripts across all normal and cancer samples was carried out by comparing the genomic alignment coordinates of each partner fragment of the chimeric transcript and allowing up to six base pairs to vary around the breakpoint. Although 88% (1716/1959) of all chimeric transcripts detected were found in the cancer samples and only 12% (243/1959) in the normal samples, this is largely attributable to the disproportionate number of samples examined (45 cancer vs. 10 normal). When the average number of chimers detected per sample is compared, the differences are less dramatic (normal: 24/sample; cancer: 38/sample) albeit still significant (Student's t-test $p<1.05E-03$).

The unexpected abundance of chimeric transcripts in normal samples and the fact that the majority of these (> 60%, 269/424; see Figure 3.6) were also present in the cancer samples, led us to explore these chimerics in more detail. It is possible that at least some of the chimeric transcripts detected in normal tissue may represent "pro-neoplastic" fusions whose cancer causing potential is at least partially repressed in normal cells (*i.e.*, oncogene expression repressed; tumor suppressor potential amplified). For example, chimeric transcripts of the well-studied chronic myeloid leukemia causing *BCR-ABL* fusion gene have been detected at low levels in the blood cells of healthy individuals as well (Boquett et al. 2013). Similarly, the anti-apoptotic chimeric transcript comprised of the zinc finger genes *JAZF1* (JAZF zinc finger 1) and *JJAZ1* (also known as SUZ12 or SUZ12 polycomb repressive complex 2) is highly expressed in nearly 50% of all endometrial stromal sarcomas (Koontz et al. 2001; Hrzenjak et al. 2005), but has also been detected at low levels in normal endometrial stromal cells as well (Li et al. 2008).

We detected 269 chimeric transcripts that were shared between our normal and breast cancer samples. Of these, 4 were identified as in frame fusion-protein coding transcripts of potential pro-neoplastic significance (*ZBTB47-FGD1, KRI1-ATRX,*

CACNA1D-CTNNBL1, and *SCAF4-TNRC6A*) (Figure 3.15, Table B.10). RNA-Seq reads were mapped to the assembled contigs representing each of these 4 chimeras and read counts were estimated using RSEM (RNA-Seq by Expectation Maximization) (Li and Dewey 2011) and normalized using upper-quartile normalization (Bullard et al. 2010) (see Methods). Two of the chimeras (*ZBTB47-FGD1* and *KRI1-ATRX*) displayed a >2.5-fold increase in expression in cancer relative to the normal samples (Figure 3.15A & B; Table B.10). A third chimera (*SCAF4-TNRC6A*) displayed a 1.3-fold increase in expression in the cancer samples while a fourth fusion (*CACNA1D-CTNNBL1*) displayed a decrease in expression in the cancer samples (Figure 3.15 C, D; Table B.10).

In the *ZBTB47-FGD1* chimeric transcript, a BTB/POZ domain (BR-C, ttk and bab domain/Pox virus and Zinc finger virus and zinc finger domain) from *ZBTB47* (Zinc Finger And BTB Domain Containing 47) is fused with the RhoGEF (a.k.a., the Dbl homologous domain), PH (pleckstrin homology) and FYVE domains from *FGD1*. Interestingly, a previously identified oncogenic fusion gene (*Dbl*) was also found to contain a RhoGEF domain whose over-expression is essential to the *Dbl* gene's oncogenic potential (Cerione and Zheng 1996). Over expression of *FGD1* has also been previously associated with cancer progression in prostate and breast cancer (Ayala et al. 2009). The 3' member of the *KRI1-ATRX* fusion (ATRX) has been previously associated with childhood neuroblastoma (Cheung et al. 2012) and the 3' member of the *CACNA1D-CTNNBL1* fusion (*CTNNBL1*), is associated with an anti-apoptotic, tumor suppressive function (Suzuki et al. 1997; Jabbour et al. 2003) consistent with its reduced expression in our breast cancer samples.

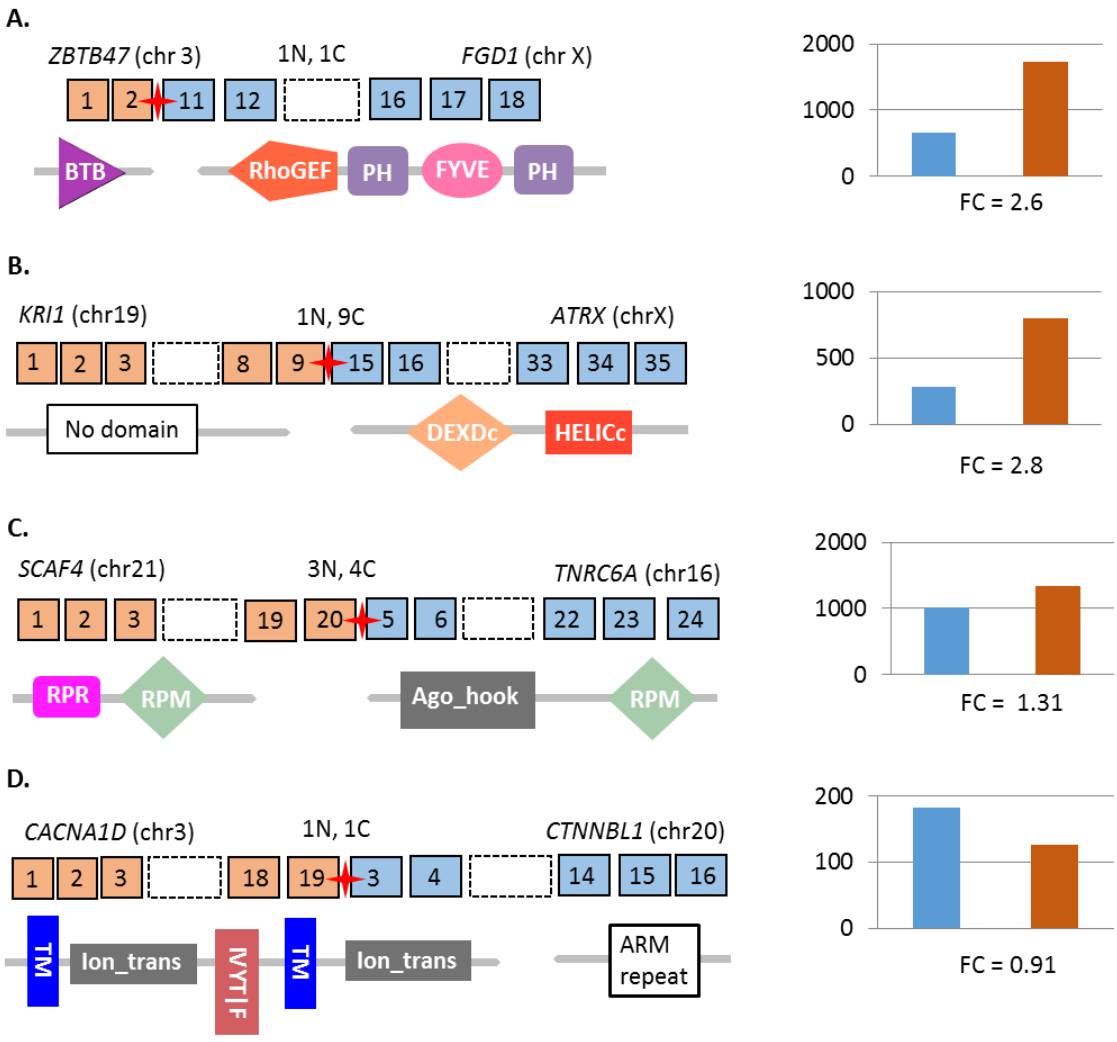

Figure 3.15. Potential pro-neoplastic gene-fusions that are functionally suppressed in normal breast tissues but activated in cancer tissues. Shown is the structure of four gene-fusions and associated protein domains that we have characterized as potential pro-neoplastic fusions. Square boxes with numbers represent exons (5' gene: orange, 3' gene: blue); exons not shown in the figure are represented by a dashed empty box; the red star represents the fusion point for each chimera; gene symbols and (chromosomal location), as well as, the number of each fusion transcript detected in normal (N) and cancer (C) samples is presented above each gene-fusion structure. Protein domains are displayed under each structure. Histograms on the right display average expression levels of the 3' members of the fusions in their native or parental (pre-fusion) genes in normal samples (blue) and the expression of the fusion transcript in cancer samples (orange) bar. Fold change is shown under each expression plot. All of the 3' partners of these fusion transcripts have been previously associated with cancer progression (see text for details).

Discussion

The oncogenic potential of gene fusions and fusion transcripts was first recognized in malignant hematological disorders and childhood sarcomas (Mitelman et al. 2004). In recent years, the importance of fusions in the onset and progression of a vast diversity of solid tumors has become more widely appreciated. The rapidly growing awareness of the extensiveness and potential importance of fusion transcripts in cancer has been facilitated by the high-throughput transcriptome sequencing of a broad spectrum of cancer types. The Cancer Genome Anatomy Project (http://cgap.nci.nih.gov/) currently lists well over 1800 fusions identified in > 63,000 cancer patient samples and it has been estimated that gene-fusions account for > 20% of human cancer morbidity (Mitelman et al. 2007).

We present here an integrated computational workflow that not only allows accurate detection of chimeric transcripts to nucleotide level resolution but also facilitates detailed molecular characterization and quantitative analysis. We employed this workflow to analyze 55 breast transcriptomes that, to our knowledge, is the first such study to explore global patterns and characteristics of chimeric transcripts in any tumor using a *de novo* assembly approach.

Since the *de novo* assembly approach allows for construction of long contigs capable of traversing multiple exons, we were able to map each known gene associated chimer to a specific splice-variant. Accurate mapping followed by hierarchical structural and functional classification enabled us to systematically infer the potential functional role and biological significance of a number of novel chimeric transcripts. While prior RNA-Seq based studies have focused primarily on the canonical gene fusion structures of fusion-protein and UTR associated alterations, our *de novo* assembly based approach allowed us to explore other classes of fusion structures such as cryptic-splice sites and non-canonical RNA structures. Although, the potential functional impact of many of these atypical structures has yet to be determined, their widespread occurrence in our

breast cancer samples strongly suggests that this class of chimeric transcripts warrants further investigation. In total, we identified 105 novel gene-fusions, 13 of which were detected across multiple patient samples.

Most previously identified gene-fusions in cancer have been associated with oncogene activation (Kumar-Sinha et al. 2006). Our findings suggest that gene-fusions can also result in significant down regulation of potentially significant genes. For example, while we identified 54 examples of genes being up regulated in cancer due to fusions with heterologous UTRs, an additional 17 such fusions resulted in a significant down regulation in gene expression including the well-known tumor suppressor gene *PTEN*.

Chimeric transcripts are typically associated with cancer cells but their presence in normal somatic cells is often overlooked. In our study, we identified a number of fusion transcripts that are present in both normal and cancer tissues but significantly differentially expressed in these two tissue types. Several of these were identified as potential pro-neoplastic fusions where domains previously associated with oncogenic functions were up regulated in cancer while those previously associated with tumor suppressor functions were down regulated in cancer.

Finally, we detected a large number of chimeric transcripts mapping partially or completely to genomic regions devoid of any known genes ("gene deserts"). We observe that the fusion transcripts involving gene-desert regions can result in the fusion of altered 5' or 3' UTRs to known protein-coding genes resulting in significant changes in gene expression. We also detected the fusion of transcripts mapping to two distinct gene-desert regions giving rise to novel RNA structures of currently unknown significance.

Overall, our *de novo* assembly approach has revealed an unexpected prevalence and diversity of chimeric transcripts in breast cancer tissues and underscores the utility of deep sequencing technologies and improved bioinformatics workflows to uncover novel and potentially significant chimeric transcripts in cancer and normal somatic tissues.

Acknowledgments

The authors thank the Office of Information Technology at Georgia Institute of Technology for providing access to computing clusters at 'Partnership for an Advanced Computing Environment' (pace.gatech.edu). This work was supported by grants from Ovarian Cycle, Deborah Nash Endowment Fund, Josephine Robinson Family and J.D. Rhodes Trust.

CHAPTER 4

IDENTIFICATION AND EXPRESSION ANALYSIS OF GENE FUSIONS AND OTHER STRUCTURAL VARIANTS IN OVARIAN CANCER USING HIGH-THROUGHPUT SEQUENCING

Abstract

Genomic rearrangements or structural variants (SVs) are one of the most common classes of mutations in cancer. We report here the results of an integrated DNA sequencing and transcriptional profiling (RNA sequence and microarray gene expression data) analysis of six ovarian cancer patient samples. Matched sets of control (whole blood) samples from these same patients were used to distinguish cancer SVs of germline origin from those arising somatically in the cancer cell lineage. We detected 10,034 ovarian cancer SVs (5518 germline derived; 4516 somatically derived) at base-pair level resolution. Only 11% of these variants were shown to have the potential to form gene-fusions and, of these, less than 20% were detected at the transcriptional level. Collectively, our findings indicate that although gene fusions and other SVs may be important factors in the onset and progression of ovarian cancer, it may not simply be the occurrence of these variants but their regulation that ultimately determines their biological and clinical significance.

Introduction

Cancer genomes are characterized by the presence of several classes of somatic mutations including point mutations, copy number alterations and chromosomal rearrangements or structural variants (SVs) (Lupski and Stankiewicz 2005; Pleasance et

al. 2010). Of these, SVs are the most frequent (Futreal et al. 2004; Stratton et al. 2009; Edwards 2010) and include tandem-duplications, inversions, deletions, insertions and inter-chromosomal translocations (Lupski and Stankiewicz 2005). Although cancer genomes may harbor hundreds to thousands of SVs, only a handful are considered of potential functional significance, typically involving protein-coding genes (Korbel et al. 2007; Stephens et al. 2009; Hillmer et al. 2011). Functionally significant SVs often involve gene-fusions that place protein coding genes under novel regulatory controls and/or result in the generation of novel fusion proteins (Rabbitts 1994; Rowley 2001; Mitelman et al. 2007). A well-known example is the reciprocal translocation between chromosome 9 and 22 resulting in expression of the *BCR-ABL* fusion protein in chronic myeloid leukemia (Nowell 1962; Rowley 1973; Lugo et al. 1990).

Advances in the application of the paired-end (or mate-pair) approach to high-throughput sequencing has made genome-wide surveys of genomic rearrangements possible (Korbel et al. 2007; Bashir et al. 2008; Campbell et al. 2008; Medvedev et al. 2009; Murphy et al. 2012) and recent studies have uncovered a number of new gene fusions and other SVs of potential functional significance in a variety of cancer genomes (Stephens et al. 2009; Quinlan et al. 2010; Hillmer et al. 2011; Jiao et al. 2011; Malhotra et al. 2013). However, the potential importance of gene-fusions and other SVs to cancer onset and progression would be compromised if these variants were not expressed. Indeed, recent studies have revealed that "normal" tissues can harbor transcriptionally repressed "pro-neoplastic" SVs that only become oncogenic when transcriptionally activated (Li et al. 2008). Thus, to fully evaluate the functional significance of gene fusions and other SVs in cancers, DNA sequence analyses should ideally be coupled with transcriptional profiling. In an effort to address this issue in ovarian cancer, we utilized an integrated computational workflow to analyze DNA sequencing and transcriptional profiling (RNA sequence and microarray gene expression data) data from six ovarian cancer patient samples. In addition, DNA sequence data from matched sets of control (whole blood) samples from

these patients were used to distinguish cancer SVs of germline origin from those arising somatically in the cancer cell lineage. We report here the detection of 10,034 ovarian cancer SVs (5518 germline derived; 4516 somatically derived) at base-pair level resolution. Only 11% of these variants were shown to have the potential to form gene-fusions and, of these, less than 20% were detected at the transcriptional level. Collectively, our results demonstrate the presence of large numbers of germline and somatically derived gene-fusions and other SVs in ovarian cancer tissues and underline the importance of processes regulating the expression of gene-fusions in cancer onset and progression.

Materials and Methods

Sequencing data acquisition

Whole genome sequencing (WGS) data for six ovarian serous cystadenocarcinoma and matched somatic control (whole blood) samples were selected from 'The Cancer Genome Atlas' (TCGA, http://cancergenome.nih.gov/) data portal (https://tcga-data.nci.nih.gov/tcga/) using dbGAP in BAM file format (see Supplementary Methods for more details).

WGS data consisted of a total of nearly 22 billion (minimum 1.3 billion – maximum 2.54 billion per sample) 75 - 100 bp long paired-end (in forward-reverse orientation) reads generated from Illumina GAII instrument. RNA-Seq data consisted of a total of nearly one billion (minimum 105 million - maximum 243 million per sample) 75 bp long paired-end reads generated from Illumina GA II system. Selected samples and sequencing data is summarized in Table C.1.

BAM files containing sequencing data were sorted using Picard tools' SortSam and converted to FastQ format using BamToFastQ program (http://genome.sph.umich.edu/wiki/BamUtil).

Genomic SV Detection using WGS

Massive amount of whole genome sequencing data presents a challenge in detecting complex structural variants with high-accuracy. In order to accurately detect and characterize genomic structural variants, we designed a streamlined workflow (summarized in Figure 4.1).

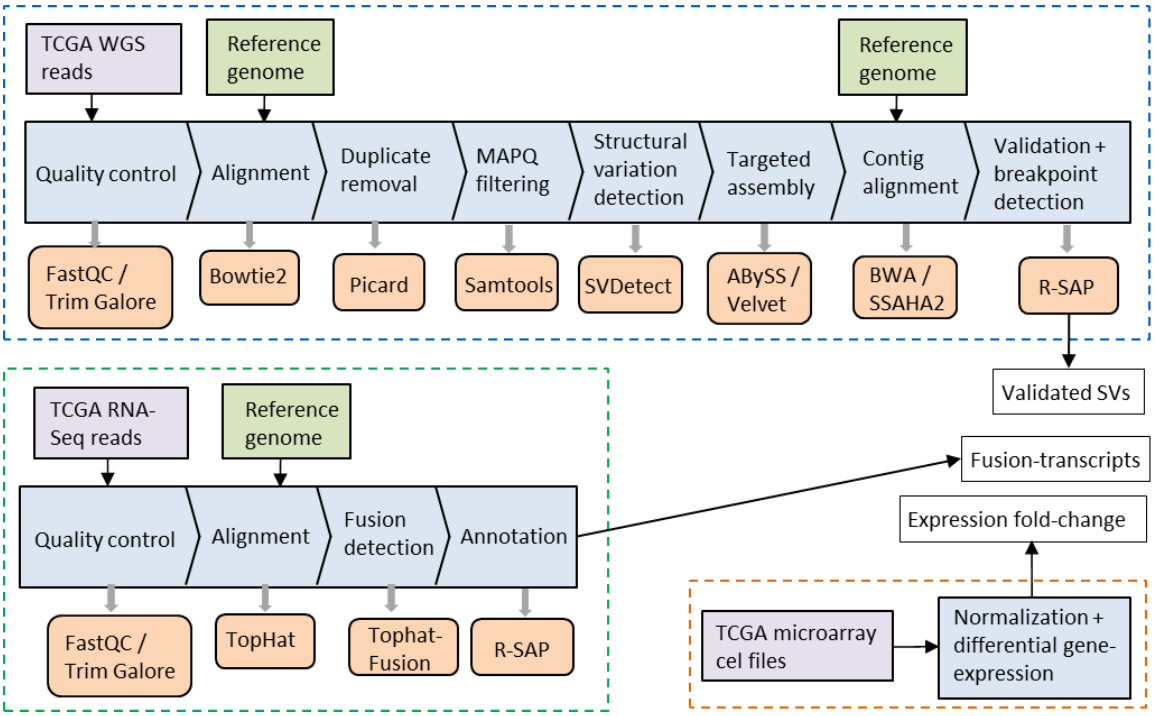

Figure 4.1. Integrative data analysis workflow for structural variants. The upper workflow summarizes detection and validation of SVs using whole genome sequence data. The bottom left workflow summarizes the detection of fusion-transcripts using RNA-Seq data. The estimation of differential gene-expression using microarray data is summarized in the bottom right of the figure.

The workflow for the WGS data is described as follows:

SV detection:

Overall quality of the WGS reads were assessed using FastQ. Low quality (Q < 20) bases and adapter sequences were removed from the ends of the reads. The remaining reads were aligned to the human reference genome hg19 (GRCh37 assembly, UCSC genome database) using Bowtie2 (Langmead and Salzberg 2012). Unmapped reads were stored in a separate file. PCR duplicates were removed from the alignment files using Picard tools' MarkDuplicate program. Since the highly repetitive/low complexity genomic regions may result in ambiguous or low confidence alignments, we filtered out all alignments with mapping quality (MAPQ) < 35. Various classes of large structural variants (SVs) were detected using SVDetect (Zeitouni et al. 2010). The SVDetect algorithm searches for clusters of paired-ends reads creating distinct signatures of structural variants in the alignment file. SV signatures are called if anyone or both of the inherent characteristic of paired-end sequencing constraints (i.e., library insert-size, alignment orientation of mates relative to each other) are violated. Based on the clusters of paired-end signatures, the SVs calls are generated and the location of breakpoints is estimated. Genomic loci involved in a SV (a.k.a."links") are required to be supported by a minimum number of paired-end reads as determined by the sequencing depth of coverage (Korbel et al. 2009). Since our samples have different sequencing depths of coverage, different cutoff values were determined for each sample (summarized in Table C.2).

Filtering:

We observed that more than 50% of the SV calls were 'small_duplications' that could be the result of artifacts generated during the library preparation. Thus, we conservatively removed such calls as well those described as 'co-amplicons' and 'undefined' calls generate from ambiguous paired-end signatures. We further removed all

the SV calls that had more than 50% overlap with the low-complexity genomic regions. Since, reference human genome quality is questionable around the centromere and telomere regions and near the assembly gaps, we also removed SVs mapping within 100 kilo base-pairs of these regions. Finally, we also removed called SVs that mapped either to mitochondrial or Y chromosome or currently un-localized regions of the genome ("Un", "hap", etc.).

Targeted assembly of SVs:

The paired-end read approach for SV detection does not provide base-pair level breakpoint information but rather provides genomic regions that may contain potential breakpoints. Also, short (75 – 100bp) read mapping to the reference genome may generate false clusters of paired-end reads resulting in false SV calls. In order to confirm SV calls generated by SVDetect and to detect the breakpoint at the base-pair resolution, we performed a targeted *de novo* assembly for each SV call. De novo assembly is performed by progressively merging redundant DNA sequences with shared overlapping ends determined by a pre-specified parameter called 'k-mer' length. The goal is to reconstruct the exact DNA sequence underlying the SV. For the assembly of each SV call, we included sequencing reads mapping within the 500 bps on either side of the genomic regions involved in an SV call. Also included are reads that initially could not be mapped to the reference genome. Since a complete assembly cannot be achieved using single k-mer length, we performed multiple k-mer length assemblies by varying k-mer from half of the read length (37 to 50 bp) to the complete read length (75 to 100 bps) in 2 bp increments. Multiple k-mer assemblies were performed using ABySS (Simpson et al. 2009) and later merged using Trans-ABySS (Robertson et al. 2010) that also removes redundant assembled sequences from the assembly. In order to further expand the assembly set, we performed multiple k-mer assemblies using an additional assembly program, Velvet (Zerbino and Birney 2008).

Validation and breakpoint detection:

Assembled DNA sequences (also called as contigs) were mapped to the human reference genome (hg19) using the BWA (Li and Durbin 2010) program that can independently align parts (also known as fragments) of a DNA sequence to discrete genomic loci. Such mapping is called split-mapping (Figure 4.2). Genomic coordinates of the paired-end based SV calls from SVDetect were compared with the fragmented alignments of the assembled contigs and breakpoints were determine for SV calls supported by the assembly. For each SV, two breakpoints are detected each corresponding to the genomic locus participating in the SV formation. Validation and breakpoint detection was carried out by using our previously developed pipeline, R-SAP (RNA-Seq analysis pipeline) (Mittal and McDonald 2012), that accurately detects fragmented alignments (split-mapping) representing potential gene-fusions and/or genomic rearrangements. R-SAP modules were slightly modified to include intragenic SVs such as deletions and insertions and other complex SV signatures such as transpositions that were not detected in the original R-SAP configuration. In order to minimize false SV calls supported by the assembly, the assembled contigs were aligned to the reference human genome using an additional alignment algorithm SSAHA2 (Ning et al. 2001), and the SVs again validated again using R-SAP. In this way, we with a stringently defined set of SVs for which breakpoints could be detected at the base-pair resolution.

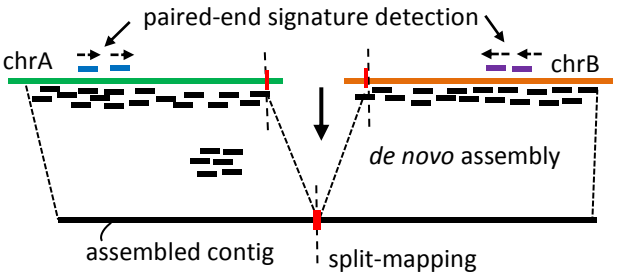

Figure 4.2. Validation and breakpoint detection. Assembly of a SV call representing a translocation event between two chromosomes (green and orange) is illustrated. SV calls are generated by SVDetect using paired-end signatures (blue and purple boxes represent paired-mates). Reads mapping to the genomic regions surrounding them (black boxes) are assembled using *de novo* assembly that also included initially unmapped reads. Assembled contigs shown here as a black line represent the DNA sequence underlying the translocation event. Contigs are mapped back to the reference genome and if split-mapping is observed, a SV call is considered validated and breakpoints (shown in red) are considered detected.

Fusion transcript detection using RNA-Seq

RNA-Seq reads obtained from TCGA were initially subjected to quality and adapter filtering using FastQC and TrimGalore. Reads were then aligned to the reference human genome in paired-end mode using TopHat using the 'fusion-search' mode. TopHat-fusion (Kim and Salzberg 2011) searches for potential breakpoints using the 'split-read' alignment of sequencing reads that are also supported by additional 'paired-end' reads. Potential fusions reported by TopHat were further evaluated using the reference transcript annotations that we defined as the merged set of Ensembl (version 73) and lncRNAs available from UCSC genome database(Hubbard et al. 2002; Karolchik et al. 2004; Cabili et al. 2011). We further required that each fusion be supported by at least one split-read and one paired-end read alignment. We conservatively discarded fusions where both ends of the fusion were confined to a single gene loci.

Gene-expression analysis

We downloaded gene-expression microarray data for the ovarian cancer samples using TCGA data portal. Due to the unavailability gene expression data from of our matched normal or control set, we utilized as a control microarray data form eight samples collected from healthy ovarian tissue from independent patients (described in Table C.3).

The microarray expression data was generated by RNA hybridization to the Affymetrix HT_HG-U133A gene chips and data files were provided in 'cel' format. Expression values were estimated and normalized by the RMA normalization method from the cel files using Affymetirx Expression Consol. For each gene, average expression across all of the eight normal samples and the average value is used as the denominator for the gene expression fold change calculation in ovarian cancer samples.

Results

DNA sequence analyses

More than 10,000 structural variants (SVs) identified in six ovarian cancer patient samples

DNA sequencing data of matched sets of six ovarian serous cystadenocarcinoma and six somatic control (whole blood) tissues were downloaded from the 'The Cancer Genome Atlas' (TCGA, http://cancergenome.nih.gov/) data portal (https://tcga-data.nci.nih.gov/tcga/) using dbGAP in BAM file format. The raw data consisted of 22 billion 75-100 bp paired-end reads (minimum 1.3 billion – maximum 2.54 billion per sample; Table C.1). An integrated computational workflow was developed to facilitate the data analysis (Figure 4.1, see Methods for details).

Initial alignments resulted in the mapping of 84% of the DNA-Seq reads to the human reference genome. A subsequent series of stringent filtering and validation steps (see Methods) resulted in a total of 35,721 SV calls. To confirm these SVs and to determine breakpoints at base-pair level resolution, targeted *de novo* assembly was performed for each SV call (Figure 4.2). After correcting for multiplicity of confirmed SVs (presence of the same SV across multiple samples), a total of 14,719 unique SVs were detected across all samples (Table C.4). Of these, 32% (4,685) were uniquely present in the somatic control (blood) samples, 31% (4,516) were uniquely present in the cancer samples and 37% (5518) were present in both the control and the cancer samples (Figure 4.3, Figure 4.4). We classified those SVs detected in both the cancer and somatic control samples as germline derived cancer variants since the presence of precisely the same SV in divergent somatic cell types implies a common clonal (germline) origin. Those SVs detected exclusively in the cancer samples were classified as somatically derived cancer variants arising in the cancer cell lineage. Of the 10,034 SVs detected in the cancer samples, 5518 or 55% were germline derived and 4516 or 45% were somatically derived.

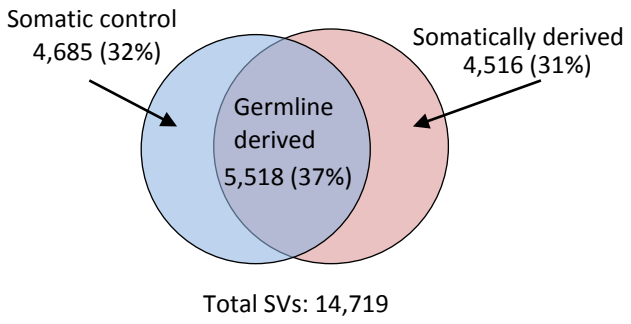

Figure 4.3. Comparison between germline and cancer SVs. Circles represent the total number of SVs detected in somatic control (whole blood) (blue circle) and cancer (red circle) tissue samples collected from six ovarian cancer patients. SVs corresponding to the overlap region identifies germline derived SVs while non-overlapping cancer SVs are somatically derived.

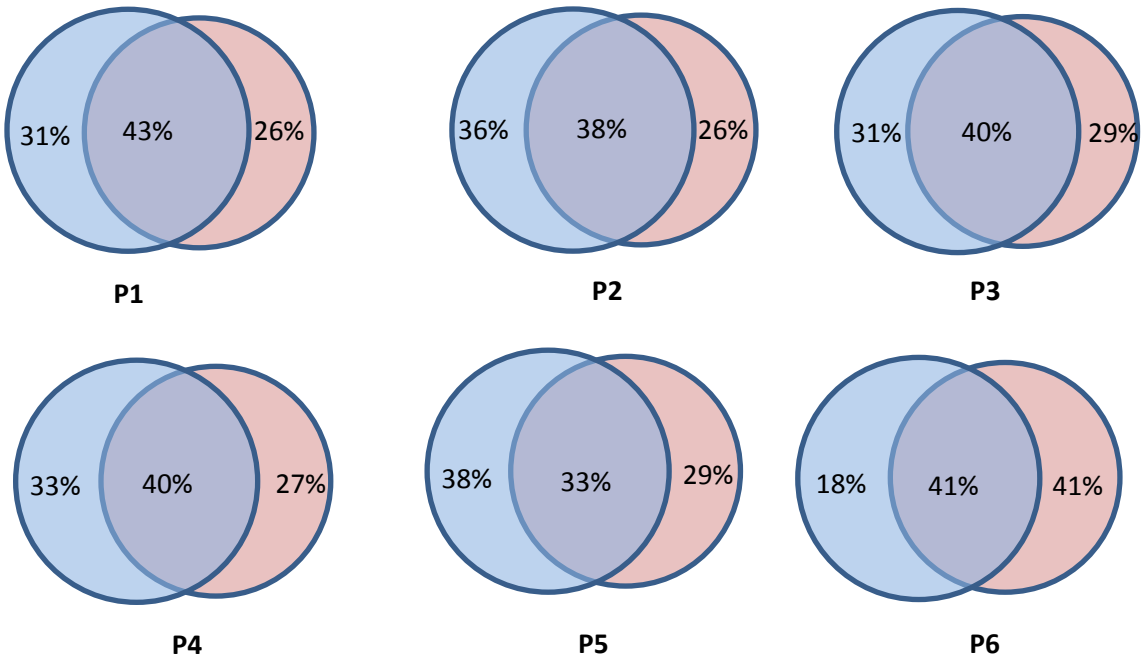

Patient Id	Somatic control	Somatically derived	Germline derived	Total
P1	711	616	986	2313
P2	1793	1316	1876	4985
P3	1414	1331	1859	4604
P4	1555	1238	1844	4637
P5	2126	1635	1866	5627
P6	654	1516	1478	3648

Figure 4.4. Comparison between germline and cancer SVs for individual patient samples. Circles represent the total number of SVs detected in somatic control (whole blood) (blue circle) and cancer (red circle) tissue samples collected from each of 6 ovarian cancer patients. SVs corresponding to the overlap region identifies germline derived SVs while non-overlapping cancer SVs are somatically derived.

The SVs were comprised of seven structural classes: inversions, transpositions, tandem-duplications (100 bps - 10 million bps in size), deletions (>20 bps), insertions (>20 bps), inverted-duplications and translocations. The distribution of these SVs across all samples is summarized in Figure 4.5. The most frequent class of SVs were deletions and germline derived deletions were >2X more frequent than somatically derived deletions. Germline and somatically derived inversions and transpositions were present in approximately equal frequencies while somatically derived SVs were more frequent than

germline derived variants for all other classes of SVs (insertions, inverted-duplications, and translocations).

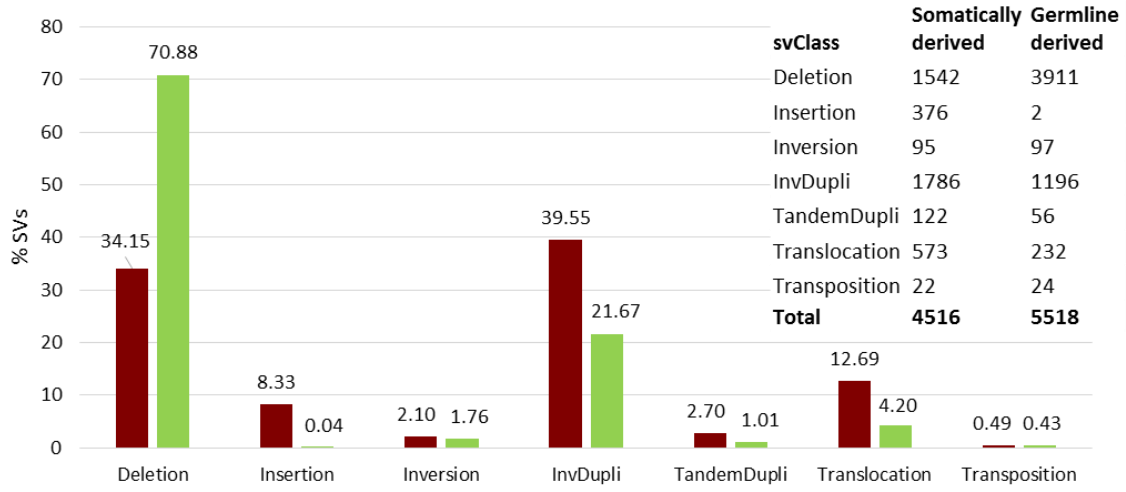

svClass	Somatically derived	Germline derived
Deletion	1542	3911
Insertion	376	2
Inversion	95	97
InvDupli	1786	1196
TandemDupli	122	56
Translocation	573	232
Transposition	22	24
Total	**4516**	**5518**

Figure 4.5. Distribution of SVs across structural categories. Somatically derived (red) and germline derived (green) SVs were further categorized according to the underlying genomic rearrangement. Deletions were the most abundant category accounting for the majority (~71%) of the germline derived SVs. Corresponding data is shown in the table (top right corner). InvDupli: inverted-duplications, TandemDupli: tandem-duplication.

Analysis of the frequency of recurrence of SVs across samples indicates that germline derived SVs have the highest rate of multiplicity (Figure 4.6). Nearly 55% of germline derived SVs are present in multiple patient samples reflecting naturally occurring variation in the human population. In contrast, only 6% of the somatically derived SVs were detected in more than one tissue sample.

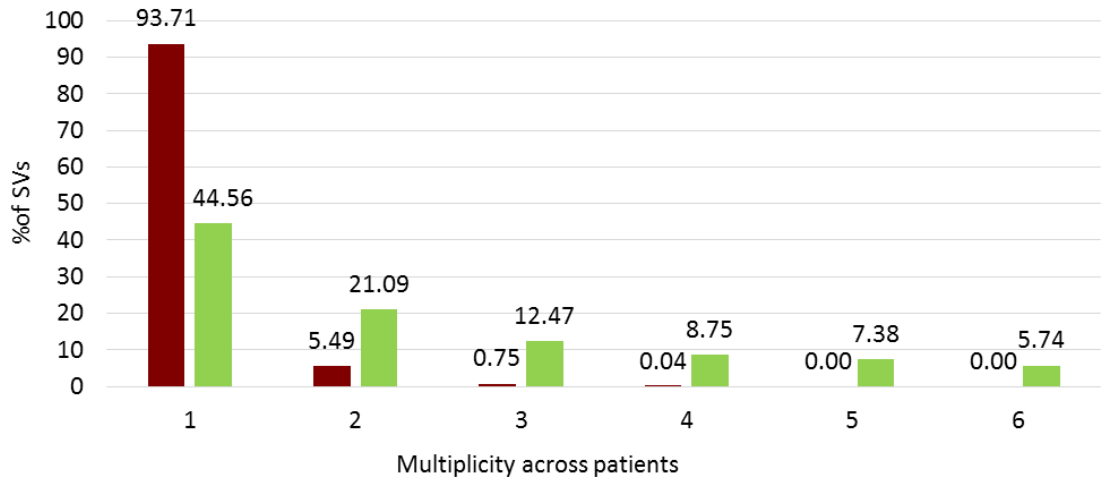

Multiplicity	somatically derived	germline derived
1	4232	2459
2	248	1164
3	34	688
4	2	483
5	0	407
6	0	317
Total	**4516**	**5518**

Figure 4.6. Multiplicity of SVs across samples. X-axis represents multiplicity (number of occurrences) of somatically derived (shown in red bars) and germline derived (shown in green bars) SVs across cancer samples. Y-axis represents percentage of SVs present in a particular multiplicity. Table at the bottom contains data corresponding to the figure.

Ovarian Cancer SVs can be divided into 3 groups based upon the location of chromosomal breakpoints

Detected SVs were annotated using a combined set of 224,555 normal reference transcripts (Ensembl annotations, release 73 and lncRNAs from the UCSC genome database). We classified SVs detected in our cancer samples into three groups based on the location of breakpoints relative to the reference transcripts as follows: inter-genic SVs are defined as variants with breakpoints mapping to two or more annotated genes located at distant genomic locations; intra-genic SVs are variants with breakpoints mapping

within a single annotated gene; and gene-desert SVs are variants with breakpoints mapping to distant locations within genomic regions devoid of annotated genes ("gene deserts") (Figure 4.7). Intra-genic SVs are the most abundant class (50%, 5,031/10,034) followed by gene-desert (39%, 3,942/10,034) and Inter-genic (11%, 1,061/10,034) SVs (Figure 4.8, Figure 4.9A). Inter-genic SVs are >2X more abundant among somatically derived variants than among germline derived variants (677 vs. 384, Figure 4.9B) while the number of intra-genic (2,151 vs. 2,880) and gene-desert SVs (1,688 vs. 2,254) are approximately equal among somatically derived and germline derived variants.

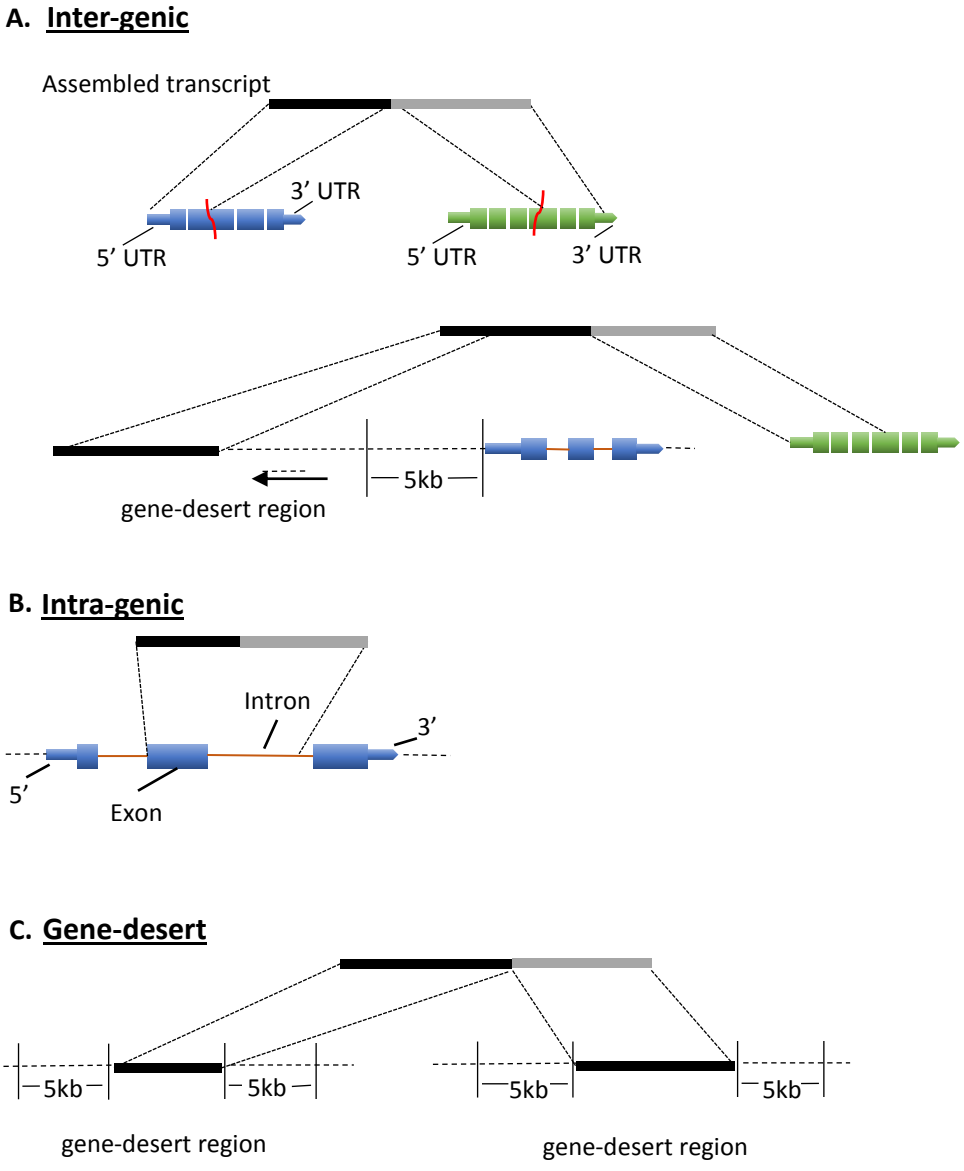

Figure 4.7. Structural classification scheme for SVs. SVs are depicted by black-grey boxes, reference transcripts are represented by the blue and green boxes. Thick boxes represent open-reading-frame or coding sequences (CDS) while thin boxes represent 5'UTR (on the left) and 3'UTR (on the right).
Inter-genic SVs (**A**) – breakpoints map to annotated genes located at distant genomic locations; intra-genic SVs (**B**)- breakpoints map within the same gene; gene desert (**C**)- breakpoints map to un-annotated genomic regions (gene deserts).

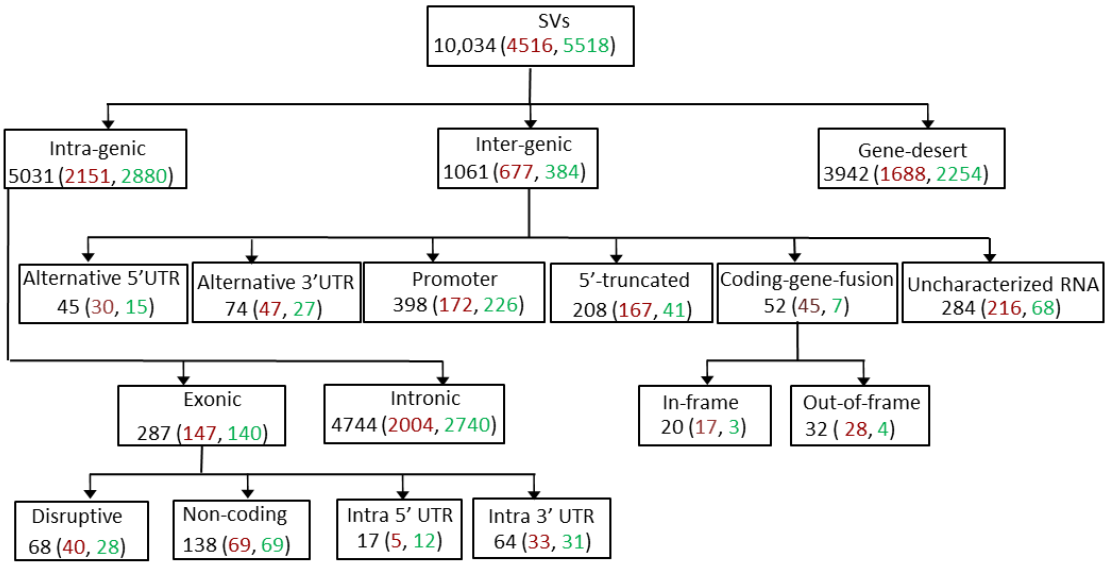

Figure 4.8. Characterization of SVs. Genomic coordinates of SVs and their breakpoint were compared with the reference transcripts that served as the basis of hierarchical classification into functionally relevant classes. The total number of SVs in each class is shown in black font while the numbers in parenthesis represent the distribution of somatically derived (red) and germline derived (green) SVs.

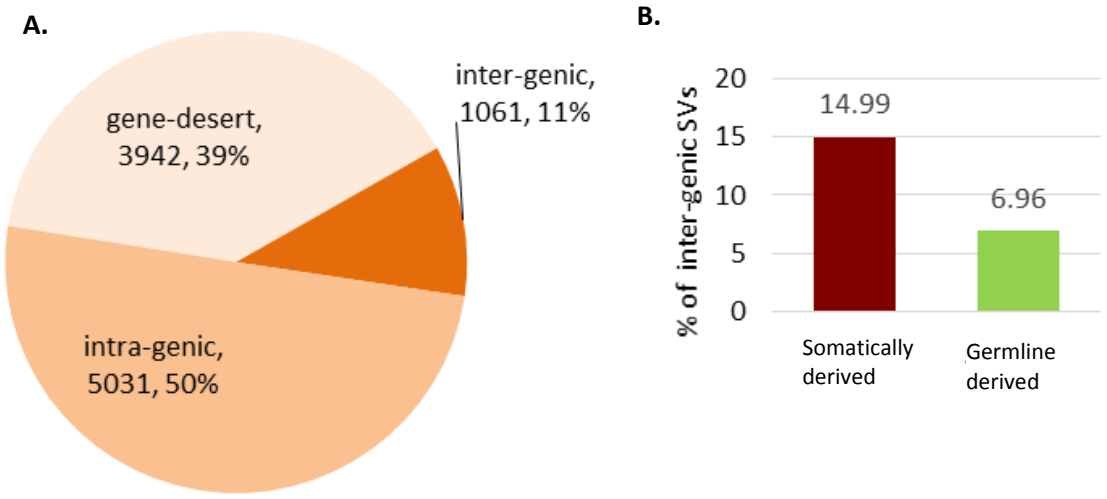

Figure 4.9. Distribution SVs across functional characterization classes. A. Distribution of total detected SVs among functional classes. **B.** Distribution of inter-genic SVs between somatically derived and germline derived SVs. Inter-genic SVs are significantly enriched (p-value < 0.05) for somatically derived variants.

Inter-genic SVs encompass multiple classes of fusion-genes

We further divided inter-genic SVs based on the location of breakpoints within the various gene regions, *i.e.*, the promoter region (defined as breakpoint regions within 5 kb up-steam of the transcriptional start site), the 5' and 3' untranslated leader regions (UTRs), and the protein coding sequence (CDS) (Table C.5). Inter-genic SVs where the 5'- partner gene sequence is fused with either a non-protein coding gene (*e.g.*, lncRNA) or with an unannotated region of the genome (gene-desert) are classified as 5' truncated SVs. Finally, inter-genic variants that do not manifest canonical gene structures (5'UTR-promoter-CDS-3'UTR), display gene components in incorrect orientation (*e.g.*, 5' UTR-CDS-promoter-3'UTR, gene desert-3' CDS, *etc*.) or otherwise cannot be functionally evaluated are classified as uncharacterized RNA (Table C.5).

The relative distribution of these sub-classes of inter-genic SVs in the cancer samples is shown in (Figure 4.10A). The most abundant (37%, 398/1061) sub-class of inter-genic variants is associated with alterations in the promoter region of genes. These altered promoter variants along with the less frequent alternative 5' UTR (4%, 45/1061) and 3' UTR (7%, 74/1061) sub-classes all have the potential to alter the expression of associated genes without altering coding sequences. Inter-genic SVs associated with the coding regions of genes also have the potential to alter the expression levels (e.g., the 5' partner gene typically provides the promoter region in addition to 5' coding sequences while the 3' partner may bring novel microRNA binding sites in its 3' UTR) but may also generate novel fusion proteins if reading frames are maintained. While only 5% (20/1061) of the inter-genic SVs involve the fusion of coding regions of different genes, 38% (20/52) of these variants were in frame. Interestingly, the vast majority of the in-frame gene fusions (85%, 17/20) were somatically rather than germline derived suggesting that these *de novo* SVs have either been selectively favored in the cancer cell

lineages or selected against in germline lineages or both. The majority of the coding region inter-gene fusions (62%, 32/52) were out-of-frame.

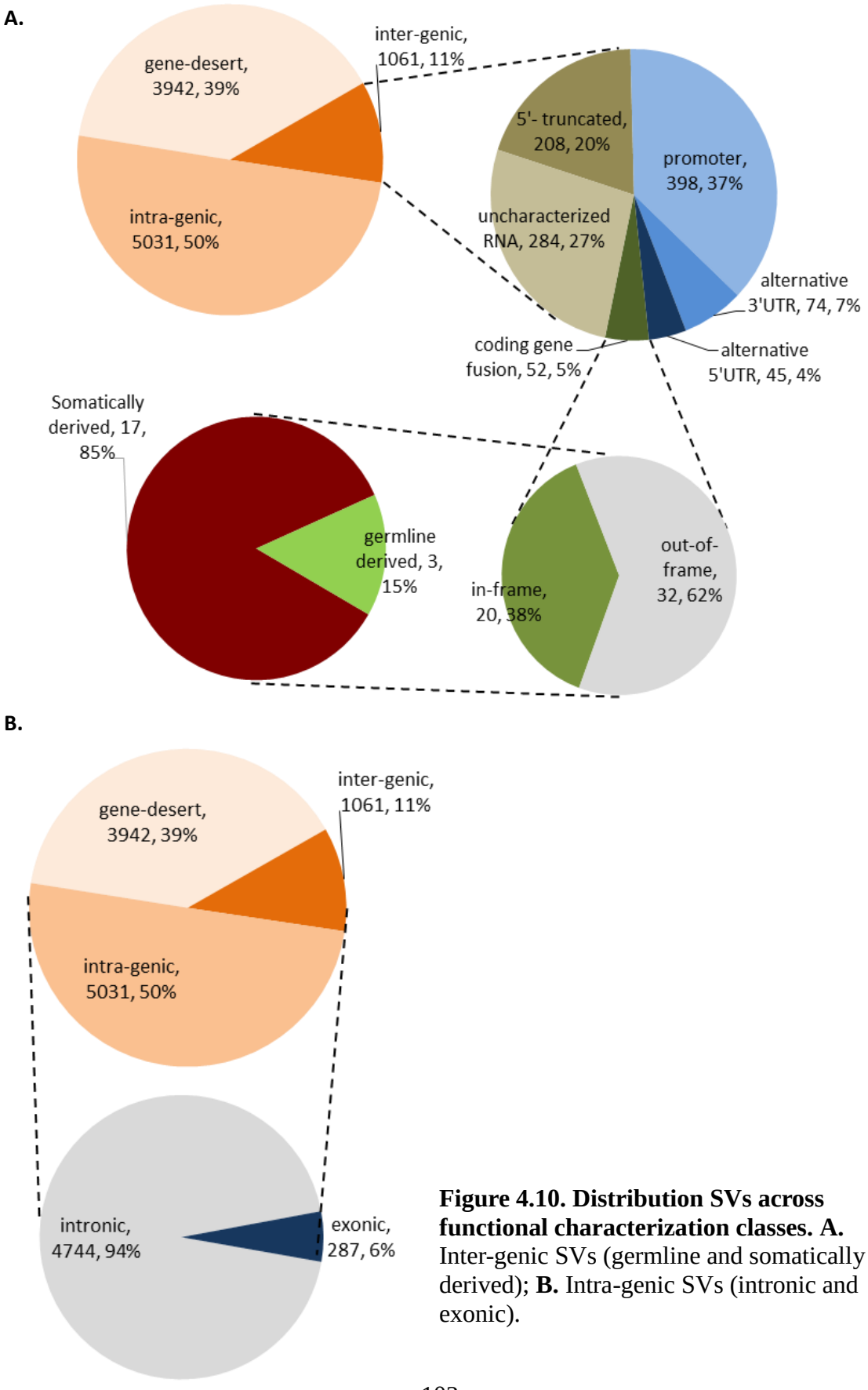

Figure 4.10. Distribution SVs across functional characterization classes. A. Inter-genic SVs (germline and somatically derived); **B.** Intra-genic SVs (intronic and exonic).

The breakpoints of most intra-genic SVs map to introns

The Intra-genic class of SVs was sub-divided into those with breakpoints mapping completely within the same intron (intronic) and those where at least one breakpoint mapped to an exon (exonic) . The vast majority of intra-genomic SVs (94%, 4,744/5,031) were intronic (Figure 4.10B, Table C.6). Although intronic variants may affect splicing functions, they do not affect coding regions *per se*. Only 6% (287/5,031) of the intra-genic SVs grouped into the exonic sub-class. The majority of these exonic variants (138/287 or 48%) mapped to non-protein coding genes (*e.g.*, lncRNAs) and are thus of currently undefined significance. The breakpoints of the remaining exonic variants mapped predominantly within 5' or 3' UTRs (5'UTRs: 17/287 or 6%; 3'UTRs: 64/287 or 22%). These intra-genic variants could potentially alter regulatory sequences involved in gene expression (e.g., upstream regulatory sequences in 5'UTRs or microRNA binding sites in 3'UTRs). The breakpoint of 24 % (68/287) of the exonic variants mapped to coding regions (CDS), which are presumed to disrupt the ORF and are labeled "disruptive" (Table C.6).

Many of the SVs map to gene desert regions

Although nearly 39% (3,942/10,034) of the detected SVs were classified as gene-desert variants (Figure 4.8, 4.9A), their potential functional significance cannot be reliably inferred since the structure of transcriptional units within gene-desert regions is currently unknown.

Gene expression analyses

A minority of gene fusions is transcribed

Inter-genic SVs have the potential to generate gene-fusions. Thus, in an effort to explore the extent to which this class of potential gene fusions were being expressed in our cancer samples, we downloaded from the TCGA data portal the results of RNA

sequencing (RNA seq) and microarray (Affymetrix) profiling studies carried out on these same samples. The raw RNA-seq data consisted of 1 billion 75 bp paired-end reads (minimum 105 million - maximum 243 million per sample) (Table C.1). These data were again analyzed using the computational workflow outlined in Figure 4.1 (see Methods for details).

Since inter-genic SVs with breakpoints mapping to the promoter region (398/1061) cannot be qualitatively distinguished using the RNA seq data, they were excluded from the RNA seq analysis but are included in the microarray expression analysis described below. All other classes of inter-genic SVs/gene fusions (coding region, 5' truncated, alternative 5' UTR, alternative 3' UTR and uncharacterized RNAs) were included in the RNA seq analysis. The breakpoints of these gene fusion transcripts were detected in the RNA-Seq data using split-read mapping (see Methods). Since introns are spliced out during mRNA processing and absent in the RNA-Seq data, we adjusted intronic SV breakpoints to the closest exon included in the gene fusion. SVs were categorized as "detected" by RNA seq if transcripts were found in at least one of the 6 cancer samples examined. Based on this criterion, 16% (103/663) of these potential gene fusions were found to be expressed in the cancer samples. The percentage of the transcribed germline derived fusions (19%, 30/158) was slightly higher than the somatically derived fusions (15%, 73/505) (Table C.1, Table C.7).

Only somatically derived coding sequence gene fusions are expressed

All 8 coding-gene fusions detected at the transcript level were somatically derived. Six of these fusions were in frame. In-frame fusions typically result in novel-fusion proteins that bring different protein domains together. We analyzed the rearrangement of protein domains resulting from the 6 in-frame gene fusions using

SMART database (http://smart.embl-heidelberg.de/) (Letunic et al. 2012). The fusion-gene structures and protein domain arrangements are shown in Figure 4.11.

A.

INTER-INV_TRANSLOC-UNBAL-chr2-115640273-115640523

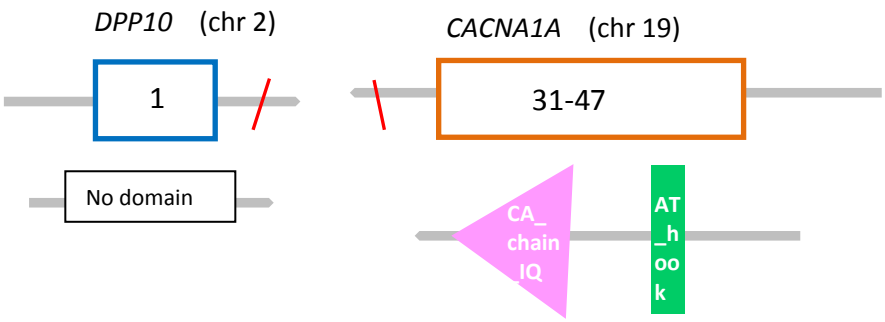

B.

INTRA-DELETION-UNBAL-chr1-32966800-32967047

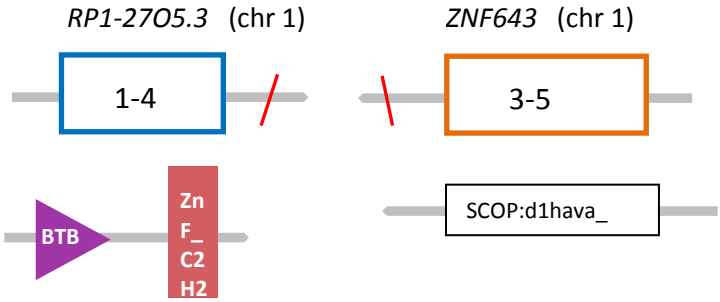

C.

INTRA-INVERSION-UNBAL-chr13-99068288-99068436

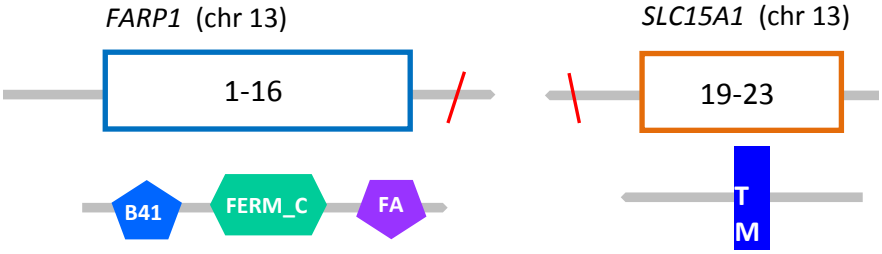

D.

INTRA-INVERSION-UNBAL-chr9-34244770-

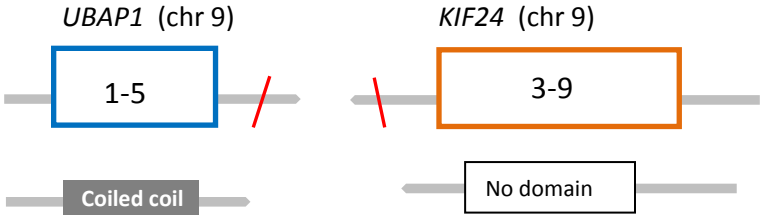

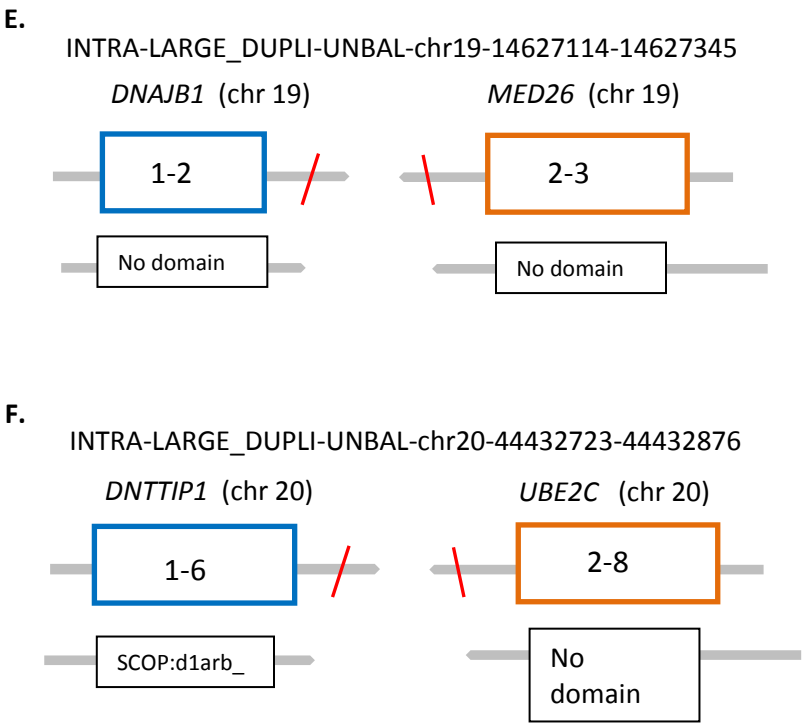

Figure 4.11. Structure of the six transcribed SVs resulting in in-frame gene-fusions. Figure represents the structure of the gene-fusion and associated protein domains. Square boxes with numbers represent exons (5' partner gene: blue, 3' partner gene: orange), red lines represent the fusion breakpoint, gene symbols corresponding chromosomes (in parenthesis) are shown on top of each gene fusion structure).

Two of the six in-frame gene fusions, *FARP1*-SLC15A1 (13q32.2 inversion) and *RP1-27O5.3–ZNF643* 1p34.2 - 1p35.1 deletion 1p34.2 - 1p35.1 deletion), resulted in a novel juxtaposition of protein-coding domains. The domains associated with the FARP1-SLC15A1 fusions are involved in a variety of signal transduction pathways that have previously been shown to influence cell-cell adhesion, cell migration and morphogenesis (Clucas and Valderrama 2014). Similarly, the BTB/POZ domain (Broad-Complex, Tramtrack and Bric a brac) contained within the region of the *RP1-2705.3* gene involved in the *RP1-27O5.3*–ZNF643 fusion has been previously implicated in ovarian cancer growth and recurrence (Nakayama et al. 2006). The potential functional significance of the remaining 4 somatically derived coding region gene fusions is currently unknown

(Figure 4.11). Other classes of transcribed inter-genic SVs include alternative 5' UTRs (4%, 2/45), alternative 3' UTRs (9%, 7/74), 5'-truncated (19%, 39/208), and uncharacterized RNAs (17%, 47/284) (Table 4.1, Table C.7).

Table 4.1. Summary of the number of the various types of SVs detected in the DNA sequencing analysis and their expression as detected by RNA seq or microarray studies (see text for details).

A. Somatically derived

	SVs (DNA level)	Transcribed	differential expression (microarray)	Total
5'-truncated	167	29	NA	29
coding-gene-fusion	45	8	NA	8
Uncharacterized RNA	216	33	NA	33
alternative 5'UTR	30	1	7	8
alternative 3'UTR	47	2	14	16
Promoters	172	NA	21	21
Total	**677**			**115**

B. Germline derived

	SVs (DNA level)	Transcribed	differential expression (microarray)	Total
5'-truncated	41	10	NA	10
coding-gene-fusion	7	0	NA	0
Uncharacterized RNA	68	14	NA	14
alternative 5'UTR	15	1	5	5[a]
alternative 3'UTR	27	5	4	8[a]
Promoters	226	NA	16	16
Total	**384**			**53**

[a] Overlap between RNA-Seq and microarray detection

Microarray analysis

Inter-genic SVs with breakpoints mapping within the promoter region or within the 5' or 3' UTRs leave coding regions unchanged but may be expected to alter patterns of gene expression. In order to search for possible quantitative changes in expression associated with these inter-genic SVs, we utilized the results of gene-expression microarray analyses downloaded from the TCGA data portal for the same six ovarian cancer patient samples (Note that the 5'-truncated, coding-region and uncharacterized RNA fusions are not distinguishable in microarray studies and thus were analyzed exclusively in the RNA seq analyses discussed above). Since gene expression profiles of normal ovarian tissue from these patient samples were not available, for controls, we downloaded and utilized the results of gene expression microarray profiles of normal ovarian tissue from 8 other age-matched women (Table C.3). Expression values were computed and normalized using the RMA normalization of the cel file data using the Affymetirx Expression Consol. Fold-change in expression relative to the average of the eight normal samples was computed for each of the genes associated with inter-genic altered promoters, as well as altered 5' and 3' UTRs SVs (Table 4.1, Table C.7).

Of the 517 (249 somatically derived and 268 germline derived) gene-fusions (promoter, alternative 5'UTR and alternative 3' UTR only) analyzed, 13% (42 somatically derived + 25 germline derived)/517) were differentially expressed (Table 4.1) including 37 that were up-regulated and 49 that were down-regulated relative to controls (Table C.7).

Chromosomal translocations are most frequently associated with changes in gene expression

Chromosomal translocations are the physical basis of gene fusions and, as shown in Figure 4.12, they are also the most frequent class of variants associated with significant

changes in gene expression both for somatically derived (61/122 or 50%) and germline derived SVs (30/65 or 46%). Although only 6% ((573 + 232)/ (4516 + 5518), Figure 4.5) of all SVs are associated with translocations, our transcriptional analysis indicates that they are the most likely class of SVs to be associated with changes in gene expression (Figure 4.12, Table 4.2, Table C.8).

Table 4.2. Summary of the number of various functional classes of SVs across multiple structural classes of SVs.

	Somatically derived		Germline derived	
svClass	All	Transcribed	All	Transcribed
deletion	92	17	154	16
insertion	13	2	0	0
inversion	45	10	17	4
inv-dupli	86	8	74	5
tandem-dupli	49	21	7	2
translocation	398	57	125	26
transposition	4	0	7	0
Total	**677**	**115**	**384**	**53**

A.

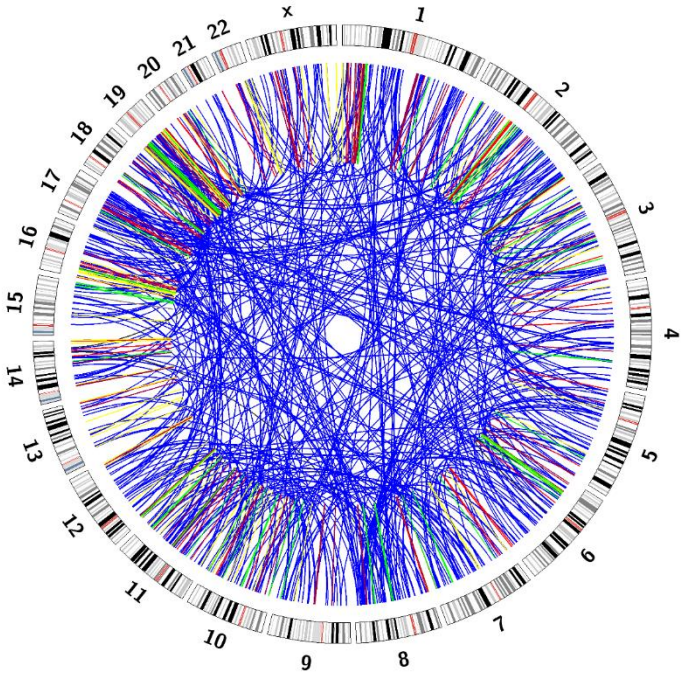
x
1
2
3
4
5
6
7
8
9
10
11
12
13
14
15
16
17
18
19
20
21
22

B.

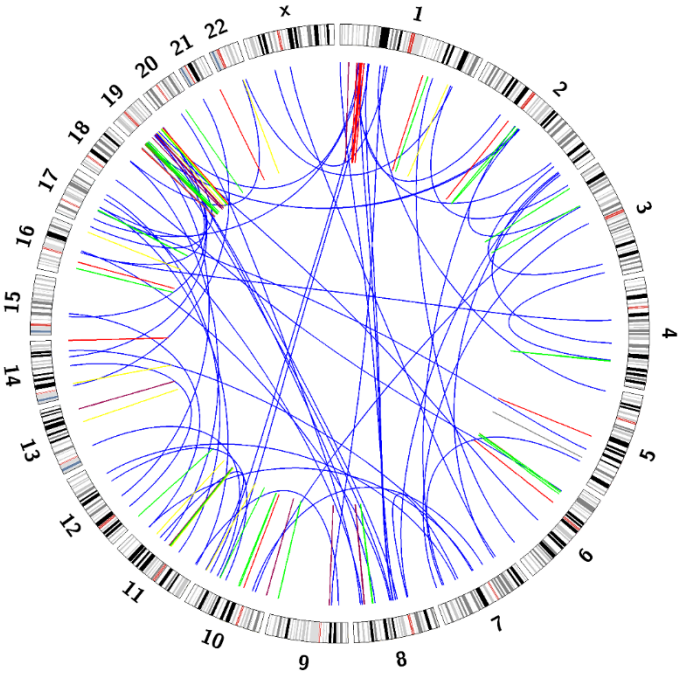
x
1
2
3
4
5
6
7
8
9
10
11
12
13
14
15
16
17
18
19
20
21
22

C.

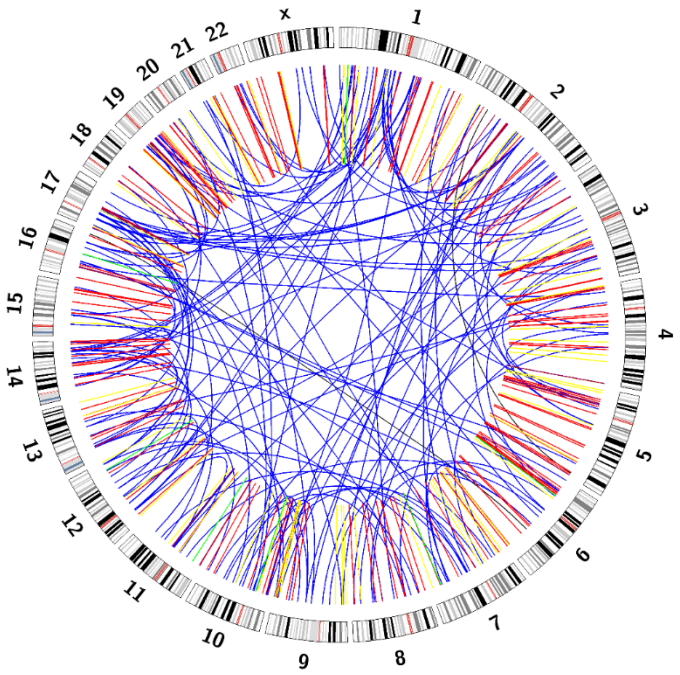

D.

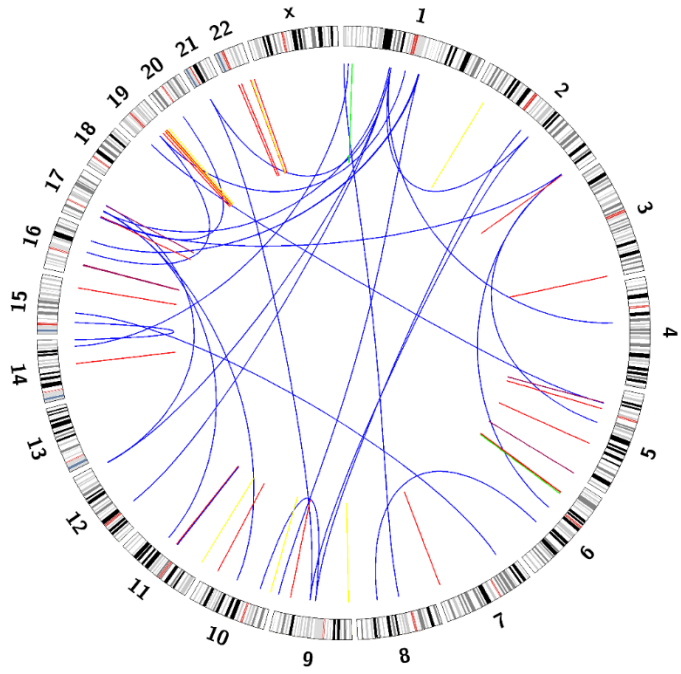

Figure 4.12. Genomic distribution of inter-genic SVs. A. displays the distribution of somatically derived inter-genic SVs, **B.** displays the distribution of those somatically derived inter-genic SVs that were either transcribed (detected using RNA-Seq) or resulted in differential gene-expression (measured using gene-expression microarrays). Similar distributions for germline derived SVs are shown in **C** and **D**. Each line (blue: translocation, red: deletion, green: tandem-duplication, yellow: inverted-duplication, orange: inversion, grey: insertion, dark grey: transposition) connecting two different chromosomes (outer circle) represents inter-chromosomal and straight lines restricted to a single chromosome represent intra-chromosomal rearrangements.

Discussion

In this study, we followed an integrated high-throughput computational workflow to accurately detect a remarkably large number (10,034) of SVs in cancerous tissue samples isolated from 6 ovarian cancer patients. This value is considerably larger than previous estimates of the number of SVs in other types of cancer tissues and cell lines (e.g., (Hillmer et al. 2011) possibly due to the greater accuracy afforded by our *de novo* assembly approach and/or because of the exceptional chromosomal instability known to be associated with ovarian cancers (Wang et al. 2012).

The majority (5518) of our identified SVs were determined to be of germline origin, apparently reflective of the abundance of naturally occurring SVs believed to be segregating in human populations (Conrad et al. 2010). An additional large number of the SVs (4516) identified in the ovarian cancer samples were determined to be of somatic origin arising *de novo* in the cancer cell lineage. Somatically derived SVs have recently been reported to constitute a major fraction of somatic tissue genetic variation in humans (O'Huallachain et al. 2012) and our findings are consistent with these reports.

While a major fraction of the SVs identified in our study were shown to map to un-annotated regions of the genome (gene deserts), the functional significance of these variants is currently unknown. In contrast, inter-genic SVs, while constituting only 11% of the SVs identified in our study, are the basis of gene-fusions- a well defined class of SVs demonstrated to be of functional significance in the onset and progression of a variety of cancers (Korbel et al. 2007; Stephens et al. 2009; Hillmer et al. 2011).

To our knowledge, ours is the first study to analyze both the presence and expression of SVs in the same panel of ovarian cancer patient samples. Among the most notable findings coming out of this comparative analysis is the remarkably low proportion of cancer SVs that are being transcribed. Only 20% of the gene fusions detected in our DNA seq analysis were detectable in the RNA seq analysis of the same samples. Remarkably, none of the germline derived gene fusions but all of the

somatically derived gene fusions were detectable on the RNA level. This observation suggests the existence of a regulatory mechanism or mechanisms that can effectively suppress those older more established SVs segregating in natural populations, but that is (are) lost or otherwise rendered ineffective in suppressing *de novo* variants arising in cancer cell lineages. Consistent with this possibility is the recent finding that a microRNA (miR-203) that targets and suppresses expression of the BCR-ABL fusion protein is hypermethylated in several hematopoietic tumors including chronic myelogenous leukemias and some lymphoblastic leukemias. Re-expression of this microRNA has been shown to significantly reduce BCR-ABL fusion protein levels and to coincidently inhibit tumor cell proliferation (Bueno et al. 2008). The relevance of such regulatory mechanisms to the fact that several gene fusions previously identified as biomarkers of cancer have recently been found to be present in normal healthy individuals (Nambiar and Raghavan 2013) remains to be determined.

Further evidence of the importance of the regulation of gene fusions and other SVs in cancer comes from our microarray analyses. We found that 10-30% of both germline and somatically derived fusions display a significant change in the expression of those genes involved in the fusion relative to normal controls. In several cases, changes in the expression of the protein coding domains involved in the fusions have been previously associated with cancer onset or progression.

Collectively, our findings are consistent with other recent studies indicating that gene fusions and other SVs may be more important factors in the onset and progression of cancer than previously envisioned (Robinson et al. 2011) . Our results further indicate, however, that it may not simply be the occurrence of these variants in cancers but their regulation that ultimately determines their biological and clinical significance.

Acknowledgements

The authors thank the Office of Information Technology at Georgia Institute of Technology for providing access to computing clusters at 'Partnership for an Advanced Computing Environment' (pace.gatech.edu) and Roman Mezencev (Georgia Institute of Technology) for his suggestions during the statistical analysis. This work was supported by grants from Ovarian Cycle, Deborah Nash Endowment Fund, Josephine Robinson Family and J.D. Rhodes Trust.

CHAPTER 5

CONCLUSIONS

In this dissertation work one of the most common mutations in cancer, gene-fusions, and their global patterns in breast and ovarian cancer was studied by using high-throughput DNA sequencing technologies. Chapter 2 describes the bioinformatics pipeline called R-SAP that we developed and implemented to systematically analyze and characterize cancer transcriptomes. In Chapter 3, R-SAP is integrated with additional, more specialized tools, to study gene-fusions in 55 breast cancer and healthy transcriptomes using RNA-Seq data. Overall a *de novo* assembly approach uncovered novel and potentially functional chimeric transcripts and revealed an unexpected prevalence and diversity of chimera in breast cancer tissues. In Chapter 4, gene-fusions are studied at the genome level using whole genome sequencing (WGS) data from ovarian cancer and matched somatic control samples. This study provides insight into the structure of genomic rearrangements underlying the gene-fusion structures observed in the cancer transcriptome. Further integration of RNA-Seq and WGS data analyses reveals the transcriptional consequences of germline and cancer specific structural variants.

Gene-fusion or chimeric transcripts that originate as a result of genomic rearrangements have been implicated in the onset and progression of a variety of cancers (Futreal et al. 2004; Lupski and Stankiewicz 2005; Mitelman et al. 2007). Recurrent gene-fusions that are also causally implicated in cancer are considered as potential biomarkers and therapeutic targets (Mitelman 2000; Laxman et al. 2008). Recent advancements in massively parallel RNA sequencing (or 'RNA-Seq') of the cellular transcriptome is a promising approach for the identification and characterization of fusion-gene transcripts (Maher et al. 2009a; Metzker 2010). Massive amounts of

sequencing data generated from the complex cellular transcriptome poses bioinformatics challenges that require highly specialized tools (Wang et al. 2013).

CHAPTER 2 presents our R-SAP program, a high-performance and highly-customizable user friendly bioinformatics pipeline for the analysis of RNA-Seq data. A built in multi-threading capability allows R-SAP to attain a near linear scalability in computation time while analyzing high-volumes of sequencing data. One of the characteristic features of the pipeline is its ability to accurately detect and annotate chimeric transcripts for their functional inference using a hierarchical characterization and classification system. R-SAP's applicability is demonstrated (CHAPTER 2) using MAQC human reference RNA-Seq data (Mane et al. 2009). Validation of the chimer-detection module shows 80% sensitivity using a curated set of 206 chimers from ChimerDB2.0 (Kim et al. 2010). The remaining 20% of reads were filtered out by R-SAP as 'ambiguous' fusions since they were originating from the repetitive regions of the genome.

In order for R-SAP to accommodate short (< 150 bp) sequencing reads such as those generated from Illumina and IonTorrent sequencing systems, we configured it to work with transcriptome assemblers such as Cufflinks, Scripture and Trans-ABySS. This compatibility is achieved by making use of the standard file formats such as GTF (Gene Transfer Format) or and BED (Browser Extensible Data) that are standard output from currently used assembly programs. We demonstrate the applicability of R-SAP to transcriptome assembly in CHAPTER 3 and further expand its applicability to whole genome sequence data analysis in CHAPTER 4.

While prior RNA-Seq studies have primarily focused on the canonical gene fusion structures of fusion-protein and promoter associated transcriptional deregulation, global patterns of chimers in cancer had yet to be explored. CHAPTER 3 presents the development and use of an integrated computational pipeline for the *de novo* assembly and comprehensive characterization of chimeric transcripts in 55 primary breast cancer

and normal tissue samples. *De novo* assembly resulted in longer contigs that not only provided greater accuracy in reference genome mapping but also allowed for more reliable identification of splice-variants because longer contigs typically extend across multiple exons. The integrated workflow developed in CHAPTER 3 demonstrates that specialized bioinformatics tools can complement each other and work synergistically. For example, although R-SAP has inherent filters to exclude ambiguous chimers, it cannot filter out the miss-assembled transcripts. But with a reconfirmation step using Bowtie and original RNA-Seq reads, we were able to significantly reduce R-SAP's false positive calls. By following a hierarchical functional classification, we were able to uncover a variety of fusion structure classes such as cryptic-splice sites and non-canonical RNA structures. Although, their functional consequences cannot be determine currently, their widespread presence is intriguing enough for further investigation.

Comparative analysis of chimeric transcripts between normal (or control) and cancer samples resulted in 269 shared chimeras. The presence of chimeric transcripts in normal samples is typically overlooked but their differential expression in cancer cells relative to the normal tissue is indicative of their 'pro-neoplastic' potential (Li et al. 2008). In CHAPTER 3, we identified four potential 'pro-neoplastic' fusions that involved protein-domains previously implicated in cancer. Such chimeric transcripts are potential candidates for use as biomarkers for early diagnosis..

Recent studies (Consortium et al. 2007; Qu and Fang 2013) have shown that transcription is not limited to genes. Previously considered 'gene-desert' regions can be transcribed in a highly cell type specific manner (Cabili et al. 2011; Prensner et al. 2011). In our study, we found that gene-desert regions can also participate in chimera formation and serve as alternative UTRs to known protein-coding genes resulting in altered gene-expression.

Gene-fusions predominantly result from genomic-rearrangements that are also known as structural variants (SVs). CHAPTER 4 presents the study of SVs in ovarian cancer using high-throughput whole genome sequencing data. Breakpoints associated with SVs were detected at the nucleotide level resolution by implementing an integrated computational workflow that also incorporates R-SAP (CHAPTER 2). Systematic and hierarchical characterization of SVs using the known gene-model revealed several non-canonical gene-fusion structures that were also observed in the breast cancer transcriptome (CHAPTER 3). The results provide evidence of the genomic origin of the diverse gene-fusion structures. Our analysis of genomic rearrangements in ovarian cancer also confirms our previous observation (CHAPTER 3) of participation of gene-desert regions in creating gene-fusion structures that can lead to transcriptional deregulation.

SVs are mainly associated with cancer but in our study we also observed SVs in the germline samples. We evaluated the differences in the functional significance between germline-derived and cancer specific (somatically derived) SVs at the transcriptional level using RNA-Seq and gene-expression microarray. Interestingly, somatically derived SVs are more likely to result in gene-fusion chimeric transcripts and also result in transcriptional deregulation as compared with the germline-derived SVs. For example, transcription of in-frame coding gene-fusions was detected only for somatically-derived cancer specific SVs and none for germline-derived SVs. Also, somatically derived SVs resulted in significantly higher numbers of transcriptionally deregulated genes than germline-derived SVs (CHAPTER 4). We suspected that the differences in functional consequences of SVs could be attributable to the differences in the structure of the underlying genomic rearrangements. We observed that the majority of the germline SVs were simple deletions, while somatically derived SVs were enriched for more complex genomic rearrangements such as translocations and tandem-duplications.

Overall we observed that out of all the detected SVs, only 11% result in potential gene-fusion structures and out of these, only 20% were detected at the transcriptional level. Additionally, only somatically derived in-frame coding-gene fusions are expressed (CHAPTER 4). Collectively, our results demonstrate the presence of large numbers of germline and somatically derived gene-fusions and other SVs in ovarian cancer tissues and the importance of processes regulating the expression of gene-fusions in cancer onset and progression.

APPENDIX A

SUPPLEMENTARY INFORMATION FOR CHAPTER 2

Supplementary Methods

Description of pipeline parameters that are adjusted in order to change the stringency during the pipeline run

- Percent identity cutoff: Minimum percent identity to call an alignment hit as high-scoring (default value is 95%). This cutoff is also the minimum identity required by each alignment pair in the chimeric transcript detection step.
- Percent coverage cutoff: Minimum alignment query coverage to call an alignment as high-scoring (default value is 90%).
- Deletion cutoff: Minimum number of skipped exonic bases from the reference genome due to the gapped alignment of query read before the read is characterized as exon-deletion (default value is 10 bp).
- Exon extension cutoff: Minimum number of extended bases outside the exon boundaries to characterize it as internal-exon-extension (if extension is in intron) or alternativeTSS or alternativePolyadenylation (if the extension is out of the transcriptional boundaries) (default value is two bp).
- Gene radius: Maximum extension of the known transcript in the upstream or downstream region to include intergeninc region mapped reads in the known gene models (default value is 5000 bp). This value can be set to zero if all the intergenic mapped reads need to be characterized as gene-desert.
- Gap tolerance: Maximum number of bases required on the query read before it is designated as chimeric transcript and searched for the alignment pair (default value is 20 bp). This cutoff is also the maximum allowed query bases between the fragmented alignments of the query sequence.

- Annotation mode: Two possible values; “unique”, “multi”. “Unique” is the default setting that will cause the pipeline to characterize each high-scoring read to only one best fitting known transcript. If set as “multi”, reads will be characterized with all the known transcripts the read mapped to.

Obtaining data from ChimerDB 2.0

ChimerDB 2.0 (http://ercsb.ewha.ac.kr:8080/FusionGen) (Kim et al. 2010) is a database of chimeric transcripts (or fusion gene transcripts) that are detected from the publicly available nucleotide sequences available in databases such as GenBank and SRA (short read archive). It also reports gene fusion pairs that are previously reported in literature. We downloaded GenBank accession IDs and corresponding fusion gene pairs for the chimeric transcripts present in ChimerDB 2.0. Downloaded fusion gene pairs were cross-referenced against the fusion gene pairs that were reported in literature and also available at Chimer DB 2.0. We retained only those GenBank accession IDs that had fusion gene pairs that were also reported previously in the literature. Nucleotide sequences for the retained GenBank accession IDs were obtained using nucleotide database (http://www.ncbi.nlm.nih.gov/nuccore) at NCBI. The resulting 206 sequences were defined as high-confidence dataset of chimeric transcripts that were used as the test data for testing the chimer detection module in R-SAP.

Raw RNA-Seq data cleaning

454 sequencing reads for MAQC Reference Human dataset were masked for low-complexity repeats (including simple repeats) using DustMakser (Morgulis et al. 2006) program before aligning them to the reference genome. Masked regions were trimmed using in-house perl scripts. Trimmed reads shorter than 20bp were excluded because of the BLAT’s (Kent 2002) limitation to align such sort reads with high accuracy.

Alignment screening and top-scoring hit selection

Command line BLAT (downloaded from http://users.soe.ucsc.edu/~kent/src/) generated psl and pslx output files don't have alignment percent identity, percent query sequence coverage and alignment score. These values were necessary for each alignment hit in order to sort and prioritize all possible reference genome hits for each sequencing read.

For alignment score and alignment percent identity calculations, we incorporated the code available at http://www.genome.ucsc.edu/FAQ/FAQblat.html#blat4 in our alignment-screening module.

Percent query coverage was calculated as:
((alignment end position in query- alignment start position in query)/(query length)) X 100

In order to obtain the best possible alignment (top-hit), all the alignment hits were sorted hierarchically first on alignment score, then on percent query coverage (if scores of the two alignment hits were equal) and finally on percent alignment identity (if coverage were equal).

Gene expression microarray data analysis

Cel files from Affymetrix Human U133Plus2.0 and Affymetrix Human Exon 1.0 ST V2 obtained from GEO (Gene Expression Omnibus at: http://www.ncbi.nlm.nih.gov/geo/) were analyzed using Affymetrix Expression Consol 1.1 provided on Affymetrix website www.affymetrix.com. Samples were RMA normalized, and transcript/gene level expression analysis and probe-set annotation was done using annotation files (hg18) downloaded from http://www.affymetrix.com/support/index.affx.

TaqMan qRT-PCR data analysis

Four replicates of TaqMan qRT-PCR measurements for MAQC Human Reference sample were obtained from GEO. Original dataset consisted of normalized expression values and their presence/absence calls for 1044 probes. Expression value for each probe was taken as the mean expression values across the four replicates. A probe was considered expressed if it had at least 75% presence call (present call in at least three replicates). 973 expressed probes were retained after the filtering. Expressed probes were then assigned to RefSeq transcripts (hg18) using TaqMan probe annotations provided under GEO's platform record for TaqMan (platform: GPL4097). 962 probes were successfully assigned to RefSeq transcripts and 727 of them were also detected (R-SAP RPKM > 0) in MAQC Human Reference RNA-Seq data.

ENCODE Gm12878 cell line RNA-Seq data analyses

Running TopHat:

TopHat v1.3.1 (Trapnell et al. 2009) (available at http://tophat.cbcb.umd.edu/) was used for the human reference genome (hg18) alignment of ENCODE Gm12878 RNA-Seq reads. TopHat was run as:

tophat -m 1 -F 0 -g 1 --coverage-search <bowtie_index> <input_fastq_file>

Using "–g 1" parameter, we allowed only uniquely mapped reads to be reported by TopHat. Overall 38,524,540 (out of 87,929,372) reads were mapped to the reference genome. TopHat outputs alignments in bam format that is used as input for Cufflinks (Trapnell et al. 2010).

Running Cufflinks:

a. Assembly mode:

Aligned reads from TopHat were assembled using Cufflinks v1.1.0 (available at http://cufflinks.cbcb.umd.edu/). Cufflinks was run as:

cufflinks -u -F 0.0 <tophat-alignments>

Transcriptome assembly resulted in 76,101 assembled transcripts. Cufflinks assembled transcripts are reported in GTF format that contains genomic coordinates of transcript an putative exons.

a. *Abundance quantification mode:*

In order to estimate the expression values of RefSeq (hg18) transcripts, we ran Cufflinks v1.1.0 in its quantification mode. Aligned reads from TopHat and RefSeq transcripts in GTF format were used as input for Cufflinks. Cufflinks was run as:
cufflinks -G Hg18RefSeq.gtf -u -F 0.0 --overhang-tolerance 3 <tophat-alignments>

Parameter "--overhang-tolerance 3" was used to match R-SAP's default cutoff for "exon-extension" (3 bp). Cufflinks reports abundance estimates as FPKM (fragments per kilobase of transcript per million fragments mapped) that are comparable to RPKM (reads per kilobase of transcript per million reads mapped) for single end read data.

Running Cuffcompare:

Cufflinks assembled transcripts (from previous step) were compared with RefSeq (hg18) transcripts using Cuffcompare. Cuffcompare is a module in Cufflinks program that compares multiple transcript sets (including reference transcripts) in order to generate transcript structural variant classifications. Cuffcompare was run as:

cuffcompare -r Hg18RefSeq.gtf -R -C <cufflinks-transcript-assembly>

Running RSEM:

RSEM v1.1.13 (Li and Dewey 2011) (available at http://deweylab.biostat.wisc.edu/rsem/) estimates transcript expression values by aligning RNA-Seq reads to reference transcript sequences. RSEM uses BowTie as an aligner that is run inherently from RSEM. In order to run RSEM, we supplied original fastq files for the Gm12878 RNA-Seq data and RefSeq (hg18) transcript sequences that were obtained using UCSC Table browser (http://genome.ucsc.edu/cgi-bin/hgTables).
RSEM was run in two steps:

1. Preparing reference transcript sequence index:
   rsem-prepare-reference <bowtie-path> <Hg18RefSeq.fa>

2. Estimating expression:

rsem-calculate-expression --out-bam --seed-length 28 <bowtie-path> --bowtie-n 3 --bowtie-e 200 --bowtie-m 1 --phred33-quals
--fragment-length-mean 200 --fragment-length-sd 80 <input-fastq-file> <reference-transcript-sequence-index>

Cufflinks default values for fragment length distribution mean and standard deviation were used for RSEM run. RSEM estimated
RSEM reports two measures of abundance estimates: Expected read count from each transcript and estimated fraction of transcripts made up by a given isoform or gene (τ value). τ value is generally converted to TPM (transcripts per million) by multiplying by 10^6 in order to get the expression value of transcripts. TPM value is not directly

comparable to RPKM or FPKM value. We converted TPM values to comparable RPKM values using the conversion formula provided in (Li and Dewey 2011):

$$RPKM_i = (10^9 x\ \tau_i)/(\sum_j \tau_i l_j)$$

Here i corresponds to the i^{th} RefSeq transcript and j varies from 1 to total number of RefSeq transcripts. l_j is the length (in bp) of j^{th} transcript.

Table A.1. Data sources and types of datasets that were used for the demonstration of R-SAP's application as well as its performance assessment and testing.

Data	Data type	Platform	Sample	Database	Database ID/Accession
MAQC RNA-seq	Single end sequencing reads	Roche 454	MAQC Universal Human Reference RNA (Sample A)	SRA (Short read archive at NCBI)	SRX002934 (Runs: SRR013995, SRR013996, SRR013997, SRR013998, SRR013999)
MAQC expression microarray	Cel files (intensities)	Affymetrix Human U133Plus2.0	MAQC Universal Human Reference RNA (Sample A)	GEO (Gene expression omnibus at NCBI)	GSM589512
MAQC TaqMan qRT-PCR	Normalized expression values	TaqMan Human MAQC (TAQ, platform id: GPL4097)	MAQC Universal Human Reference RNA (Sample A)	GEO (Gene expression omnibus at NCBI)	GSM129638, GSM129639 GSM129640, GSM129641
ENCODE RNA-seq	Paired end 75 bp long reads (insert length 200 bp)	Illumina Genome Analyzer	Gm12878 cell line complete Poly-A selected	UCSC DCC (UCSC ENCODE Data coordination center)	wgEncodeCaltechRnaSeqG m12878R2x75NaIl200Fast qRd1Rep1
ENCODE expression microarray	cel files (microarray intensities)	Affymetrix Human Exon 1.0 ST arrays	Gm12878 cell line	GEO (Gene expression omnibus at NCBI)	GSM472901

Table A.2. GenBank accession IDs for the 206 EST and mRNA sequences that were used as the high confidence test dataset for testing the chimer-detection module of R-SAP. 164 (~80% of 206) Accession IDs (in red color) were reported as chimer-transcripts by R-SAP.

AB000268.1	AF492832.1	AY624559.1	EU446645.1	AB300355.1
AB001342.1	AJ131466.1	AY624560.1	FM165197.1	AB300356.1
AB038155.1	AJ131467.1	AY633656.1	FM165198.1	AB300357.1
AB274722.1	AJ251843.1	AY803272.1	L03357.1	AF047022.1
AB275889.1	AJ251844.1	BC008826.1	L22179.1	AF125093.1
AF024541.1	AJ251845.1	D90075.1	M13096.1	AF143407.1
AF031404.1	AJ295163.1	DQ084494.1	M19730.1	AF186109.1
AF041811.2	AJ297349.1	DQ204770.1	M25946.1	AF230662.1
AF060927.1	AJ298917.1	DQ204771.1	M30829.1	AF231996.1
AF060928.1	AJ299261.1	DQ204772.1	M30832.1	AF254086.1
AF060929.1	AJ299262.1	DQ204773.2	M31213.1	AF272376.1
AF060930.1	AJ301611.1	DQ437654.1	M73779.1	AF295356.1
AF060931.1	AJ301612.1	DQ437655.1	S50916.1	AF297746.1
AF102845.1	AJ303089.1	DQ451148.1	S72478.1	AF297747.1
AF113911.1	AJ417079.1	DQ831522.1	S72604.1	AF310722.1
AF123094.1	AJ438986.1	DQ841178.1	S75763.1	AF390893.1
AF125808.1	AJ549094.1	DQ845345.1	S77574.1	AF524261.1
AF125809.1	AJ549095.1	DQ845346.1	U02308.1	AF533988.1
AF177236.1	AJ549096.1	DQ886024.1	U02368.1	AY186998.1
AF177237.1	AJ972402.1	DQ898313.1	U41814.1	AY380223.1
AF177238.1	AM491359.1	DQ898314.1	X03541.1	AY380226.1
AF177239.1	AM491360.1	DQ912588.1	X06418.1	D45915.1
AF186110.1	AM491361.1	DQ912589.1	X62947.1	EU327511.1
AF231995.1	AM491362.1	DQ912590.1	X98708.1	FM165196.1
AF254087.1	AM491363.1	EF051633.1	X98709.1	M82827.1
AF254088.1	AY040324.1	EF158045.1	X98710.1	S71225.1
AF272374.1	AY040555.1	EF374064.1	Y08643.1	S72479.1
AF272375.1	AY043457.1	EF406122.1	Y15913.1	S72621.1
AF272383.1	AY138857.1	EF423615.1	Y15914.1	S72865.1
AF272384.1	AY138858.1	EF525170.1	Y15915.1	S74529.1
AF272385.1	AY138859.1	EF632110.1	Y15916.1	S79325.1
AF297748.1	AY138860.1	EU090248.1	Y15917.1	S79332.1
AF297749.1	AY186997.1	EU090249.1	Y15918.1	S81242.1
AF364037.1	AY187920.1	EU216064.1	Y15919.1	U35622.2
AF373587.1	AY187921.1	EU216066.1	Y15920.1	U41743.1
AF395885.1	AY187922.1	EU216070.1	Y15921.1	X07537.1
AF422798.1	AY380222.1	EU216071.1	Y16346.1	X79200.1
AF477006.1	AY380224.1	EU236680.1	Z35761.1	X85960.1
AF487522.1	AY380225.1	EU236948.1	AB000267.1	
AF487905.1	AY624556.1	EU314929.1	AB001343.1	
AF487906.1	AY624557.1	EU364772.1	AB012575.1	
AF492831.1	AY624558.1	EU432099.1	AB300354.1	

Table A.3. Intron-retention events detected in MAQC Reference Human dataset using R-SAP from high-scoring reads that were also characterized as internal-exon-extension.

Characterization sub-category	Reads (Represented RefSeq transcripts)
Internal-exon-extension	18,419 (7,648)
Complete intron-retention	361 (275)
Total number of retained introns	305

Table A.4. Distribution of "multiple-annotations" reads that were detected in MAQC Reference Human dataset using R-SAP. Since more than one type of novel transcriptional event was detected in each of the "multiple-annotations" reads, reads representing characterization sub-categories here may be overlapping. "Exon-skipping" and "intron-retention" events are already included in "exon-deletion" and "internal-exon-extension" events.

Total Multiple-annotations	3020
Sub-categories (characterization)	Reads
Exon-deletion	2889
(Exon-skipping)	(579)
Internal-exon-extension	1867
(Intron-retention)	(13)
AlternativeTSS	563
AlternativePolyadenylation	782

Table A.5. Distribution of Trans-ABySS characterized reads that were also classified as "high-scoring" by R-SAP previously using MAQC Human Reference RNA-Seq data. RefSeq transcripts (hg18) were used as annotated set of transcripts. "novel-transcript" are those that could not be mapped to any of the known RefSeq exon by Trans-ABySS. Novel transcriptional event sub-categories (AS3, AS, AS53, novel_exon, novel_intron, novel_utr, retained_intron and skipped_exon) have 121 overlapping reads between them. Filtered-out reads are those that were not reported in any category by Trans-ABySS.

Sub-categories (characterization)	**Reads (% total "high-scoring")**	**Associated RefSeq transcripts**
AS3	1447 (0.29%)	960
AS5	1503 (0.30%)	1031
AS53	24 (0.004%)	22
novel_exon	608 (0.12%)	462
novel_intron	259 (0.05%)	212
novel_utr	357 (0.072%)	190
retained_intron	2 (0.0004%)	1
skipped_exon	768 (0.15%)	568
Total novel-transcriptional events (121 overlapping subtracted from the total sum)	4847(0.98%)	2548
Mapping within known exons	123066 (25.05%)	16211
Total exon-associated	127913 (26.04%)	18759
Novel-transcripts	144173 (29.35%)	NA
Total reported	272086 (55.4%)	18759
Filtered-out	219031 (44.6%)	
Total high-scoring	491117	

Table A.6. Distribution of transcripts that were assembled from ENCODE Gm12878 RNA-Seq data using Cufflinks and then characterized by R-SAP. RefSeq transcripts (hg18) were used as reference set of transcripts.

Sub-categories (characterization)	Reads (% Cufflinks assembled transcripts)	Represented RefSeq transcripts
Exon-skipping	1,389 (1.82%)	1,186
Exon-deletion	597 (0.78%)	548
AlternativeTSS	1,957 (2.57%)	4,382
Alternative Polyadenylation	2,848 (3.74%)	5,361
Internal-exon-extension	15,416 (20.25%)	6,744
Intron-retention	3,563 (4.68%)	2,059
Multiple-annotations (additional exon-skipping, exon-deletion, alternativeTSS, alternativePolyA, internal-exon-extension and intron-retention)	14,255 (18.73%)	7,667
Total novel-transcripts	40,025 (52.59%)	13,638
Exon-only	8,940 (11.74%)	8,275
Intron-only	10,172 (13.36%)	3,772
Neighboring-exons	3,166 (4.16%)	2,282
Gene-desert	8.582 (11.27%)	
Uncharacterized	5,216 (6.85%)	
Total Cufflinks assembled transcripts	76,101	

Table A.7. Distribution of transcripts that were assembled from ENCODE Gm12878 RNA-Seq data using Cufflinks and then classified by Cuffcompare into structurally variant classes of RefSeq transcripts (hg18).

Cuffcompare classification	Classification code	Number of reads (% of assembled transcripts)	Associated RefSeq transcripts
Potential novel-isoform	j	24,752 (32.52%)	9240
Full match + contained	=, c	14,015 (18.41%)	11046
Falling entirely within intron	i	10,149 (13.33%)	3765
Possible polymerase run (2kb away from reference transcript)	p	1,772 (2.32%)	1361
Unknown, intergenic	u	10,131 (13.31%)	0
Generic reference exon overlap	o	1,389 (1.82%)	1257
Exonic overlap (on opposite strand)	x	765 (1%)	586
Intron overlap (on opposite strand)	s	306 (0.4%)	297
Single exon with partial intron overlap (pre-mRNA fragment)	e	12,822 (16.84%)	4016
Total assembled transcripts		76,101	

Table A.8. Comparison between R-SAP's characterizations and Cuffcompare's classification of transcripts that were previously assembled from ENCODE Gm12878 RNA-Seq dataset using Cufflinks (also see Table 5 and Supplementary Table S6 and S7 for detailed distribution and comparison of other sub-categories).

R-SAP characterization	Cuffcompare classification(code)	Number of associated assembled transcripts		Overlap		
		R-SAP	Cuffcompare	#Reads	%Cuffcompare	%R-SAP
Exon-only	Complete match + contained (=,c)	8940	14015	8699	62%	97.3%
Intron-only	Intron-only (i)	10172	10149	10137	99.9%	99.6%
Neighboring-exon	Polymerase run (p)	3166	1772	1772	100%	55.6%
Gene-desert	Unknown-intergenic (u)	8582	10131	8582	84.71%	100%

Table A.9. Sequencing reads, reference genome alignment and R-SAP characterization statistics for the ENCODE RNA-seq data for Gm12878 cell line. RPKM values were estimated using exon-only reads that were also classified as high-scoring reads by R-SAP.

Category	Reads
Raw sequencing reads	87,929,372
Total reference genome mapped	54,095,800
Uniquely mapped	49,533,283
Multi-hits	4,562,517
High-scoring	32,815,685
Exon-only	22,390,589
Total RefSeq transcripts detected using Exon-only reads	24,080

Table A.10. New intronic-exons detected in human RefSeq transcripts (hg18) by R-SAP from intron-only reads in MAQC Reference Human RNA-Seq dataset.

Please see table on our website:
http://www.mcdonaldlab.biology.gatech.edu/dissertations/mittal.htm

APPENDIX B

SUPPLEMENTARY INFORMATION FOR CHAPTER 3

Supplementary Methods

RNA-Seq data pre-processing

Forty-five breast adenocarcinoma (BRCA) primary tumors and 10 adjacent normal breast tissue samples were selected from 'The Cancer Genome Atlas project' (TCGA) data portal) and subsequently RNA-Seq raw data files were downloaded from NCBI-SRA using dbGAP. RNA-Seq data files were downloaded 'sra' format that were further converted to FastQ format files using sra-toolkit (http://eutils.ncbi.nih.gov/Traces/sra/?view=software).

Filtering of the assembled contigs and chimer detection

Assembled contigs were aligned to the human reference human genome (hg19 from UCSC genome database) using 'Blast Like Alignment Tool (BLAT) (Kent 2002) that is a specialized program for aligning long RNA stretches to the reference genome. BLAT reports independent alignment of different fragments of the RNA sequences and allows long gaps in the alignment that can be representative of introns present in a RNA sequence. We observed the presence of short stretches of homopolymers (poly As and poly Ts) towards the ends of the assembled contigs. Such repeats may affect the overall alignment and may create ambiguous alignments. We, therefore, trimmed homopolymer repeats as well as other low complexity repeats detected using RepeatMasker (http://www.repeatmasker.org) and Tandem Repeat Finder (http://tandem.bu.edu/trf/trf.html,). Alignment files were exported in '.pslx' format from BLAT then were supplied to R-SAP as input for detecting chimeric transcripts. Chimeric transcripts result in fragmented (or split-) alignments where fragments of the chimeric

transcripts map to discrete genomic loci. R-SAP detects such alignments and derives the underlying fusion structure using the known gene models. We combined Ensembl and lncRNA annotations (available from UCSC genome database) in order to generate a comprehensive set of known gene models. R-SAP characterized each chimeric transcript based upon the genic regions (5'UTR, CDS or 3'UTR) of the reference transcripts intersecting with the genomic loci involved in the chimeric transcript formation.

Expression quantification

We performed a two-way expression estimation on the filtered set of 1959 chimeric transcripts. First we estimated the expression of the reference transcripts (comprised of Ensembl and lncRNA annotation set) that were involved in the chimer transcript formation. Reference transcript sequences were obtained from the UCSC genome database and filtered RNA-Seq reads were mapped using Bowtie. Alignment files were obtained in "bam" format that were sorted using Samtools (Li et al. 2009). Abundance was estimated as expected read counts by using RSEM ((RNA-Seq by Expectation Maximization) (Li and Dewey 2011). Expression values of reference transcripts were used to calculate the fold change of 5'- and 3'- UTR change associated chimers in cancer samples relative to the normal samples. Expression values were then normalized using "Upper quartile normalization" (Bullard et al. 2010).

In order to determine the "pro-neoplastic" potential chimeric transcripts (see main text), we relied upon the expression of the chimeric transcript itself rather than the associated reference transcripts. We estimated the expression of shared (detected in normal and cancer samples) in each of the corresponding samples. RNA-Seq reads were mapped to the assembled contig representing the chimera and read counts were then estimated using RSEM. Read counts were normalized using upper-quartile normalization as proposed by Bullard et al. (Bullard et al. 2010). Expression fold change in cancer

relative to normal was computed using the average expression values measured across cancer and normal samples.

Table B.1. Summary statistics on raw and processed RNA-Seq data from the 55 breast samples used in this study. Additional columns contain statistics on assembled contigs, initial and final number of chimeric transcripts after filtering. The first sheet in the excel file contains the data columns and a key describing the data is on the second excel sheet.

Please see table on our website:
http://www.mcdonaldlab.biology.gatech.edu/dissertations/mittal.htm

Table B.2. Detailed alignment and annotation information on 1959 filtered chimeric transcripts from 55 samples analyzed in the study. Each chimeric transcript is represented by a unique ID in the first column. Structural and functional classification (as described in the text) information is presented in columns S, T and U. Cells in the gene name columns ('geneName1' and 'geneName2') with value "none" represent gene-desert regions. The first sheet in the excel file contains the data columns and a key describing the data is on the second excel sheet.

Please see table on our website:
http://www.mcdonaldlab.biology.gatech.edu/dissertations/mittal.htm

Table B.3: Distribution of structural and functional classes for chimers found only in normal tissue samples. (A similar table for cancer specific chimers is included in the main text.)

	inter-genic	gene-desert-I	gene-desert-II	**Total**
fusion-protein	9	NA	NA	9
3' truncated-protein	22	4	NA	26
5' UTR-change	6	2	NA	8
3'UTR-change	18	1	NA	19
cryptic splice-site	41	6	NA	47
novel RNA	39	6	1	46
Total	135	19	1	155

Table B.4: Distribution of structural and functional classes for chimeras found in both normal and in cancer tissue samples. (A similar table for cancer specific chimers is included in the main text.)

	inter-genic	gene-desert-I	gene-desert-II	**Total**
fusion-protein	23	NA	NA	23
3' truncated-protein	53	4	NA	57
5' UTR-change	6	0	NA	6
3'UTR-change	52	0	NA	52
cryptic splice-site	33	15	NA	48
novel RNA	79	4	0	83
Total	246	23	0	269

Table B.5: Recurrence of chimeric transcripts across cancer samples. Recurrence is defined as the number of samples in which a specific chimeric transcript was detected. The frequency is the chimeric transcript count divided by the total number of chimeric transcripts.

Recurrence	frequency	percentage
1	1309	93.97
2	55	3.95
3	17	1.22
4	5	0.36
5	5	0.36
6	1	0.07
7	0	0.00
8	0	0.00
9	1	0.07
Total	**1393**	

Table B.6. Cancer specific in-frame fusions where at least one protein domain from each (5' and 3') of the participating genes is covered by the ORFs involved in the chimera formation. Protein domain names (as defined by SMART database) are present in columns K and T. The first sheet in the excel file contains the data columns and a key describing the data is on the second excel sheet.

Please see table on our website:
http://www.mcdonaldlab.biology.gatech.edu/dissertations/mittal.htm

Table B.7. Cancer specific in-frame fusions where 3' partner gene is up-regulated by > 2X relative to the intact gene in normal tissue samples. Expression is the normalized RNA-Seq read counts as estimated using RSEM and followed by upper quartile normalization. Expression fold change for the 3'- gene is present in column U. The first sheet in the excel file contains the data columns and a key describing the data is on the second excel sheet.

Please see table on our website:
http://www.mcdonaldlab.biology.gatech.edu/dissertations/mittal.htm

Table B.8. Cancer specific chimeric transcripts with fused 5' or 3' UTRs and having the ORF of the coding gene intact and displaying > 2X change in expression relative to the intact gene's expression in normal tissue. The first sheet in the excel file contains the key defining column entries. The second sheet contains data for chimeras with a fused 5' UTR; the third sheet contains data for chimeras with a fused 3' UTR. For 5'-UTR fusions, the expression fold change for the 3' partner gene is calculated; for 3' UTR fusions, the expression fold change for the 5' partner gene is calculated. The upper portion in each data sheet summarizes the down-regulated genes and the lower portion summarizes the up-regulated genes.

Please see table on our website:
http://www.mcdonaldlab.biology.gatech.edu/dissertations/mittal.htm

Table B.9. Detailed information for gene-desert-I and gene-desert-II chimeric transcripts. The first sheet of the excel file contains the key defining column entries. The data for cancer specific, normal control and shared chimeric transcripts is presented separately in second, third and fourth sheets, respectively. Cells in the gene name columns ('geneName1' and 'geneName2') with value "none" represent gene-desert regions.

Please see table on our website:
http://www.mcdonaldlab.biology.gatech.edu/dissertations/mittal.htm

Table B.10. Chimeric transcripts comprised of in-frame fusion gene transcripts present in both normal and cancer samples. Expression levels are presented as normalized RNA-Seq read counts as estimated using RSEM and upper quartile normalization. The first sheet of the excel file contains the key defining column entries. The second sheet presents the chimeric transcript annotation information. Third sheets presents the expression values across normal and cancer samples respectively. The structures of these fusion genes is presented in Figure 3.15.

Please see table on our website:
http://www.mcdonaldlab.biology.gatech.edu/dissertations/mittal.htm

APPENDIX C

SUPPLEMENTARY MATERIAL FOR CHAPTER 4

Supplementary Methods

Preprocessing of the whole-genome sequence (WGS) data

Whole genome sequencing data from TCGA was downloaded in BAM format that also contains metadata about the sequencing libraries. We noticed that the presence of multiple read-group in each BAM file. Read-groups are typically generated as a result of multiple sequencing runs of the, use of multiple lanes on the sequencer or difference in sequencing library preparation protocol for the same sample. For each BAM file, we collected the more precise information on read-group insert-size distribution by using SortSam (http://picard.sourceforge.net/command-line-overview.shtml#SortSam) followed by http://picard.sourceforge.net/command-line-overview.shtml#CollectInsertSizeMetrics.

Read-groups with the similar mean insert-size and similar insert-size distributions were merged into single read-groups. Merging of the read-groups resulted in two read-groups per sample. Estimated mean insert-size and standard-deviation for the insert-size for each group are summarized in Supplementary Table 2. Since intra-chromosomal variants detection is done by considering the insert-size and standard-deviation of the distribution into account, downstream analysis (up to the SV (structural variant) breakpoint detection using *de novo* assembly) was done on per 'read-group basis. After the breakpoint detection, validated SVs from multiple read-groups were merged using the SV structure and breakpoint information and a non-redundant set of validated SVs was created for each sample.

Inclusion of unmapped reads in the *de novo* assembly of SVs

After reference genome alignment of the WGS reads, on an average there were 300 million reads that were left unmapped. A subset of these reads may represent those that are spanning the breakpoints of SVs. So we included the unmapped reads in the de novo assembly of each SV. Since, on average, there were 19,500 SVs, it was not feasible to include all of the unmapped reads for the assembly of each SV. Instead, we defined a subset, called 'neighborhood junction reads', of all the unmapped reads for each SVs. Unmapped reads were mapped to the reference genome using the 'local alignment' mode of BowTie2 (Langmead and Salzberg 2012). Unmapped reads that were mapping partially within the 500 bp region around the SVs, were selected for the *de novo* assembly.

Trimming of assembled contigs

We observed the presence of simple or low-complexity repeats around the edges of the assembled contig resulting from the *de novo* assembly. Such repeats can create in false or ambiguous 'split' mapping structures during the reference genome alignment and can result in false SV validation calls. Also, they can increase the alignment time significantly since human genome is enriched with simple We, therefore, detected these repeats at the edges of contigs using RepeatMasker (http://www.repeatmasker.org) and TRF (Tandem Repeat Finder)(Benson 1999) and trimmed off using custom Perl script.

Table C.1. Summary statistics on processed whole genome sequencing data and detected structural variants from 12 samples (6 control (whole blood), 6 cancer patient samples). Additional columns include statistics on reference genome alignment, SV detections, assembled contigs and validation rate of SVs and number of RNA-Seq reads. First sheet in the excel file contains the keys describing the data columns in the second sheet.
Please see table on our website:
http://www.mcdonaldlab.biology.gatech.edu/dissertations/mittal.htm

Table C.2. Table describing read-groups in the ovarian WGS data and various cutoffs used for the SV detection. Each sample is represented by two read-groups that were originally determined by TCGA following the manual merging of the similar read-groups. Mean insert-size, standard deviation of the insert-size distribution and SVDetect cutoff were empirically derived using the reference genome alignment of paired-end WGS reads. First sheet in the excel file describes the data columns in the second sheet.

Please see table on our website:
http://www.mcdonaldlab.biology.gatech.edu/dissertations/mittal.htm

Table C.3. Summary of the ovarian samples used to perform the microarray gene-expression by TCGA. Each sample is represented by two read-groups that were originally determined by TCGA following the manual merging of the similar read-groups. Mean insert-size, standard deviation of the insert-size distribution and SVDetect cutoff were empirically derived using the reference genome alignment of paired-end WGS reads. First sheet in the excel file describes the data columns in the second sheet.

TCGA sample Id	Tissue	Tissue source	Microarray chip version
TCGA-01-0628-11A	ovary	Solid Tissue Normal	Affymetrix HT_HG-U133A
TCGA-01-0630-11A	ovary	Solid Tissue Normal	Affymetrix HT_HG-U133A
TCGA-01-0631-11A	ovary	Solid Tissue Normal	Affymetrix HT_HG-U133A
TCGA-01-0633-11A	ovary	Solid Tissue Normal	Affymetrix HT_HG-U133A
TCGA-01-0636-11A	ovary	Solid Tissue Normal	Affymetrix HT_HG-U133A
TCGA-01-0637-11A	ovary	Solid Tissue Normal	Affymetrix HT_HG-U133A
TCGA-01-0639-11A	ovary	Solid Tissue Normal	Affymetrix HT_HG-U133A
TCGA-01-0642-11A	ovary	Solid Tissue Normal	Affymetrix HT_HG-U133A
TCGA-04-1371-01A	ovary	Primary solid Tumor	Affymetrix HT_HG-U133A
TCGA-13-0723-01A	ovary	Primary solid Tumor	Affymetrix HT_HG-U133A
TCGA-13-0725-01A	ovary	Primary solid Tumor	Affymetrix HT_HG-U133A
TCGA-13-0751-01A	ovary	Primary solid Tumor	Affymetrix HT_HG-U133A
TCGA-13-0890-01A	ovary	Primary solid Tumor	Affymetrix HT_HG-U133A
TCGA-13-1411-01A	ovary	Primary solid Tumor	Affymetrix HT_HG-U133A
TCGA-24-0982-01A	ovary	Primary solid Tumor	Affymetrix HT_HG-U133A
TCGA-24-1103-01A	ovary	Primary solid Tumor	Affymetrix HT_HG-U133A
TCGA-25-1319-01A	ovary	Primary solid Tumor	Affymetrix HT_HG-U133A

Table C.4. Detailed alignment and annotation information on 14,719 validated SVs from 12 ovarian samples (6 control (whole blood) and 6 ovarian cancer patient samples) analyzed in the study. The table contains 4,516 somatically derived, 5,518 germline derived and 4,685 somatic control SVs that were originally detected by SVDetect and later validated using *de novo* assembly. This table is a non-redundant table i.e. corrected for the multiplicity of SVs across samples and frequency across samples is recorded in column O, P and Q. Each SV is represented by a unique Id in the first column that is followed by columns with SV class, genomic coordinates and breakpoint information for the SV. Columns T ('headTx')to AA ('tailGeneStrand') contain information on the genes that overlap SV breakpoints were 'NA' indicates no overlap with any known gene. Last three columns define SVs characterization and functional classification. First sheet in the excel file contains the keys describing data columns in the second sheet.

Please see table on our website:
http://www.mcdonaldlab.biology.gatech.edu/dissertations/mittal.htm

Table C.5. Table summarizing the potential functional impacts each class of inter-genic SV.

Functional class	potential functional impacts	Detectable by RNA-Seq?
altered promoter	Change in gene-expression	No
alternative 5'UTR	Change in gene-expression	Yes
alternative 3'UTR	Change in gene-expression	Yes
5'-truncated	C-terminal truncated protein from the 5'- (or head) gene, gene-expression may also change	Yes
coding-gene-fusion (in-frame)	Will encode for a fusion-protein	Yes
coding-gene-fusion (out-of-frame)	will undergo NMD	Yes
uncharacterized RNA	function cannot be inferred but will potentially form structural RNAs	Yes

Table C.6. Distribution of somatically and germline derived SVs that were characterized as intra-genic SVs. SVs were classified based on the location of breakpoints within the same gene. Since intra-genic SVs do not create gene-fusions, they were not pursued in the RNA-Seq and gene-expression microarray analysis.

Characterization class	somatically derived	germline derived
exonic	**147**	**140**
5'UTR	5	12
3'UTR	33	31
disruptive	40	28
non-coding	69	69
intronic	2004	2740
Total	**2151**	**2880**

Table C.7. Somatically and germline derived inter-genic SVs that were detected by RNA-Seq or resulted in differential gene-expression as measured by microarray. The table is divided in two parts, Table 7a contains transcription detected by RNA-Seq; Table 7b contains SVs resulting in differential gene-expression measured by microarray. Each table is presented in a different excel sheet. Upper half of the sheet contains 'somatically derived' SVs and lower half contains 'germline derived' SVs. Two additional sheets contain keys describing the data columns present in Table 7A and 7B.

Please see table on our website:
http://www.mcdonaldlab.biology.gatech.edu/dissertations/mittal.htm

Table C.8. Detailed distribution of functional classes of inter-genic SVs among various structural classes of SVs. Structural classes of SVs are 'deletion', 'insertion', 'inversion', 'inverted-duplication', 'tandem-duplication', 'translocation' and 'transposition'. Table 8A (upper half) contains data for somatically derived SVs while Table 8B (lower half) belongs to germline derived SVs.

Please see table on our website:
http://www.mcdonaldlab.biology.gatech.edu/dissertations/mittal.htm

REFERENCES

ACS ACS. 2013. Cancer Facts & Figures 2013. In *Atlanta: American Cancer Society; 2013*.

Akiva P, Toporik A, Edelheit S, Peretz Y, Diber A, Shemesh R, Novik A, Sorek R. 2006. Transcription-mediated gene fusion in the human genome. *Genome research* **16**(1): 30-36.

Alsafadi S, Scott V, Pautier P, Goubar A, Lazar V, Dessen P, Lacroix L, Duvillard P, Morice P, André F et al. 2011. Identification of SORBS2 as a Candidate Marker To Predict Metastatic Relapse in Breast Cancer [abstract]. In *American Association for Cancer Research*, Vol 71, pp. P5-01-07.

Aparicio SA, Caldas C, Ponder B. 2000. Does massively parallel transcriptome analysis signify the end of cancer histopathology as we know it? *Genome biology* **1**(3): REVIEWS1021.

Aplan PD. 2006. Causes of oncogenic chromosomal translocation. *Trends in genetics : TIG* **22**(1): 46-55.

Asmann YW, Hossain A, Necela BM, Middha S, Kalari KR, Sun Z, Chai HS, Williamson DW, Radisky D, Schroth GP et al. 2011. A novel bioinformatics pipeline for identification and characterization of fusion transcripts in breast cancer and normal cell lines. *Nucleic acids research* **39**(15): e100.

Asmann YW, Necela BM, Kalari KR, Hossain A, Baker TR, Carr JM, Davis C, Getz JE, Hostetter G, Li X et al. 2012. Detection of redundant fusion transcripts as biomarkers or disease-specific therapeutic targets in breast cancer. *Cancer research* **72**(8): 1921-1928.

Ayala I, Giacchetti G, Caldieri G, Attanasio F, Mariggio S, Tete S, Polishchuk R, Castronovo V, Buccione R. 2009. Faciogenital dysplasia protein Fgd1 regulates invadopodia biogenesis and extracellular matrix degradation and is up-regulated in prostate and breast cancer. *Cancer research* **69**(3): 747-752.

Barthel SR, Gavino JD, Wiese GK, Jaynes JM, Siddiqui J, Dimitroff CJ. 2008. Analysis of glycosyltransferase expression in metastatic prostate cancer cells capable of

rolling activity on microvascular endothelial (E)-selectin. *Glycobiology* **18**(10): 806-817.

Barzilai A, Rotman G, Shiloh Y. 2002. ATM deficiency and oxidative stress: a new dimension of defective response to DNA damage. *DNA repair* **1**(1): 3-25.

Baselga J, Tripathy D, Mendelsohn J, Baughman S, Benz CC, Dantis L, Sklarin NT, Seidman AD, Hudis CA, Moore J et al. 1996. Phase II study of weekly intravenous recombinant humanized anti-p185HER2 monoclonal antibody in patients with HER2/neu-overexpressing metastatic breast cancer. *Journal of clinical oncology : official journal of the American Society of Clinical Oncology* **14**(3): 737-744.

Bashir A, Volik S, Collins C, Bafna V, Raphael BJ. 2008. Evaluation of paired-end sequencing strategies for detection of genome rearrangements in cancer. *PLoS computational biology* **4**(4): e1000051.

Benson G. 1999. Tandem repeats finder: a program to analyze DNA sequences. *Nucleic acids research* **27**(2): 573-580.

Berger MF, Levin JZ, Vijayendran K, Sivachenko A, Adiconis X, Maguire J, Johnson LA, Robinson J, Verhaak RG, Sougnez C et al. 2010. Integrative analysis of the melanoma transcriptome. *Genome research* **20**(4): 413-427.

Birney E Stamatoyannopoulos JA Dutta A Guigo R Gingeras TR Margulies EH Weng Z Snyder M Dermitzakis ET Thurman RE et al. 2007. Identification and analysis of functional elements in 1% of the human genome by the ENCODE pilot project. *Nature* **447**(7146): 799-816.

Boboila C, Jankovic M, Yan CT, Wang JH, Wesemann DR, Zhang T, Fazeli A, Feldman L, Nussenzweig A, Nussenzweig M et al. 2010. Alternative end-joining catalyzes robust IgH locus deletions and translocations in the combined absence of ligase 4 and Ku70. *Proceedings of the National Academy of Sciences of the United States of America* **107**(7): 3034-3039.

Bongarzone I, Vigneri P, Mariani L, Collini P, Pilotti S, Pierotti MA. 1998. RET/NTRK1 rearrangements in thyroid gland tumors of the papillary carcinoma family: correlation with clinicopathological features. *Clinical cancer research : an official journal of the American Association for Cancer Research* **4**(1): 223-228.

Boquett JA, Alves JR, de Oliveira CE. 2013. Analysis of BCR/ABL transcripts in healthy individuals. *Genetics and molecular research : GMR* **12**(4): 4967-4971.

Boveri T. 1914. Zur Frage der Entstehung Maligner Tumoren. *Gustav Fischer*: 1-64.

Bueno MJ, Perez de Castro I, Gomez de Cedron M, Santos J, Calin GA, Cigudosa JC, Croce CM, Fernandez-Piqueras J, Malumbres M. 2008. Genetic and epigenetic silencing of microRNA-203 enhances ABL1 and BCR-ABL1 oncogene expression. *Cancer cell* **13**(6): 496-506.

Bullard JH, Purdom E, Hansen KD, Dudoit S. 2010. Evaluation of statistical methods for normalization and differential expression in mRNA-Seq experiments. *BMC bioinformatics* **11**: 94.

Cabili MN, Trapnell C, Goff L, Koziol M, Tazon-Vega B, Regev A, Rinn JL. 2011. Integrative annotation of human large intergenic noncoding RNAs reveals global properties and specific subclasses. *Genes & development* **25**(18): 1915-1927.

Campbell PJ, Stephens PJ, Pleasance ED, O'Meara S, Li H, Santarius T, Stebbings LA, Leroy C, Edkins S, Hardy C et al. 2008. Identification of somatically acquired rearrangements in cancer using genome-wide massively parallel paired-end sequencing. *Nature genetics* **40**(6): 722-729.

Carninci P, Yasuda J, Hayashizaki Y. 2008. Multifaceted mammalian transcriptome. *Current opinion in cell biology* **20**(3): 274-280.

Cerione RA, Zheng Y. 1996. The Dbl family of oncogenes. *Current opinion in cell biology* **8**(2): 216-222.

Chen ST, Choo KB, Hou MF, Yeh KT, Kuo SJ, Chang JG. 2005a. Deregulated expression of the PER1, PER2 and PER3 genes in breast cancers. *Carcinogenesis* **26**(7): 1241-1246.

Chen Z, Trotman LC, Shaffer D, Lin HK, Dotan ZA, Niki M, Koutcher JA, Scher HI, Ludwig T, Gerald W et al. 2005b. Crucial role of p53-dependent cellular senescence in suppression of Pten-deficient tumorigenesis. *Nature* **436**(7051): 725-730.

Cheung NK, Zhang J, Lu C, Parker M, Bahrami A, Tickoo SK, Heguy A, Pappo AS, Federico S, Dalton J et al. 2012. Association of age at diagnosis and genetic mutations in patients with neuroblastoma. *JAMA : the journal of the American Medical Association* **307**(10): 1062-1071.

Clucas J, Valderrama F. 2014. ERM proteins in cancer progression. *Journal of cell science* **127**(Pt 2): 267-275.

Conrad DF, Pinto D, Redon R, Feuk L, Gokcumen O, Zhang Y, Aerts J, Andrews TD, Barnes C, Campbell P et al. 2010. Origins and functional impact of copy number variation in the human genome. *Nature* **464**(7289): 704-712.

Consortium EP Birney E Stamatoyannopoulos JA Dutta A Guigo R Gingeras TR Margulies EH Weng Z Snyder M Dermitzakis ET et al. 2007. Identification and analysis of functional elements in 1% of the human genome by the ENCODE pilot project. *Nature* **447**(7146): 799-816.

Cooke MS, Evans MD, Dizdaroglu M, Lunec J. 2003. Oxidative DNA damage: mechanisms, mutation, and disease. *FASEB journal : official publication of the Federation of American Societies for Experimental Biology* **17**(10): 1195-1214.

Cormen T, Stein C, Rivest R, Leiserson C. 2001. *Introduction to Algorithms*. McGraw-Hill Higher Education.

Cory S. 1986. Activation of cellular oncogenes in hemopoietic cells by chromosome translocation. *Advances in cancer research* **47**: 189-234.

Costa V, Angelini C, De Feis I, Ciccodicola A. 2010. Uncovering the complexity of transcriptomes with RNA-Seq. *Journal of biomedicine & biotechnology* **2010**: 853916.

Dean M. 2009. ABC transporters, drug resistance, and cancer stem cells. *Journal of mammary gland biology and neoplasia* **14**(1): 3-9.

Deutsch EW, Lam H, Aebersold R. 2008. PeptideAtlas: a resource for target selection for emerging targeted proteomics workflows. *EMBO reports* **9**(5): 429-434.

Druker BJ, Sawyers CL, Kantarjian H, Resta DJ, Reese SF, Ford JM, Capdeville R, Talpaz M. 2001. Activity of a specific inhibitor of the BCR-ABL tyrosine kinase

in the blast crisis of chronic myeloid leukemia and acute lymphoblastic leukemia with the Philadelphia chromosome. *The New England journal of medicine* **344**(14): 1038-1042.

Duncan TJ, Rolland P, Deen S, Scott IV, Liu DT, Spendlove I, Durrant LG. 2007. Loss of IFN gamma receptor is an independent prognostic factor in ovarian cancer. *Clinical cancer research : an official journal of the American Association for Cancer Research* **13**(14): 4139-4145.

Edwards PA. 2010. Fusion genes and chromosome translocations in the common epithelial cancers. *The Journal of pathology* **220**(2): 244-254.

Fletcher JI, Haber M, Henderson MJ, Norris MD. 2010. ABC transporters in cancer: more than just drug efflux pumps. *Nature reviews Cancer* **10**(2): 147-156.

Flicek P, Amode MR, Barrell D, Beal K, Billis K, Brent S, Carvalho-Silva D, Clapham P, Coates G, Fitzgerald S et al. 2014. Ensembl 2014. *Nucleic acids research* **42**(Database issue): D749-755.

Flouriot G, Brand H, Seraphin B, Gannon F. 2002. Natural trans-spliced mRNAs are generated from the human estrogen receptor-alpha (hER alpha) gene. *The Journal of biological chemistry* **277**(29): 26244-26251.

Forbes SA, Bhamra G, Bamford S, Dawson E, Kok C, Clements J, Menzies A, Teague JW, Futreal PA, Stratton MR. 2008. The Catalogue of Somatic Mutations in Cancer (COSMIC). *Current protocols in human genetics / editorial board, Jonathan L Haines [et al]* **Chapter 10**: Unit 10 11.

Forbes SA, Bindal N, Bamford S, Cole C, Kok CY, Beare D, Jia M, Shepherd R, Leung K, Menzies A et al. 2011. COSMIC: mining complete cancer genomes in the Catalogue of Somatic Mutations in Cancer. *Nucleic acids research* **39**(Database issue): D945-950.

Frenkel-Morgenstern M, Lacroix V, Ezkurdia I, Levin Y, Gabashvili A, Prilusky J, Del Pozo A, Tress M, Johnson R, Guigo R et al. 2012. Chimeras taking shape: potential functions of proteins encoded by chimeric RNA transcripts. *Genome research* **22**(7): 1231-1242.

Fu X, Fu N, Guo S, Yan Z, Xu Y, Hu H, Menzel C, Chen W, Li Y, Zeng R et al. 2009. Estimating accuracy of RNA-Seq and microarrays with proteomics. *BMC genomics* **10**: 161.

Fugazzola L, Pilotti S, Pinchera A, Vorontsova TV, Mondellini P, Bongarzone I, Greco A, Astakhova L, Butti MG, Demidchik EP et al. 1995. Oncogenic rearrangements of the RET proto-oncogene in papillary thyroid carcinomas from children exposed to the Chernobyl nuclear accident. *Cancer research* **55**(23): 5617-5620.

Fujita PA, Rhead B, Zweig AS, Hinrichs AS, Karolchik D, Cline MS, Goldman M, Barber GP, Clawson H, Coelho A et al. 2011. The UCSC Genome Browser database: update 2011. *Nucleic acids research* **39**(Database issue): D876-882.

Futreal PA, Coin L, Marshall M, Down T, Hubbard T, Wooster R, Rahman N, Stratton MR. 2004. A census of human cancer genes. *Nature reviews Cancer* **4**(3): 177-183.

Garcia-Blanco MA. 2003. Messenger RNA reprogramming by spliceosome-mediated RNA trans-splicing. *The Journal of clinical investigation* **112**(4): 474-480.

Gery S, Virk RK, Chumakov K, Yu A, Koeffler HP. 2007. The clock gene Per2 links the circadian system to the estrogen receptor. *Oncogene* **26**(57): 7916-7920.

Gorunova L, Hoglund M, Andren-Sandberg A, Dawiskiba S, Jin Y, Mitelman F, Johansson B. 1998. Cytogenetic analysis of pancreatic carcinomas: intratumor heterogeneity and nonrandom pattern of chromosome aberrations. *Genes, chromosomes & cancer* **23**(2): 81-99.

Greenman C, Stephens P, Smith R, Dalgliesh GL, Hunter C, Bignell G, Davies H, Teague J, Butler A, Stevens C et al. 2007. Patterns of somatic mutation in human cancer genomes. *Nature* **446**(7132): 153-158.

Griffith M, Griffith OL, Mwenifumbo J, Goya R, Morrissy AS, Morin RD, Corbett R, Tang MJ, Hou YC, Pugh TJ et al. 2010. Alternative expression analysis by RNA sequencing. *Nature methods* **7**(10): 843-847.

Gu W, Zhang F, Lupski JR. 2008. Mechanisms for human genomic rearrangements. *PathoGenetics* **1**(1): 4.

Guffanti A, Iacono M, Pelucchi P, Kim N, Solda G, Croft LJ, Taft RJ, Rizzi E, Askarian-Amiri M, Bonnal RJ et al. 2009. A transcriptional sketch of a primary human breast cancer by 454 deep sequencing. *BMC genomics* **10**: 163.

Gui C, Hagenbuch B. 2009. Role of transmembrane domain 10 for the function of organic anion transporting polypeptide 1B1. *Protein science : a publication of the Protein Society* **18**(11): 2298-2306.

Guttman M, Garber M, Levin JZ, Donaghey J, Robinson J, Adiconis X, Fan L, Koziol MJ, Gnirke A, Nusbaum C et al. 2010. Ab initio reconstruction of cell type-specific transcriptomes in mouse reveals the conserved multi-exonic structure of lincRNAs. *Nature biotechnology* **28**(5): 503-510.

Harris TJ, McCormick F. 2010. The molecular pathology of cancer. *Nature reviews Clinical oncology* **7**(5): 251-265.

Hillmer AM, Yao F, Inaki K, Lee WH, Ariyaratne PN, Teo AS, Woo XY, Zhang Z, Zhao H, Ukil L et al. 2011. Comprehensive long-span paired-end-tag mapping reveals characteristic patterns of structural variations in epithelial cancer genomes. *Genome research* **21**(5): 665-675.

Hrzenjak A, Moinfar F, Tavassoli FA, Strohmeier B, Kremser ML, Zatloukal K, Denk H. 2005. JAZF1/JJAZ1 gene fusion in endometrial stromal sarcomas: molecular analysis by reverse transcriptase-polymerase chain reaction optimized for paraffin-embedded tissue. *The Journal of molecular diagnostics : JMD* **7**(3): 388-395.

Huang CR, Schneider AM, Lu Y, Niranjan T, Shen P, Robinson MA, Steranka JP, Valle D, Civin CI, Wang T et al. 2010. Mobile interspersed repeats are major structural variants in the human genome. *Cell* **141**(7): 1171-1182.

Hubbard T, Barker D, Birney E, Cameron G, Chen Y, Clark L, Cox T, Cuff J, Curwen V, Down T et al. 2002. The Ensembl genome database project. *Nucleic acids research* **30**(1): 38-41.

Jabbour L, Welter JF, Kollar J, Hering TM. 2003. Sequence, gene structure, and expression pattern of CTNNBL1, a minor-class intron-containing gene--evidence for a role in apoptosis. *Genomics* **81**(3): 292-303.

Jiao X, Rosenlund M, Hooper SD, Tellgren-Roth C, He L, Fu Y, Mangion J, Sjoblom T. 2011. Structural alterations from multiple displacement amplification of a human genome revealed by mate-pair sequencing. *PloS one* **6**(7): e22250.

Ju YS, Lee WC, Shin JY, Lee S, Bleazard T, Won JK, Kim YT, Kim JI, Kang JH, Seo JS. 2012. A transforming KIF5B and RET gene fusion in lung adenocarcinoma revealed from whole-genome and transcriptome sequencing. *Genome research* **22**(3): 436-445.

Karolchik D, Barber GP, Casper J, Clawson H, Cline MS, Diekhans M, Dreszer TR, Fujita PA, Guruvadoo L, Haeussler M et al. 2014. The UCSC Genome Browser database: 2014 update. *Nucleic acids research* **42**(Database issue): D764-770.

Karolchik D, Hinrichs AS, Furey TS, Roskin KM, Sugnet CW, Haussler D, Kent WJ. 2004. The UCSC Table Browser data retrieval tool. *Nucleic acids research* **32**(Database issue): D493-496.

Kaye FJ. 2009. Mutation-associated fusion cancer genes in solid tumors. *Molecular cancer therapeutics* **8**(6): 1399-1408.

Kent WJ. 2002. BLAT--the BLAST-like alignment tool. *Genome research* **12**(4): 656-664.

Kim D, Salzberg SL. 2011. TopHat-Fusion: an algorithm for discovery of novel fusion transcripts. *Genome biology* **12**(8): R72.

Kim P, Yoon S, Kim N, Lee S, Ko M, Lee H, Kang H, Kim J. 2010. ChimerDB 2.0--a knowledgebase for fusion genes updated. *Nucleic acids research* **38**(Database issue): D81-85.

Knezevich SR, McFadden DE, Tao W, Lim JF, Sorensen PH. 1998. A novel ETV6-NTRK3 gene fusion in congenital fibrosarcoma. *Nature genetics* **18**(2): 184-187.

Koontz JI, Soreng AL, Nucci M, Kuo FC, Pauwels P, van Den Berghe H, Dal Cin P, Fletcher JA, Sklar J. 2001. Frequent fusion of the JAZF1 and JJAZ1 genes in endometrial stromal tumors. *Proceedings of the National Academy of Sciences of the United States of America* **98**(11): 6348-6353.

Korbel JO, Abyzov A, Mu XJ, Carriero N, Cayting P, Zhang Z, Snyder M, Gerstein MB. 2009. PEMer: a computational framework with simulation-based error models for inferring genomic structural variants from massive paired-end sequencing data. *Genome biology* **10**(2): R23.

Korbel JO, Urban AE, Affourtit JP, Godwin B, Grubert F, Simons JF, Kim PM, Palejev D, Carriero NJ, Du L et al. 2007. Paired-end mapping reveals extensive structural variation in the human genome. *Science* **318**(5849): 420-426.

Koudritsky M, Domany E. 2008. Positional distribution of human transcription factor binding sites. *Nucleic acids research* **36**(21): 6795-6805.

Kudo T, Ikehara Y, Togayachi A, Morozumi K, Watanabe M, Nakamura M, Nishihara S, Narimatsu H. 1998. Up-regulation of a set of glycosyltransferase genes in human colorectal cancer. *Laboratory investigation; a journal of technical methods and pathology* **78**(7): 797-811.

Kulesh DA, Clive DR, Zarlenga DS, Greene JJ. 1987. Identification of interferon-modulated proliferation-related cDNA sequences. *Proceedings of the National Academy of Sciences of the United States of America* **84**(23): 8453-8457.

Kumar-Sinha C, Tomlins SA, Chinnaiyan AM. 2006. Evidence of recurrent gene fusions in common epithelial tumors. *Trends in molecular medicine* **12**(11): 529-536.

-. 2008. Recurrent gene fusions in prostate cancer. *Nature reviews Cancer* **8**(7): 497-511.

Langmead B, Salzberg SL. 2012. Fast gapped-read alignment with Bowtie 2. *Nature methods* **9**(4): 357-359.

Langmead B, Trapnell C, Pop M, Salzberg SL. 2009. Ultrafast and memory-efficient alignment of short DNA sequences to the human genome. *Genome biology* **10**(3): R25.

Laxman B, Morris DS, Yu J, Siddiqui J, Cao J, Mehra R, Lonigro RJ, Tsodikov A, Wei JT, Tomlins SA et al. 2008. A first-generation multiplex biomarker analysis of urine for the early detection of prostate cancer. *Cancer research* **68**(3): 645-649.

Lee LR, Teng PN, Nguyen H, Hood BL, Kavandi L, Wang G, Turbov JM, Thaete LG, Hamilton CA, Maxwell GL et al. 2013. Progesterone enhances calcitriol

antitumor activity by upregulating vitamin D receptor expression and promoting apoptosis in endometrial cancer cells. *Cancer prevention research* **6**(7): 731-743.

Lengauer C, Kinzler KW, Vogelstein B. 1998. Genetic instabilities in human cancers. *Nature* **396**(6712): 643-649.

Letunic I, Doerks T, Bork P. 2012. SMART 7: recent updates to the protein domain annotation resource. *Nucleic acids research* **40**(Database issue): D302-305.

Li B, Dewey CN. 2011. RSEM: accurate transcript quantification from RNA-Seq data with or without a reference genome. *BMC bioinformatics* **12**: 323.

Li B, Ruotti V, Stewart RM, Thomson JA, Dewey CN. 2010a. RNA-Seq gene expression estimation with read mapping uncertainty. *Bioinformatics* **26**(4): 493-500.

Li H, Durbin R. 2010. Fast and accurate long-read alignment with Burrows-Wheeler transform. *Bioinformatics* **26**(5): 589-595.

Li H, Handsaker B, Wysoker A, Fennell T, Ruan J, Homer N, Marth G, Abecasis G, Durbin R, Genome Project Data Processing S. 2009. The Sequence Alignment/Map format and SAMtools. *Bioinformatics* **25**(16): 2078-2079.

Li H, Wang J, Mor G, Sklar J. 2008. A neoplastic gene fusion mimics trans-splicing of RNAs in normal human cells. *Science* **321**(5894): 1357-1361.

Li J, Jiang H, Wong WH. 2010b. Modeling non-uniformity in short-read rates in RNA-Seq data. *Genome biology* **11**(5): R50.

Li J, Xu Y, Long XD, Wang W, Jiao HK, Mei Z, Yin QQ, Ma LN, Zhou AW, Wang LS et al. 2014. Cbx4 governs HIF-1alpha to potentiate angiogenesis of hepatocellular carcinoma by its SUMO E3 ligase activity. *Cancer cell* **25**(1): 118-131.

Lindgreen S. 2012. AdapterRemoval: easy cleaning of next-generation sequencing reads. *BMC research notes* **5**: 337.

Loeb LA, Harris CC. 2008. Advances in chemical carcinogenesis: a historical review and prospective. *Cancer research* **68**(17): 6863-6872.

Look AT. 1997. Oncogenic transcription factors in the human acute leukemias. *Science* **278**(5340): 1059-1064.

Lugo TG, Pendergast AM, Muller AJ, Witte ON. 1990. Tyrosine kinase activity and transformation potency of bcr-abl oncogene products. *Science* **247**(4946): 1079-1082.

Lupski JR, Stankiewicz P. 2005. Genomic disorders: molecular mechanisms for rearrangements and conveyed phenotypes. *PLoS genetics* **1**(6): e49.

Maeda K, Horikoshi T, Nakashima E, Miyamoto Y, Mabuchi A, Ikegawa S. 2005. MATN and LAPTM are parts of larger transcription units produced by intergenic splicing: intergenic splicing may be a common phenomenon. *DNA research : an international journal for rapid publication of reports on genes and genomes* **12**(5): 365-372.

Maher CA, Kumar-Sinha C, Cao X, Kalyana-Sundaram S, Han B, Jing X, Sam L, Barrette T, Palanisamy N, Chinnaiyan AM. 2009a. Transcriptome sequencing to detect gene fusions in cancer. *Nature* **458**(7234): 97-101.

Maher CA, Palanisamy N, Brenner JC, Cao X, Kalyana-Sundaram S, Luo S, Khrebtukova I, Barrette TR, Grasso C, Yu J et al. 2009b. Chimeric transcript discovery by paired-end transcriptome sequencing. *Proceedings of the National Academy of Sciences of the United States of America* **106**(30): 12353-12358.

Malhotra A, Lindberg M, Faust GG, Leibowitz ML, Clark RA, Layer RM, Quinlan AR, Hall IM. 2013. Breakpoint profiling of 64 cancer genomes reveals numerous complex rearrangements spawned by homology-independent mechanisms. *Genome research* **23**(5): 762-776.

Mane SP, Evans C, Cooper KL, Crasta OR, Folkerts O, Hutchison SK, Harkins TT, Thierry-Mieg D, Thierry-Mieg J, Jensen RV. 2009. Transcriptome sequencing of the Microarray Quality Control (MAQC) RNA reference samples using next generation sequencing. *BMC genomics* **10**: 264.

Mani RS, Chinnaiyan AM. 2010. Triggers for genomic rearrangements: insights into genomic, cellular and environmental influences. *Nature reviews Genetics* **11**(12): 819-829.

Martin JA, Wang Z. 2011. Next-generation transcriptome assembly. *Nature reviews Genetics* **12**(10): 671-682.

Maskos U, Southern EM. 1992. Oligonucleotide hybridizations on glass supports: a novel linker for oligonucleotide synthesis and hybridization properties of oligonucleotides synthesised in situ. *Nucleic acids research* **20**(7): 1679-1684.

McPherson JD. 2009. Next-generation gap. *Nature methods* **6**(11 Suppl): S2-5.

McWhirter JR, Galasso DL, Wang JY. 1993. A coiled-coil oligomerization domain of Bcr is essential for the transforming function of Bcr-Abl oncoproteins. *Molecular and cellular biology* **13**(12): 7587-7595.

Medvedev P, Stanciu M, Brudno M. 2009. Computational methods for discovering structural variation with next-generation sequencing. *Nature methods* **6**(11 Suppl): S13-20.

Metzker ML. 2010. Sequencing technologies - the next generation. *Nature reviews Genetics* **11**(1): 31-46.

Mignone F, Gissi C, Liuni S, Pesole G. 2002. Untranslated regions of mRNAs. *Genome biology* **3**(3): REVIEWS0004.

Mitelman F. 2000. Recurrent chromosome aberrations in cancer. *Mutation research* **462**(2-3): 247-253.

Mitelman F, Johansson B, Mertens F. 2004. Fusion genes and rearranged genes as a linear function of chromosome aberrations in cancer. *Nature genetics* **36**(4): 331-334.

-. 2007. The impact of translocations and gene fusions on cancer causation. *Nature reviews Cancer* **7**(4): 233-245.

Mitelman F, Mertens F, Johansson B. 2005. Prevalence estimates of recurrent balanced cytogenetic aberrations and gene fusions in unselected patients with neoplastic disorders. *Genes, chromosomes & cancer* **43**(4): 350-366.

Mittal VK, McDonald JF. 2012. R-SAP: a multi-threading computational pipeline for the characterization of high-throughput RNA-sequencing data. *Nucleic acids research* **40**(9): e67.

Morgulis A, Gertz EM, Schaffer AA, Agarwala R. 2006. A fast and symmetric DUST implementation to mask low-complexity DNA sequences. *Journal of computational biology : a journal of computational molecular cell biology* **13**(5): 1028-1040.

Morozova O, Marra MA. 2008. Applications of next-generation sequencing technologies in functional genomics. *Genomics* **92**(5): 255-264.

Mortazavi A, Williams BA, McCue K, Schaeffer L, Wold B. 2008. Mapping and quantifying mammalian transcriptomes by RNA-Seq. *Nature methods* **5**(7): 621-628.

Murphy SJ, Cheville JC, Zarei S, Johnson SH, Sikkink RA, Kosari F, Feldman AL, Eckloff BW, Karnes RJ, Vasmatzis G. 2012. Mate pair sequencing of whole-genome-amplified DNA following laser capture microdissection of prostate cancer. *DNA research : an international journal for rapid publication of reports on genes and genomes* **19**(5): 395-406.

Nacu S, Yuan W, Kan Z, Bhatt D, Rivers CS, Stinson J, Peters BA, Modrusan Z, Jung K, Seshagiri S et al. 2011. Deep RNA sequencing analysis of readthrough gene fusions in human prostate adenocarcinoma and reference samples. *BMC medical genomics* **4**: 11.

Nagalakshmi U, Wang Z, Waern K, Shou C, Raha D, Gerstein M, Snyder M. 2008. The transcriptional landscape of the yeast genome defined by RNA sequencing. *Science* **320**(5881): 1344-1349.

Nakayama K, Nakayama N, Davidson B, Sheu JJ, Jinawath N, Santillan A, Salani R, Bristow RE, Morin PJ, Kurman RJ et al. 2006. A BTB/POZ protein, NAC-1, is related to tumor recurrence and is essential for tumor growth and survival. *Proceedings of the National Academy of Sciences of the United States of America* **103**(49): 18739-18744.

Nambiar M, Raghavan SC. 2013. Chromosomal translocations among the healthy human population: implications in oncogenesis. *Cellular and molecular life sciences : CMLS* **70**(8): 1381-1392.

Ng HH, Ciccone DN, Morshead KB, Oettinger MA, Struhl K. 2003. Lysine-79 of histone H3 is hypomethylated at silenced loci in yeast and mammalian cells: a potential mechanism for position-effect variegation. *Proceedings of the National Academy of Sciences of the United States of America* **100**(4): 1820-1825.

Ning Z, Cox AJ, Mullikin JC. 2001. SSAHA: a fast search method for large DNA databases. *Genome research* **11**(10): 1725-1729.

Nowell PC. 1962. The minute chromosome (Phl) in chronic granulocytic leukemia. *Blut* **8**: 65-66.

O'Huallachain M, Karczewski KJ, Weissman SM, Urban AE, Snyder MP. 2012. Extensive genetic variation in somatic human tissues. *Proceedings of the National Academy of Sciences of the United States of America* **109**(44): 18018-18023.

Ozsolak F, Milos PM. 2011. RNA sequencing: advances, challenges and opportunities. *Nature reviews Genetics* **12**(2): 87-98.

Pan Q, Shai O, Lee LJ, Frey BJ, Blencowe BJ. 2008. Deep surveying of alternative splicing complexity in the human transcriptome by high-throughput sequencing. *Nature genetics* **40**(12): 1413-1415.

Parker BC, Annala MJ, Cogdell DE, Granberg KJ, Sun Y, Ji P, Li X, Gumin J, Zheng H, Hu L et al. 2013. The tumorigenic FGFR3-TACC3 gene fusion escapes miR-99a regulation in glioblastoma. *The Journal of clinical investigation* **123**(2): 855-865.

Parra G, Reymond A, Dabbouseh N, Dermitzakis ET, Castelo R, Thomson TM, Antonarakis SE, Guigo R. 2006. Tandem chimerism as a means to increase protein complexity in the human genome. *Genome research* **16**(1): 37-44.

Patani N, Jiang W, Mokbel K. 2008. Prognostic utility of glycosyltransferase expression in breast cancer. *Cancer genomics & proteomics* **5**(6): 333-340.

Pierotti MA. 2001. Chromosomal rearrangements in thyroid carcinomas: a recombination or death dilemma. *Cancer letters* **166**(1): 1-7.

Pleasance ED, Cheetham RK, Stephens PJ, McBride DJ, Humphray SJ, Greenman CD, Varela I, Lin ML, Ordonez GR, Bignell GR et al. 2010. A comprehensive

catalogue of somatic mutations from a human cancer genome. *Nature* **463**(7278): 191-196.

Prechelt L. 2000. An empirical comparison of seven programming languages. *Computer* **33**(10): 23-29.

Prensner JR, Iyer MK, Balbin OA, Dhanasekaran SM, Cao Q, Brenner JC, Laxman B, Asangani IA, Grasso CS, Kominsky HD et al. 2011. Transcriptome sequencing across a prostate cancer cohort identifies PCAT-1, an unannotated lincRNA implicated in disease progression. *Nature biotechnology* **29**(8): 742-749.

Pruitt KD, Tatusova T, Maglott DR. 2007. NCBI reference sequences (RefSeq): a curated non-redundant sequence database of genomes, transcripts and proteins. *Nucleic acids research* **35**(Database issue): D61-65.

Qu H, Fang X. 2013. A brief review on the Human Encyclopedia of DNA Elements (ENCODE) project. *Genomics, proteomics & bioinformatics* **11**(3): 135-141.

Quinlan AR, Clark RA, Sokolova S, Leibowitz ML, Zhang Y, Hurles ME, Mell JC, Hall IM. 2010. Genome-wide mapping and assembly of structural variant breakpoints in the mouse genome. *Genome research* **20**(5): 623-635.

Rabbitts TH. 1994. Chromosomal translocations in human cancer. *Nature* **372**(6502): 143-149.

Reddy EP, Reynolds RK, Santos E, Barbacid M. 1982. A point mutation is responsible for the acquisition of transforming properties by the T24 human bladder carcinoma oncogene. *Nature* **300**(5888): 149-152.

Reiter A, Lengfelder E, Grimwade D. 2004. Pathogenesis, diagnosis and monitoring of residual disease in acute promyelocytic leukaemia. *Acta haematologica* **112**(1-2): 55-67.

Ren R. 2005. Mechanisms of BCR-ABL in the pathogenesis of chronic myelogenous leukaemia. *Nature reviews Cancer* **5**(3): 172-183.

Richardson C, Jasin M. 2000. Frequent chromosomal translocations induced by DNA double-strand breaks. *Nature* **405**(6787): 697-700.

Richter BG, Sexton DP. 2009. Managing and analyzing next-generation sequence data. *PLoS computational biology* **5**(6): e1000369.

Risch HA, McLaughlin JR, Cole DE, Rosen B, Bradley L, Fan I, Tang J, Li S, Zhang S, Shaw PA et al. 2006. Population BRCA1 and BRCA2 mutation frequencies and cancer penetrances: a kin-cohort study in Ontario, Canada. *Journal of the National Cancer Institute* **98**(23): 1694-1706.

Ritchie W, Granjeaud S, Puthier D, Gautheret D. 2008. Entropy measures quantify global splicing disorders in cancer. *PLoS computational biology* **4**(3): e1000011.

Robertson G, Schein J, Chiu R, Corbett R, Field M, Jackman SD, Mungall K, Lee S, Okada HM, Qian JQ et al. 2010. De novo assembly and analysis of RNA-seq data. *Nature methods* **7**(11): 909-912.

Robinson DR, Kalyana-Sundaram S, Wu YM, Shankar S, Cao X, Ateeq B, Asangani IA, Iyer M, Maher CA, Grasso CS et al. 2011. Functionally recurrent rearrangements of the MAST kinase and Notch gene families in breast cancer. *Nature medicine* **17**(12): 1646-1651.

Roix JJ, McQueen PG, Munson PJ, Parada LA, Misteli T. 2003. Spatial proximity of translocation-prone gene loci in human lymphomas. *Nature genetics* **34**(3): 287-291.

Rosenbloom KR, Sloan CA, Malladi VS, Dreszer TR, Learned K, Kirkup VM, Wong MC, Maddren M, Fang R, Heitner SG et al. 2013. ENCODE data in the UCSC Genome Browser: year 5 update. *Nucleic acids research* **41**(Database issue): D56-63.

Roth L, Nasarre C, Dirrig-Grosch S, Aunis D, Cremel G, Hubert P, Bagnard D. 2008. Transmembrane domain interactions control biological functions of neuropilin-1. *Molecular biology of the cell* **19**(2): 646-654.

Rowley JD. 1973. Letter: A new consistent chromosomal abnormality in chronic myelogenous leukaemia identified by quinacrine fluorescence and Giemsa staining. *Nature* **243**(5405): 290-293.

-. 2001. Chromosome translocations: dangerous liaisons revisited. *Nature reviews Cancer* **1**(3): 245-250.

Saini V, Hose CD, Monks A, Nagashima K, Han B, Newton DL, Millione A, Shah J, Hollingshead MG, Hite KM et al. 2012. Identification of CBX3 and ABCA5 as putative biomarkers for tumor stem cells in osteosarcoma. *PloS one* **7**(8): e41401.

Savage JR. 1993. Interchange and intra-nuclear architecture. *Environmental and molecular mutagenesis* **22**(4): 234-244.

Sboner A, Habegger L, Pflueger D, Terry S, Chen DZ, Rozowsky JS, Tewari AK, Kitabayashi N, Moss BJ, Chee MS et al. 2010. FusionSeq: a modular framework for finding gene fusions by analyzing paired-end RNA-sequencing data. *Genome biology* **11**(10): R104.

Schimke RT, Kaufman RJ, Alt FW, Kellems RF. 1978. Gene amplification and drug resistance in cultured murine cells. *Science* **202**(4372): 1051-1055.

Shi L Reid LH Jones WD Shippy R Warrington JA Baker SC Collins PJ de Longueville F Kawasaki ES Lee KY et al. 2006. The MicroArray Quality Control (MAQC) project shows inter- and intraplatform reproducibility of gene expression measurements. *Nature biotechnology* **24**(9): 1151-1161.

Simpson JT, Wong K, Jackman SD, Schein JE, Jones SJ, Birol I. 2009. ABySS: a parallel assembler for short read sequence data. *Genome research* **19**(6): 1117-1123.

Simsek D, Jasin M. 2010. Alternative end-joining is suppressed by the canonical NHEJ component Xrcc4-ligase IV during chromosomal translocation formation. *Nature structural & molecular biology* **17**(4): 410-416.

Skotheim RI, Nees M. 2007. Alternative splicing in cancer: noise, functional, or systematic? *The international journal of biochemistry & cell biology* **39**(7-8): 1432-1449.

Soda M, Choi YL, Enomoto M, Takada S, Yamashita Y, Ishikawa S, Fujiwara S, Watanabe H, Kurashina K, Hatanaka H et al. 2007. Identification of the transforming EML4-ALK fusion gene in non-small-cell lung cancer. *Nature* **448**(7153): 561-566.

Stephens PJ, McBride DJ, Lin ML, Varela I, Pleasance ED, Simpson JT, Stebbings LA, Leroy C, Edkins S, Mudie LJ et al. 2009. Complex landscapes of somatic rearrangement in human breast cancer genomes. *Nature* **462**(7276): 1005-1010.

Stratton MR, Campbell PJ, Futreal PA. 2009. The cancer genome. *Nature* **458**(7239): 719-724.

Suh KS, Malik M, Shukla A, Ryscavage A, Wright L, Jividen K, Crutchley JM, Dumont RA, Fernandez-Salas E, Webster JD et al. 2012. CLIC4 is a tumor suppressor for cutaneous squamous cell cancer. *Carcinogenesis* **33**(5): 986-995.

Sullenger BA, Gilboa E. 2002. Emerging clinical applications of RNA. *Nature* **418**(6894): 252-258.

Sultan M, Schulz MH, Richard H, Magen A, Klingenhoff A, Scherf M, Seifert M, Borodina T, Soldatov A, Parkhomchuk D et al. 2008. A global view of gene activity and alternative splicing by deep sequencing of the human transcriptome. *Science* **321**(5891): 956-960.

Sutherland GT, Janitz M, Kril JJ. 2011. Understanding the pathogenesis of Alzheimer's disease: will RNA-Seq realize the promise of transcriptomics? *Journal of neurochemistry* **116**(6): 937-946.

Suzuki Y, Yoshitomo-Nakagawa K, Maruyama K, Suyama A, Sugano S. 1997. Construction and characterization of a full length-enriched and a 5'-end-enriched cDNA library. *Gene* **200**(1-2): 149-156.

Tanner NK, Linder P. 2001. DExD/H box RNA helicases: from generic motors to specific dissociation functions. *Molecular cell* **8**(2): 251-262.

Thierry-Mieg D, Thierry-Mieg J. 2006. AceView: a comprehensive cDNA-supported gene and transcripts annotation. *Genome biology* **7 Suppl 1**: S12 11-14.

Tognon C, Knezevich SR, Huntsman D, Roskelley CD, Melnyk N, Mathers JA, Becker L, Carneiro F, MacPherson N, Horsman D et al. 2002. Expression of the ETV6-NTRK3 gene fusion as a primary event in human secretory breast carcinoma. *Cancer cell* **2**(5): 367-376.

Tomlins SA, Rhodes DR, Perner S, Dhanasekaran SM, Mehra R, Sun XW, Varambally S, Cao X, Tchinda J, Kuefer R et al. 2005. Recurrent fusion of TMPRSS2 and ETS transcription factor genes in prostate cancer. *Science* **310**(5748): 644-648.

Trapnell C, Pachter L, Salzberg SL. 2009. TopHat: discovering splice junctions with RNA-Seq. *Bioinformatics* **25**(9): 1105-1111.

Trapnell C, Williams BA, Pertea G, Mortazavi A, Kwan G, van Baren MJ, Salzberg SL, Wold BJ, Pachter L. 2010. Transcript assembly and quantification by RNA-Seq reveals unannotated transcripts and isoform switching during cell differentiation. *Nature biotechnology* **28**(5): 511-515.

Tsai AG, Lu H, Raghavan SC, Muschen M, Hsieh CL, Lieber MR. 2008. Human chromosomal translocations at CpG sites and a theoretical basis for their lineage and stage specificity. *Cell* **135**(6): 1130-1142.

Tuduri S, Crabbe L, Conti C, Tourriere H, Holtgreve-Grez H, Jauch A, Pantesco V, De Vos J, Thomas A, Theillet C et al. 2009. Topoisomerase I suppresses genomic instability by preventing interference between replication and transcription. *Nature cell biology* **11**(11): 1315-1324.

Velculescu VE, Zhang L, Zhou W, Vogelstein J, Basrai MA, Bassett DE, Jr., Hieter P, Vogelstein B, Kinzler KW. 1997. Characterization of the yeast transcriptome. *Cell* **88**(2): 243-251.

Voelkerding KV, Dames SA, Durtschi JD. 2009. Next-generation sequencing: from basic research to diagnostics. *Clinical chemistry* **55**(4): 641-658.

Vogelstein B, Papadopoulos N, Velculescu VE, Zhou S, Diaz LA, Jr., Kinzler KW. 2013. Cancer genome landscapes. *Science* **339**(6127): 1546-1558.

von Hansemann D. 1890. Ueber asymmetrische Zelltheilung in epithel Krebsen und deren biologische Bedeutung. *Virchow's Arch Path Anat* **119**: 299.

von Heijne G. 1985. Signal sequences. The limits of variation. *Journal of molecular biology* **184**(1): 99-105.

Vorburger SA, Pataer A, Swisher SG, Hunt KK. 2004. Genetically targeted cancer therapy: tumor destruction by PKR activation. *American journal of pharmacogenomics : genomics-related research in drug development and clinical practice* **4**(3): 189-198.

Wang Q, Xia J, Jia P, Pao W, Zhao Z. 2013. Application of next generation sequencing to human gene fusion detection: computational tools, features and perspectives. *Briefings in bioinformatics* **14**(4): 506-519.

Wang Z, Gerstein M, Snyder M. 2009. RNA-Seq: a revolutionary tool for transcriptomics. *Nature reviews Genetics* **10**(1): 57-63.

Wang ZC, Birkbak NJ, Culhane AC, Drapkin R, Fatima A, Tian R, Schwede M, Alsop K, Daniels KE, Piao H et al. 2012. Profiles of genomic instability in high-grade serous ovarian cancer predict treatment outcome. *Clinical cancer research : an official journal of the American Association for Cancer Research* **18**(20): 5806-5815.

Xia SJ, Barr FG. 2005. Chromosome translocations in sarcomas and the emergence of oncogenic transcription factors. *European journal of cancer* **41**(16): 2513-2527.

Zeitouni B, Boeva V, Janoueix-Lerosey I, Loeillet S, Legoix-ne P, Nicolas A, Delattre O, Barillot E. 2010. SVDetect: a tool to identify genomic structural variations from paired-end and mate-pair sequencing data. *Bioinformatics* **26**(15): 1895-1896.

Zerbino DR, Birney E. 2008. Velvet: algorithms for de novo short read assembly using de Bruijn graphs. *Genome research* **18**(5): 821-829.